U.S.NRC
United States Nuclear Regulatory Commission
Protecting People and the Environment

NUREG/CR-6994
ANL-08/37

Argonne Model Boiler Test Results

Office of Nuclear Regulatory Research

AVAILABILITY OF REFERENCE MATERIALS IN NRC PUBLICATIONS

C Reference Material

of November 1999, you may electronically access REG-series publications and other NRC records at C's Public Electronic Reading Room at ://www.nrc.gov/reading-rm.html. Publicly released ords include, to name a few, NUREG-series lications; *Federal Register* notices; applicant, nsee, and vendor documents and correspondence; C correspondence and internal memoranda; etins and information notices; inspection and stigative reports; licensee event reports; and mission papers and their attachments.

C publications in the NUREG series, NRC lations, and *Title 10, Energy*, in the Code of *eral Regulations* may also be purchased from one ese two sources.

The Superintendent of Documents
U.S. Government Printing Office
Mail Stop SSOP
Washington, DC 20402–0001
Internet: bookstore.gpo.gov
Telephone: 202-512-1800
Fax: 202-512-2250
The National Technical Information Service
Springfield, VA 22161–0002
www.ntis.gov
1–800–553–6847 or, locally, 703–605–6000

ngle copy of each NRC draft report for comment is lable free, to the extent of supply, upon written uest as follows:

Address: Office of Administration
Reproduction and Mail Services Branch
U.S. Nuclear Regulatory Commission
Washington, DC 20555-0001
Mail: DISTRIBUTION@nrc.gov
Facsimile: 301–415–2289

ne publications in the NUREG series that are ed at NRC's Web site address //www.nrc.gov/reading-rm/doc-collections/nuregs pdated periodically and may differ from the last ed version. Although references to material found Web site bear the date the material was accessed, material available on the date cited may equently be removed from the site.

Non-NRC Reference Material

Documents available from public and special technical libraries include all open literature items, such as books, journal articles, and transactions, *Federal Register* notices, Federal and State legislation, and congressional reports. Such documents as theses, dissertations, foreign reports and translations, and non-NRC conference proceedings may be purchased from their sponsoring organization.

Copies of industry codes and standards used in a substantive manner in the NRC regulatory process are maintained at—

The NRC Technical Library
Two White Flint North
11545 Rockville Pike
Rockville, MD 20852–2738

These standards are available in the library for reference use by the public. Codes and standards are usually copyrighted and may be purchased from the originating organization or, if they are American National Standards, from—

American National Standards Institute
11 West 42nd Street
New York, NY 10036–8002
www.ansi.org
212–642–4900

Legally binding regulatory requirements are stated only in laws; NRC regulations; licenses, including technical specifications; or orders, not in NUREG-series publications. The views expressed in contractor-prepared publications in this series are not necessarily those of the NRC.

The NUREG series comprises (1) technical and administrative reports and books prepared by the staff (NUREG–XXXX) or agency contractors (NUREG/CR–XXXX), (2) proceedings of conferences (NUREG/CP–XXXX), (3) reports resulting from international agreements (NUREG/IA–XXXX), (4) brochures (NUREG/BR–XXXX), and (5) compilations of legal decisions and orders of the Commission and Atomic and Safety Licensing Boards and of Directors' decisions under Section 2.206 of NRC's regulations (NUREG–0750).

U.S.NRC
United States Nuclear Regulatory Commission
Protecting People and the Environment

NUREG/CR-6994
ANL-08/37

Argonne Model Boiler Test Results

Manuscript Completed: November 2008
Date Published: December 2009

Prepared by
C.B. Bahn, K.E. Kasza, J. Park, C. Vulyak, and W.J. Shack

Argonne National Laboratory
9700 South Cass Avenue
Argonne, IL 60439

C. Harris, NRC Project Manager

NRC Job Code Y6588

Office of Nuclear Regulatory Research

Abstract

Various corrosion phenomena have been observed in the steam generator (SG) tubes of pressurized water reactors. One such type of corrosion involves impurity concentration in the narrow gap between SG tubes and supporting structures or sludge piles ("crevices"). The purpose of this study is to characterize accumulation of impurities in the crevices for varying Na-to-Cl molar ratios in water, temperature, and packing type (diamond or magnetite). This characterization is based on tests carried out at Argonne National Laboratory in a model boiler system which can simulate prototypic SG conditions. Diamond powder, which has a higher thermal conductivity than magnetite powder, can enhance the boiling rate and lead to a rapid rate of impurity accumulation. Magnetite-packed crevices, which have lower permeability, are more appropriate for the simulation of actual SG crevices than a diamond-packed crevice. A radial chemistry gradient was observed in a crevice packed tightly with magnetite powder, a finding supported by earlier experimental work. Near the tube wall, the crevice chemistry tends to vary actively because of the increased volatility effect of Cl at the heated tube wall where boiling occurs. Initially, the crevice pH near the tube wall appears to be alkaline. As the concentration progresses, however, the crevice pH becomes neutralized and even acidic because of preferential Cl concentration, enabled by a reduced boiling rate near the tube wall due to the presence of a Na-rich liquid film. Based on the test results, the chemistry variation in actual SG crevice deposits near the tube wall was estimated. Unless some impurities remain and accumulate in the crevice after each fuel cycle, during most of a typical fuel cycle, the crevice chemistry would be in a transient rather than a steady-state condition because of low impurity concentrations in the secondary system. The kinetic data obtained for the crevice chemistry evolution with low bulk impurity concentration is valuable for the estimation of actual SG crevice chemistries. Based on the crevice and bulk solution sample analyses, the volatility effect of Cl in the diamond-packed crevices becomes significant as the molar ratio decreases. Data are limited but it is likely that the volatility effect of Cl in the magnetite-packed crevices is not strongly influenced by the molar ratio variation in the bulk solution. Tests showed that once a tube crack is formed, the crack itself can act as a crevice, and in the presence of NaOH bulk chemistry, it can grow even if the sludge or debris is cleaned out of the SG.

FOREWORD

This report discusses a study conducted by Argonne National Laboratory (ANL) under contract with the U.S. Nuclear Regulatory Commission (NRC), to study the effects of steam generator secondary side water chemistry on crack initiation and propagation near crevices.

The purpose of this study is to characterize accumulation of impurities in the crevices adjacent to steam generator (SG) tubes. A model boiler system to simulate prototypical thermal hydraulic and chemistry conditions of the secondary side of SGs in pressurized water reactors was developed at ANL. The facility has prototypic crevice heat fluxes and temperatures, thus permitting the development of more prototypic crevice chemistry conditions. A crevice simulator equipped with various instruments, including thermocouples, electro-chemical potential electrodes, pH electrodes, conductivity probes, and solution sampling lines, was developed and successfully operated.

This work produced many findings regarding SG tube corrosion and deposits. The crevice pH predicted by an analytical code was compared with the measured crevice pH as a function of boiling point elevation. Initially, the crevice pH near the tube wall appears to be alkaline, however, as the impurity concentration progresses, the crevice pH becomes neutralized and even acidic. In a less permeable crevice, the volatility of Cl becomes less significant because Cl does not easily escape. This condition leads to a lowering of the crevice pH near the tube wall. The kinetic data obtained for the crevice chemistry evolution with low bulk impurity concentration is valuable for the estimation of actual SG crevice chemistries.

The chemistry variations in the deposits in an actual SG crevice near the tube wall were estimated. The Model Boiler tests showed some initial evidence that once a crack is formed, the crack itself can act as a crevice. In NaOH bulk chemistry the crack can grow even if the sludge or debris is cleaned out of the SG.

The NRC may use this research in the evaluation of industry assessments of steam generator (SG) tube integrity. These assessments are provided in support of license amendments and other licensing tasks. Additionally, these products may also provide guidance to regionally based NRC inspectors who verify proper implementation of the licensee steam generator programs.

Michael J. Case, Director
Division of Engineering
Office of Nuclear Regulatory Research
U.S. Nuclear Regulatory Commission

Contents

Figures

Tables

Executive Summary

One of the main tasks in the NRC-sponsored steam generator (SG) tube integrity program (TIP-3) was to evaluate models that predict potential degradation modes of SG tubes of pressurized water reactors (PWRs). One type of degradation that occurred in SG tubes involves impurity concentration in the narrow gap between SG tubes and supporting structures or sludge piles ("crevices"). An understanding of the chemistries in these crevices is needed for models to predict potential degradation modes of SG tubes. The chemistries vary depending on the solubility, volatility, and adsorptivity of impurities in bulk water. A thermodynamic equilibrium code, such as, MULTEQ® can predict solubility-limited cases, but in the presence of volatile species, the calculations show a wide pH variation. Therefore, volatility and adsorptivity effects of impurities have been experimentally evaluated. Earlier studies have examined the kinetics of impurity concentration and resultant crevice chemistry change in a packed crevice. However, the results are limited because the crevice pH was not monitored and prototypic thermal conditions in the crevice were not achieved in most cases. The objective of this study was to evaluate crevice chemistry evolution at a given bulk chemistry of varying Na-to-Cl molar ratio (MR) as a function of packing type with an appropriate pH sensor and a test configuration that provides prototypic thermal conditions. Since the chloride is the critical species most likely affected by volatility, this study mainly focused on the effects of chloride volatility.

A model boiler (MB) system has been developed to simulate prototypic thermal hydraulics and bulk chemistry conditions of the secondary side of SGs in PWRs. For the MB system, an instrumented crevice simulator has been developed and successfully operated. A tungsten/tungsten oxide electrode was used as a pH electrode in bulk water. The pH electrode potentials showed good linearity within the pH range of 4-8 under sodium chloride (NaCl) or sodium hydroxide (NaOH) water chemistry while the pH electrode in acidic crevices appeared relatively insensitive to pH change. Two packing materials were evaluated in this work: diamond and magnetite. Diamond packed crevices are easier to instrument, but diamond powder has very high thermal conductivity as compared with magnetite, which can enhance the boiling rate and lead to an overestimate of the impurity accumulation rate in the crevice. To simulate actual SG crevices, a magnetite-packed crevice having lower permeability is more appropriate than a diamond-packed crevice.

A tightly packed crevice with magnetite powder developed a radial chemistry gradient, consistent with earlier experimental work. The crevice chemistry tends to vary actively near the tube wall because the volatility effect of Cl becomes significant at the heated tube wall where boiling occurs. Initially, the crevice pH near the tube wall appears to be alkaline. But, as the impurity concentration progresses, the crevice pH becomes neutralized and even acidic because the reduced boiling rate near the tube wall caused by the development of Na-rich liquid film results in delayed preferential Cl concentration. Based on the test results, the chemistry variation in actual SG crevice deposits near the tube wall was projected. Unless some impurities remain and accumulate in the crevice after each fuel cycle, during a typical fuel cycle, the crevice chemistry would be in a transient rather than a steady-state condition mainly because of the low bulk impurity concentration. It is likely that the volatility effect of Cl in diamond-packed crevices becomes significant as the MR decreases from 1.0. Limited data are available for magnetite-packed crevices, but it is less likely that the volatility effect of Cl will be much influenced by bulk MR variation. Since our test results suggest that the transient behavior is more important in actual SG crevice deposits, the kinetic data for the crevice chemistry evolution with low bulk impurity concentration (~1 ppm) will be helpful for estimating actual SG crevice chemistry where the predictions of thermodynamic equilibrium codes have limited applicability.

Acknowledgments

The authors thank John Oras, Jeffrey Franklin, and Chuck Vulyak for their technical support to the experimental effort; and Ken Natesan and D. R. Diercks for their management and administrative support; Denise Moores for her administrative assistance. The authors also thank James Davis, Joseph Muscara, Todd Mintz, Eric Reichelt, Kenneth Karwoski, and Margaret Stambaugh for their NRC support and program management. The authors are grateful to Allen Baum for many helpful discussions; Al Mcilree of Electric Power Research Institute for providing alloy 690 TT tubing. This work is sponsored by the Office of Nuclear Regulatory Research, U.S. Nuclear Regulatory Commission, under Job Code Y6588; Program Manager: Margaret Stambaugh.

Acronyms and Abbreviations

BPE	Boiling Point Elevation
ECP	Electrochemical Potential
IC	Ion Chromatography
ICP/OES	Inductively Coupled Plasma/Optical Emission Spectroscopy
ID	Inner Diameter
IGA	Inter-Granular Attack
ISE	Ion Selective Electrode
MA	Mill Annealed
MB	Model Boiler
MR	Molar Ratio
NRC	Nuclear Regulatory Commission
OD	Outer Diameter
PWR	Pressurized Water Reactor
SCC	Stress Corrosion Cracking (or Crack)
SG	Steam Generator
SHE	Standard Hydrogen Electrode
SS	Stainless Steel
TC	Thermocouple
TSP	Tube Support Plate
TT	Thermally Treated

Symbols

A_i	Parameter defined in Eq. (B8)
a_{H^+}	Activity of hydrogen ion
c	Impurity concentration in crevice
c_i	Molar concentration of ion species in solution
c_o	Impurity concentration in bulk solution
c_o^o	Initial impurity concentration in bulk solution
D	Steam generator tube diameter
D_p	Particle diameter
E	Cell potential
E^o	Standard cell potential
e^-	Electron
F	Faraday's constant
G_i	Parameter defined in Eq. (B8)
H^+	Hydrogen ion
H_2O	Water
h_{fg}	Heat of vaporization
K_f	Parameter defined in Eq. (B2)
k	Permeability
L	Crevice depth
M	Metal
MO	Metal oxide
$\dot{m}_i$	Mass flow rate of liquid into the crevice
$\dot{m}_o$	Mass flow rate of liquid out of the crevice
q''	Heat flux from the tube surface in the crevice
R	Universal gas constant
T	Absolute temperature
u_i	Ionic mobility
V	Total volume in crevice
V_0	Total volume of bulk water
z_i	Charge on the species
α	Fraction of wetted length in the crevice
β'	Parameter defined in Eq. (B4)
ΔT	Primary-to-secondary saturation temperature difference
ε	Porosity in crevice
γ	Liquid-vapor distribution coefficient
Γ	Mass transfer coefficient for diffusion
κ	Conductivity of electrolyte
λ_i	Ionic molar conductivity

ρ	Density of matter
ρ_f	Density of liquid in crevice
ρ_0	Density of bulk water
τ	Tortuosity

1 Introduction

Argonne National Laboratory has participated in the Steam Generator Tube Integrity Program-3 (SG TIP-3) since 2002, which is sponsored by the U.S. Nuclear Regulatory Commission (NRC). Two of the main objectives of this program are to evaluate and experimentally validate models that predict potential degradation of steam generator (SG) tubes under normal plant operating conditions and to provide data for conducting operational assessments. The prediction models use various input data: temperature, stress distribution of SG tubes, material characteristics, chemical conditions surrounding tubes, etc. Although plant programs have been effective of managing the degradation, various corrosion phenomena have been observed in an SG of a pressurized water reactor (PWR).[1] Cracking, which is a main tube degradation phenomenon occurring in operating SG tubes, is difficult to predict mainly because these input data have too much uncertainty. Some corrosion and degradation phenomena of SG tubes involve high uncertainty for the chemical conditions.

In a locally constricted geometry on the outer-diameter (OD) side of SG tubing, trace impurities in the secondary water can concentrate to extreme pH values due to boiling. If a solution containing a solute impurity boils in a flow-restricted region, the steam phase may escape more easily from that region than any remaining liquid phase. As such boiling proceeds, the impurity concentration in the remaining liquid phase dramatically increases to a degree depending on the extent of the restriction. This impurity concentration process in a flow-restricted region is sometimes called "impurity hideout." The impurity hideout raises the boiling point of the solution by lowering the vaporization pressure and can accompany an extreme chemical condition (strong caustic or acidic). This concentration process occurs mainly at three locations in SGs: the tube-to-tube support plate (TSP) crevice, the tube-to-tubesheet crevice, and the tube-to-sludge pile crevice on the top of the tubesheet. The narrow and tight gap between the SG tube and supporting structure or sludge piles is called a "crevice." To distinguish it from other types of crevices, it is often called the "heated crevice" because inside the crevice water boiling occurs by heat transfer from the primary to secondary sides of SG tubes. At locations with concentrated solutions, OD stress corrosion cracking/intergranular attack (ODSCC/IGA) may then develop. ODSCC/IGA is one of the major tube degradation modes in SGs even though there is a gap in understanding the mechanism for the degradation mode. In heated crevices, the chemical conditions are not well understood due to the complexity of crevice concentration phenomenon, which increases the uncertainty of model predictions. To reduce this uncertainty and to mitigate ODSCC/IGA in the restricted area, research aimed at gaining a basic understanding of the concentration phenomena in heated crevices has been pursued for many years.

1.1 Model Development

To better understand the impurity hideout in heated crevices, two conceptual crevice models are discussed. Mann and Castle[2] proposed an impurity hideout model based on crevice experiments with NaCl bulk water chemistry. Figure 1 shows the Mann's model of impurity hideout in a heated, loosely packed crevice. The authors proposed that impurities initially concentrate deep within the crevice (see Figure 1 A). Diffusion and convection of impurities is very slow, and continued boiling leads to a more concentrated solution (see Figure 1 B). As impurities continue to "hide out," the boundary between the dilute and the concentrated solution approaches the mouth of the crevice (see Figure 1 C). At this stage, a small increase in the amount of the accumulated impurity leads to a rapid rise in the outward transport owing to diffusion and convection; eventually, equilibrium is established. Figure 2 shows the Mann's impurity hideout model for a crevice tightly packed with corrosion product. Such a tightly packed crevice is likely to be blanketed in steam (see Figure 2 A). Since there is no liquid access to the steam-filled region, solute concentration will occur initially at the top and bottom of the steam blanket (see Figure 2

B). As impurities accumulate, concentrated solutions will penetrate into the steam-filled region by capillary attraction until the whole crevice is again full of concentrate (see Figure 2 C).

Manns's hideout model is appropriate to explain the concentration behavior of highly soluble chemicals like NaOH, but it is too simple to apply to the hideout process in operating PWR SG crevices. For example, it is difficult to apply this model to less soluble species, like phosphates or sulfates, which are present in the secondary water of SGs. Also, the model does not consider possible effects of volatile species like chlorides on crevice hideout. When boiling occurs, volatile species is distributed to steam and liquid phases so that the hideout in the liquid phase is less effective than non-volatile species, which is called "volatility effect." Chlorine anions form soluble HCl and this soluble HCl in the liquid phase should be in equilibrium with gaseous HCl in the steam phase. Therefore, as HCl is distributed more in the steam phase, the concentration of chlorine anion becomes lower. The adsorption of sulfates and chlorides to magnetite deposits also should be considered. In a tightly packed crevice, Mann's model considers only the axial chemical gradient, but the radial gradient needs to be considered to explain hideout behavior, which has been observed by Baum's experiments[3] and Albertin el al.'s examination of the crevice section of pulled tubes.[4] Albertin et al. found that in a TSP crevice the porosity was reduced immediately at the tube surface by the precipitation of bulk contaminants, and that such a low-porosity region forms in the corrosion layer associated with the TSP, leaving a central region with relatively high porosity.[4]

Baum and Evans[5] proposed an impurity hideout model in a tightly packed crevice based on Baum's experimental work and the pulled-tube examination results. This model considered the volatility effect and the radial chemistry gradient that Mann's model did not consider. Figure 3 is a schematic of the model. The crevice solutions are formed by concentrating bulk contaminants as a result of boiling at the peripheral regions of the crevice. The concentration continues until the solution precipitates or volatilizes, or until boiling terminates because of an increased solution boiling temperature. Under the latter circumstances, the concentrated solution migrates deeper into the crevice by capillary action, into regions that would otherwise be dried out.

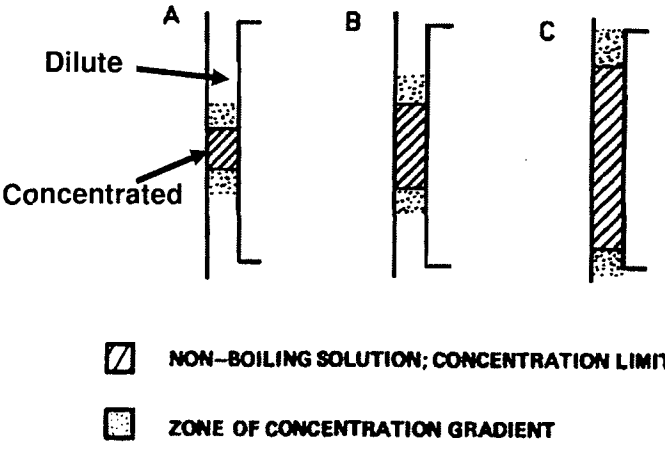

Figure 1.
Mann's model of impurity hideout in a heated, loosely packed crevice (Reprinted with permission from EPRI).[2]

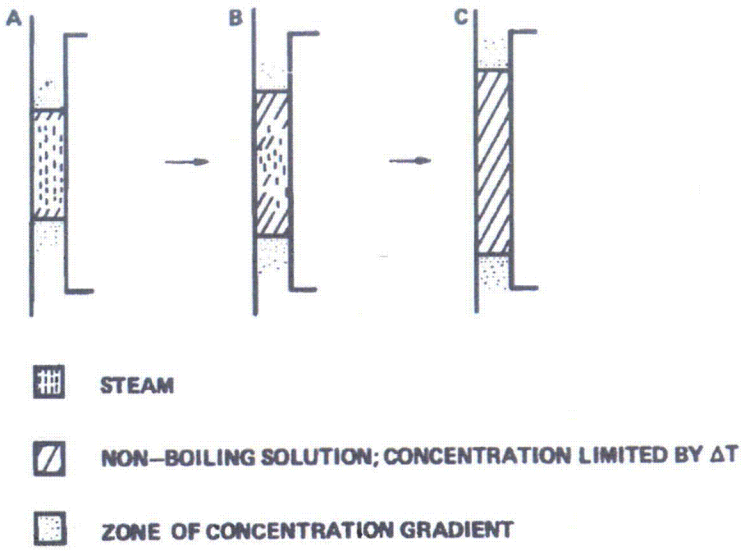

Figure 2.
Mann's model of impurity hideout in a heated, highly packed crevice (Reprinted with permission from EPRI).[2]

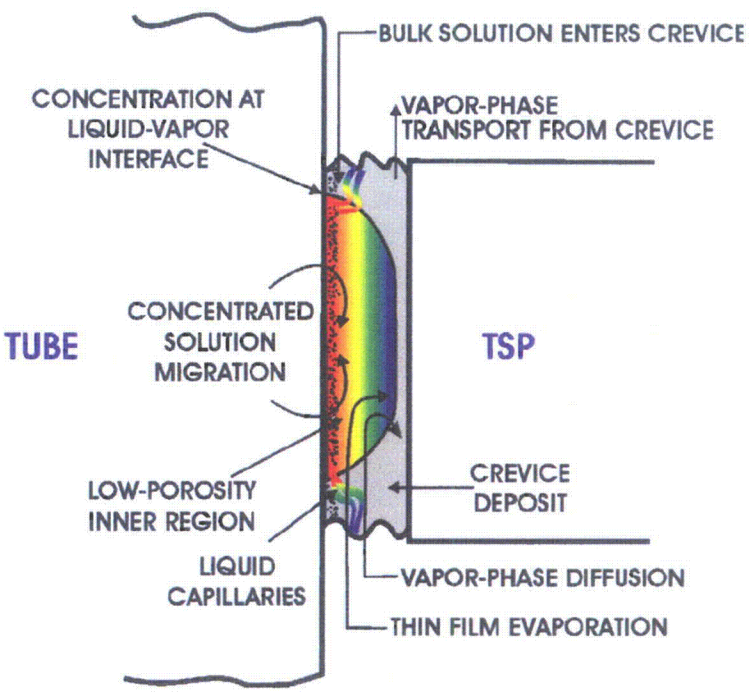

Figure 3.
Schematic showing crevice solution transport processes (Reprinted with permission from TMS).[5]

The concentrated solution near the tube wall plays an important role in tube degradation; therefore it is important to know the chemical conditions of the concentrated solution and its evolution over time. Hideout and crevice conditions depend on the solubility, volatility, and adsorptivity of bulk impurities. Thermodynamic equilibrium codes like MULTEQ® can predict solubility-limited cases, for example, the case that the impurity in the secondary water is only NaOH. In the presence of volatile species, however,

the calculation by thermodynamic equilibrium codes results in a wide pH variation because the extent of volatile species in the liquid phase depends on their concentration, the temperature, and the crevice deposit morphology. The current tools for predicting the crevice chemistry, using plant hideout return data as input, can only predict an average crevice pH. Furthermore, without a mass-balance model, the present thermodynamic equilibrium codes cannot handle adsorptivity effects. Therefore, to improve our understanding of crevice condition, the current tests would need to be updated to include the effects of both the volatility and adsorptivity of bulk impurities.

1.2 Literature Review

Much work has performed into crevice studies and they were reviewed in earlier literatures[6-8]. Some earlier work focused on thermal-hydraulic characteristics of unpacked and packed crevices and some of them evaluated chemical and electrochemical evolution. Numerical modeling including thermal-hydraulic, chemical, and electrochemical reactions has been developed. The key issues that have been pursued in earlier work but are not completely resolved yet are how much and how fast various impurities hideout can occur in packed crevices and how they determine the crevice chemistry like pH by interacting with each other and deposits.

1.2.1 Laboratory Heated Crevice Testing

Early studies into SG crevice effects were primarily focused on crevice thermal-hydraulic characteristics as reviewed by Baum[6], while studies in recent years have focused on chemical and/or electrochemical evolution in crevices. Table 1 summarizes earlier work involving laboratory-scale crevice experiments focused on crevice chemistry.

Hermer et al.[9] developed a technique to study electrochemical phenomena in crevices that simulate the TSP geometry in SGs. The electrochemical potential (ECP) was measured in a TSP crevice geometry with chemical conditions causing caustic SCC. The ECP of alloy 600 was measured versus Ag/AgCl (0.01 M KCl) reference electrodes and results indicated the formation of caustic crevice by Na hideout. Even though they tried to simulate an actual SG crevice by introducing simulated plant sludge, impurities studied in this work are limited; only Na effect was studied. Other species like chloride or sulfate should be considered to simulate actual SG crevice chemistries.

In electrochemical studies by Damien,[10] electrochemical impedance spectroscopy and potential measurements were conducted in eccentric and concentric TSP crevices that were instrumented with platinum electrodes. The electrochemical impedance spectroscopy indicated the concentration of Na and boron but it appears difficult to correlate impedance spectroscopic results with actual impurity concentration. Since the crevice was not packed with magnetite or sludge, the application of test results are limited. In our work, the electrochemical impedance spectroscopy was not used due to the calibration difficulty.

Brennenstuhl et al.[11] evaluated the electrochemical noise monitoring technique in a refreshed autoclave system for corrosion monitoring in SGs. The system arrangement was designed to simulate a magnetite-fouled SG tube/tubesheet crevice. The results showed a change in the noise activity with change in operating chemistry. The sulfate and the chloride caused alloy 800 tube materials to be anodic relative to a 410 stainless steel (SS) tubesheet, for the entire depth of the crevice, while the caustic environment resulted in the tube becoming the cathode. Exposure to the sulfate environment appeared to cause the highest level of electrochemical noise. The electrochemical noise data, however, need to be carefully interpreted because bubble agitation and boiling affect the noise signal. If the electrochemical

noise signal can be distinguished from the non-electrochemical noise, this method should be a powerful method for investigating the materials degradation under a concentrated crevice environment. Due to the prematurity of the technique, the electrochemical noise monitoring was not used in our work.

Lumsden et al.[12,13] constructed an experimental system to simulate SG thermal conditions. The system was designed such that *in situ* measurements could be made for the ECP of the tube crevice, the ECP of the free span, and the temperature profile in the crevice. The measurements were obtained for the average boiling point elevation in the crevice, the composition of the extracted crevice solutions, and the ECP of the alloy 600 tubes in the crevice and free span. After equilibrium was attained, the measured values agreed well with MULTEQ® predictions. The hideout kinetics data in this test also showed good agreement with the prediction by numerical modeling. Lumsden et al. determined the influence of the Na-to-Cl molar ratio (MR) on the ECP in the crevice for alloy 600, without a crevice pH electrode. The ECP of alloy 600 may give qualitative information on crevice pH, but an independent pH electrode, like a tungsten/tungsten oxide electrode, can monitor the crevice pH quantitatively. Only diamond powder was used as crevice packing materials in these tests. In our work, synthetic magnetite powder was used as packing materials, as well as diamond powder. The differences of two packing materials in terms of crevice hideout kinetics are experimentally shown and discussed in this report. They used an electric heater as a heating source instead of high-temperature water, which might cause non-prototypic thermal conditions inside the crevice. In our work, a test facility was designed to provide prototypic thermal conditions by introducing high-temperature water as a heating source.

Kawamura et al.[14] estimated the NaOH and H_2SO_4 concentration factor in a TSP crevice by monitoring the ECP variation of alloy 600 tubes. The ECP data clearly showed the concentration of impurities and they were converted to actual concentration data by using a calibration curve. However, the crevice was unpacked and impurity hideout behavior in unpacked crevices can be completely different from that in magnetite-packed crevices, especially for sulfuric acid because of its adsorption effect.

Kawamura and Hirano[15] estimated the sodium hydroxide concentration factor in a TSP crevice by using an *in situ* technique for high-temperature conductivity measurement. The concentration factor was about 2000 in the range of the heat flux that can establish a dry and wet condition. As reported in previous literature by the authors, the crevice was not packed with magnetite or sludge. Therefore, the application of this data is limited.

Baum[3,16] measured the temperature, impedance, and pH in a magnetite-packed TSP crevice. The experiments showed large concentration gradients between the tube and TSP sides of the crevice. The tested crevice gap size of 0.6 mm was relatively wide compared with other literature. Therefore, similar experiments having a narrower gap crevice could provide additional insights. The experiment showed that strong bases concentrated more effectively on the tube wall than strong acids because of the volatility of Cl. The crevice pH on the tube wall, when exposed to sodium and chloride mixtures, increased with increasing superheat and decreasing bulk concentration. It was proposed that Cl tends to evaporate more easily on the tube wall at larger differences between the primary and secondary saturation temperatures, ΔT. Baum also showed that sulfates were adsorbed to the magnetite particles, so that the crevice impedance and pH data did not vary significantly as the test progressed. The volatility effect of Cl and the adsorptivity of sulfate were also examined in a magnetite-packed crevice by Balakrishnan and Strati.[17]

Bahn et al.[18] measured the ECP in a tubesheet-type crevice packed with synthetic magnetite powder. They used a water loop with high flow rate as a heating source. Na concentration and resultant ECP variation with and without magnetite were compared. However, only NaOH was tested as an impurity and a pH electrode was not used.

Most of earlier studies measured the ECP of alloy 600 or Pt, but to determine the crevice pH, tungsten/tungsten oxide electrode style pH electrode was needed. Simulating prototypic thermal conditions is also an important factor, which was not achieved successfully in many cases of earlier work, for example, using an electric heater. In our work, a test facility is designed such that it provides prototypic thermal conditions in the crevice. As mentioned earlier, impurities hideout in packed crevice and their effect on the crevice chemistry are still not completely understood. Earlier work indicates that the bulk [Na]/[Cl] molar ratio may have an effect on the volatility and adsorptivity of Cl. Therefore, an examination of Na and Cl hideout behaviors in a magnetite-packed crevice by using a pH electrode under prototypic thermal conditions was conducted.

1.2.2 Crevice Numerical Modeling

A detailed model of the transport processes that produce concentrated solutions locally in PWR SGs was developed by Millett and Fenton.[19,20] The model describes the heat, mass, and momentum transfer processes that occur in porous deposits such as those found in the TSP and the tubesheet crevices and in the sludge pile on the top of the tubesheet. This model was used to predict the total amount of NaCl in the crevice solution, and the model predictions have been compared to available experimental data by Mann and Castle[2]. The model is in excellent agreement with experimental data obtained with carbon-fiber-packed crevices. However, with the given total impurity amount, this model cannot determine the crevice chemical conditions like electrochemical potential or pH because Millett's model is based on thermal-hydraulic relations and does not consider the chemical and electrochemical properties.

A new model for describing transport processes in PWR SG tube/TSP crevices has been developed by Engelhard et al.[21,22] Based on Millett's model, this model includes the influence of convective transport, diffusion, and electromigration of species in the crevice on the evolution of crevice properties. Another localized electrochemical model has been developed by Fauchon.[23] The model considers a two-phase countercurrent flow of water and steam within a porous deposit, driven by capillary forces. Convection and diffusion processes are taken into account. Several homogeneous reactions are considered as well as electrochemical reactions. The model predicts that the crevice is initially steam blanketed and slowly becomes wetted as a concentrated liquid with a higher boiling point migrates into the steam-blanketed region. Engelhardt's and Fauchon's models consider a few chemical reactions and species, including Fe^{2+}, $FeOH^{+}$, Na^{+}, Cl^{-}, H^{+}, and OH^{-}.

MULTEQ® is an interactive computer program that calculates the composition, pH, and electrochemical potential of an aqueous solution under a thermodynamic equilibrium at an elevated temperature and pressure.[24] MULTEQ® is primarily designed to be used by PWR plant chemists concerned about corrosion of SGs, but it also can be used for other applications. The code is designed to calculate the changing composition of a solution in a SG crevice or under corrosion product deposits as it undergoes concentration due to local boiling. MULTEQ® assumes that the liquid, vapor, and solid phases in the crevice are always in thermodynamic equilibrium. Since MULTEQ® is a thermodynamic equilibrium code, it cannot model realistic situations where steady state is established by two-phase flow balance or where a transient effect exists. By coupling MULTEQ® with thermal-hydraulic models and transient models, it could describe the evolution of crevice chemistry.

Table 1. Summary of earlier studies involving laboratory-scaled crevice experiments focused on the crevice chemistry measurement.

Author	Experiment	Pressure, MPa (psia)	Crevice Geometry	Packing	Heating Method	Control Method*
Hermer et al.[9]	A600 ECP measurement by using 0.01 M KCl Ag/AgCl	5.5 (800)	TSP	Sludge packed	Flowing water	ΔT
Feron[10]	Sodium & boric acid hideout with electrochemical impedance spectroscopy	6.4 (930)	TSP	Unpacked	Flowing water	ΔT
Brennenstuhl et al.[11]	Electrochemical noise measurement to monitor the effects of chemical excursions on the corrosion response of A800	5.5 (800)	Tubesheet	Magnetite packed	Electric heater	ΔT
Lumsden et al.[12,13]	NaOH & NaCl hideout studies with ECP & temperature measurement	6.4 (930)	TSP	Diamond packed	Electric heater	ΔT & q"
Kawamura et al.[14]	NaOH & sulfuric acid hideout studies with ECP measurements	5.5 (800)	TSP	Unpacked	Electric heater	q"
Kawamura et al.[15]	Na concentration factor measurement with high temperature conductivity cell	5.5-6.4 (800-930)	TSP	Unpacked	Flowing water	ΔT
Baum[3,16]	Crevice chemistry evaluation by measuring temperature, impedance, and pH difference	3.2 (468)	TSP	Magnetite packed	Flowing water	ΔT
Bahn et al.[18]	NaOH hideout studies with ECP measurements	5.5 (800)	Tubesheet	Magnetite packed	Flowing water	ΔT

* ΔT means the temperature difference between primary and secondary sides are controlled, q" means the heat flux from primary to secondary sides are controlled.

1.3 Objectives & Approach

One of the objectives of this study is to characterize the chemical conditions in a crevice for a given bulk chemistry of varying Na-to-Cl MR as a function of packing type with an appropriate pH sensor and a test configuration that provides prototypic SG thermal conditions. The generated information can then be used to evaluate the corrosion performance of SG tubing materials in isothermal autoclave-type tests and to improve modeling efforts on the degradation of SG tubes. The long-term goal is to provide the tools for quantifying volatility and adsorptivity effects on the crevice chemistry. This study focuses on the volatility effect of chloride. Of the chemical species judged to significantly affect the crevice chemistry, the chloride concentration is the most likely to be affected by volatility. The dependency of the volatility effect of Cl on the Na-to-Cl MR is also explored.

A model boiler (MB) system simulating a crevice under prototypic SG thermal conditions has been constructed for this study. The crevice is instrumented with thermocouples, ECP and pH electrodes, conductivity probes, and solution sampling lines. Bulk solution chemistry is monitored with the same instruments as used in the crevice. At first, an unpacked crevice test was performed as a reference. Then, diamond-packed crevices were tested under NaOH or NaCl bulk water chemistry. To simulate actual SG crevice conditions, magnetite-packed crevices were also tested under NaCl bulk water chemistry.

2 Experimental

2.1 Model Boiler

An MB system has been constructed at Argonne National Laboratory to simulate actual SG crevice conditions. It provides more prototypic conditions than those obtained in an isothermal autoclave or electrically heated crevice test system. The MB is designed to match prototypic conditions with regard to both the tube wall temperature and crevice heat flux. Design/operation information and shakedown test data for the MB system are presented in a previous NRC report.[25] The MB system is briefly described below.

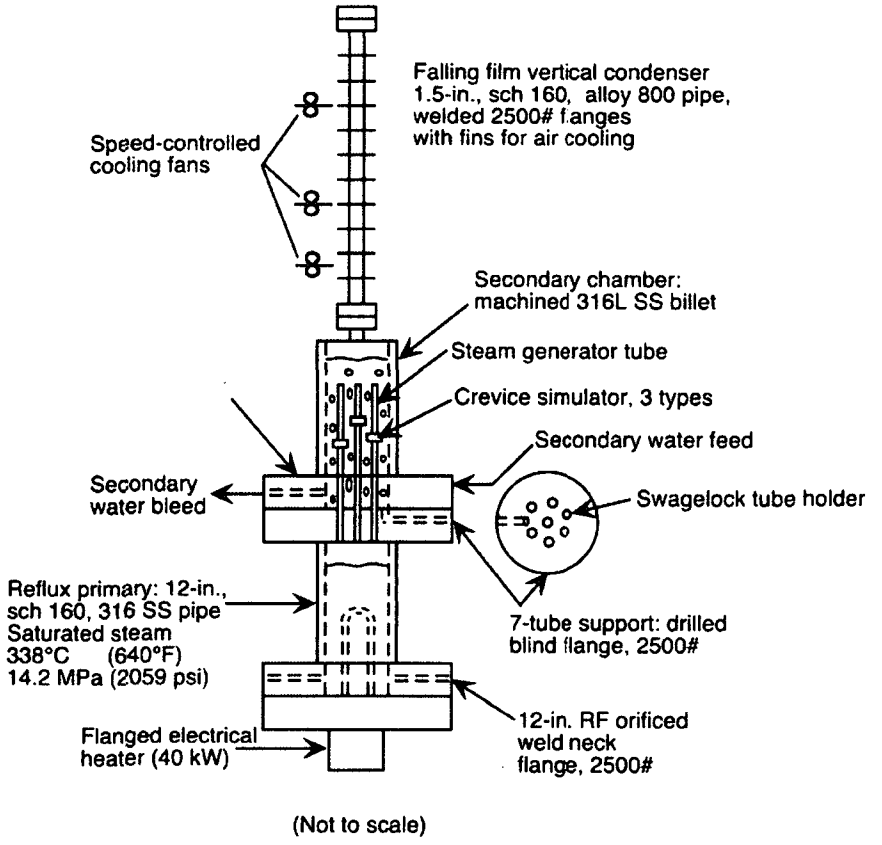

Figure 4.
Schematic of Argonne model boiler system.[25]

Figure 4 is a schematic of the MB system. The pressure vessel consists of a lower primary reflux boiler chamber, where steam is generated, and a secondary upper chamber, where boiling occurs on the outside of multiple SG tubes capped on the top and open on the bottom to the steam generated in the lower primary chamber. The MB design is simplified by introducing a static pressure vessel that is used for the secondary chamber as well as the primary chamber. The primary steam condenses on the inner walls of the tubes, creating a boundary condition of high heat flux. Primary electrical heaters (40 kW) are submerged in the primary water to provide prototypical heat fluxes. The outsides of the primary and secondary pressure vessels are surrounded by six zones of combined insulation blankets and trace electrical heaters. A thermocouple in the secondary water and a variable-speed drive fan are used to maintain the temperature and pressure on the secondary side by controlling heat rejection to the ambient air from a finned, fan-cooled steam condenser pipe. As safety features, a pressure-protection system that

uses a rupture disc is introduced in the primary and secondary chambers. The discharge lines of the rupture discs are connected to a collection tank. The MB system is surrounded by concrete protective barriers. A dedicated computer data acquisition system is used to control and monitor experimental parameters during the testing. Figure 5 shows the MB equipped with insulation and instrumentation. The discharge collection tank is located at the right side of the MB.

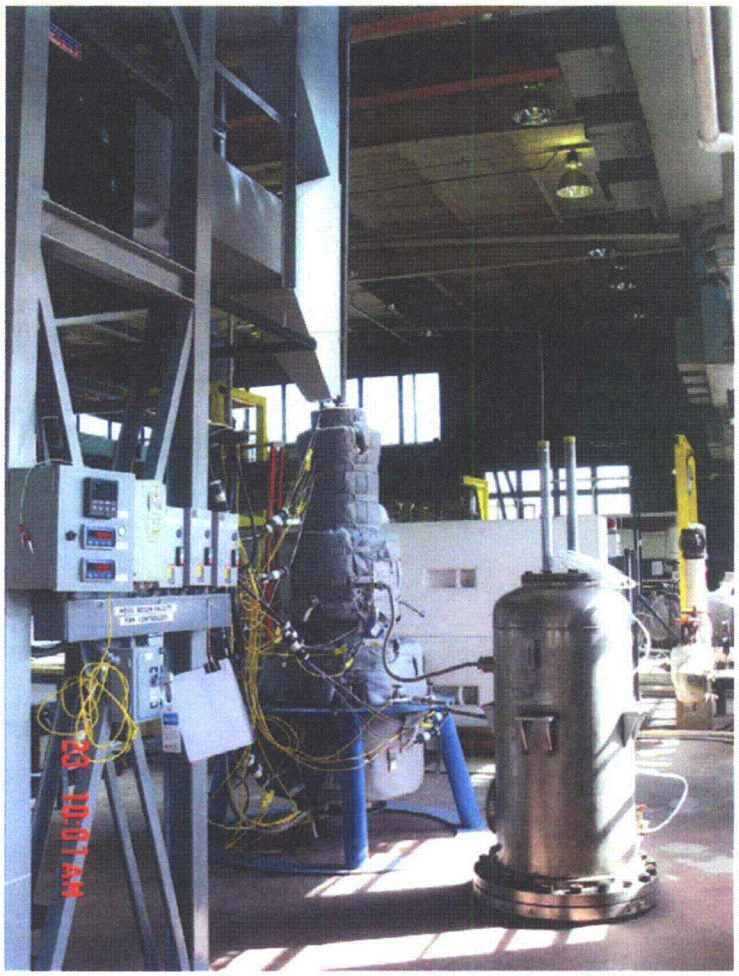

Figure 5.
Photograph showing the MB equipped with insulation and instrumentation and a discharge collection tank.

2.2 Secondary Water Control & Instrumentations

2.2.1 Water Chemistry Control

The Na-to-Cl molar ratio of the secondary test solution is controlled by mixing reagent-grade sodium chloride (NaCl) powders (Fisher Scientific, >99 % purity), concentrated hydrochloric acid (HCl) solution (Fisher Scientific, 37.4 wt%), and deionized water. In some tests, only sodium hydroxide (NaOH) powders (Fisher Scientific, 97.8 %) are used to prepare the secondary solution.

A high-pressure injector metering pump is used to control the secondary bulk water chemistry. Figure 6 shows a schematic of the injection system for the secondary bulk solution. A concentrated NaCl (or NaOH) solution is filled in a 304L SS 500-mL reservoir and deaerated with high purity Ar gas for 20-30 min before being connected to the injection line. A concentrated feed solution is delivered to the secondary chamber through a micro-bore injector tube (1/16-in. OD, 0.010-in. ID 316 SS) with the tip located at the middle of the chamber. Due to intense SG tube boiling, mixing of the secondary chamber bulk fluid is rapid and efficient. Two level sensors in the secondary chamber are used to ensure that the chamber fill level is maintained within the correct range during the pumping of new chemicals or sampling of the bulk solution. For safety, a check valve and a pressure relief valve are installed at the high pressure side of the injection pump. In addition, a manual isolation valve is installed on the injection line just before entering the MB in case the injector pump system malfunctions during a test and must be repaired. The system also has a pressure transducer for monitoring the delivery pressure and a flow meter for determining the rate of delivery. Figure 7 shows the injection pump system for controlling the bulk water chemistry in the secondary chamber. Figure 8 shows the MB high-pressure manifold access for the bulk solution feed/sampling lines in the secondary chamber, overpressure safety rupture disc, pressure transducer, and filling/drain line.

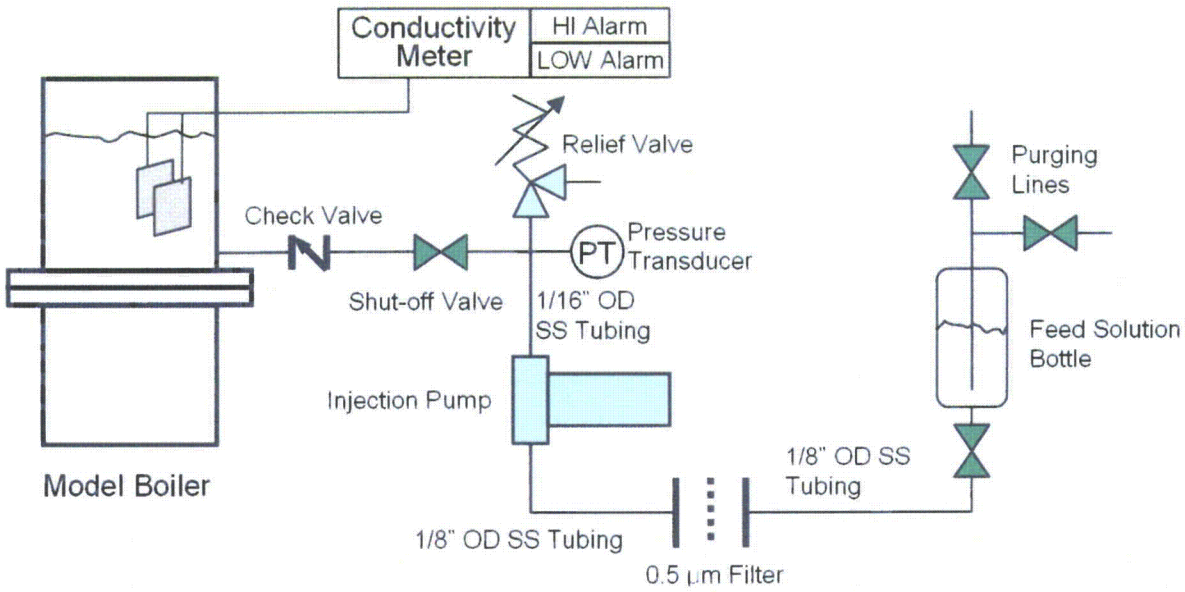

Figure 6. Schematic of injection pump system for secondary bulk solution.

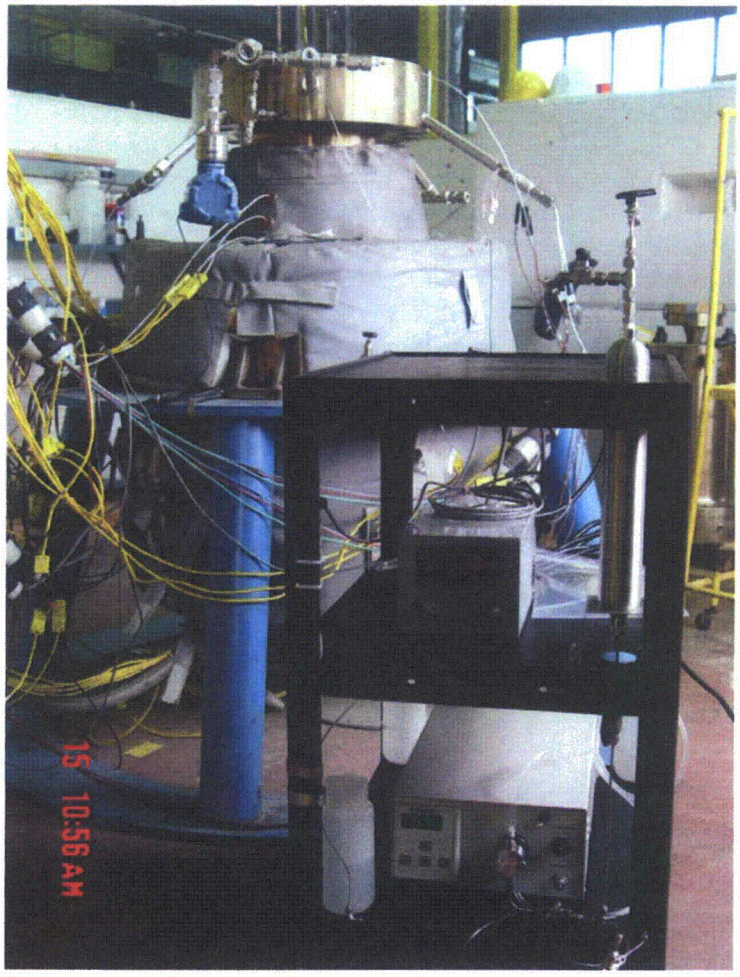

Figure 7.
Photograph of the injection pump system for controlling/changing secondary bulk water chemistry (cart on right side).

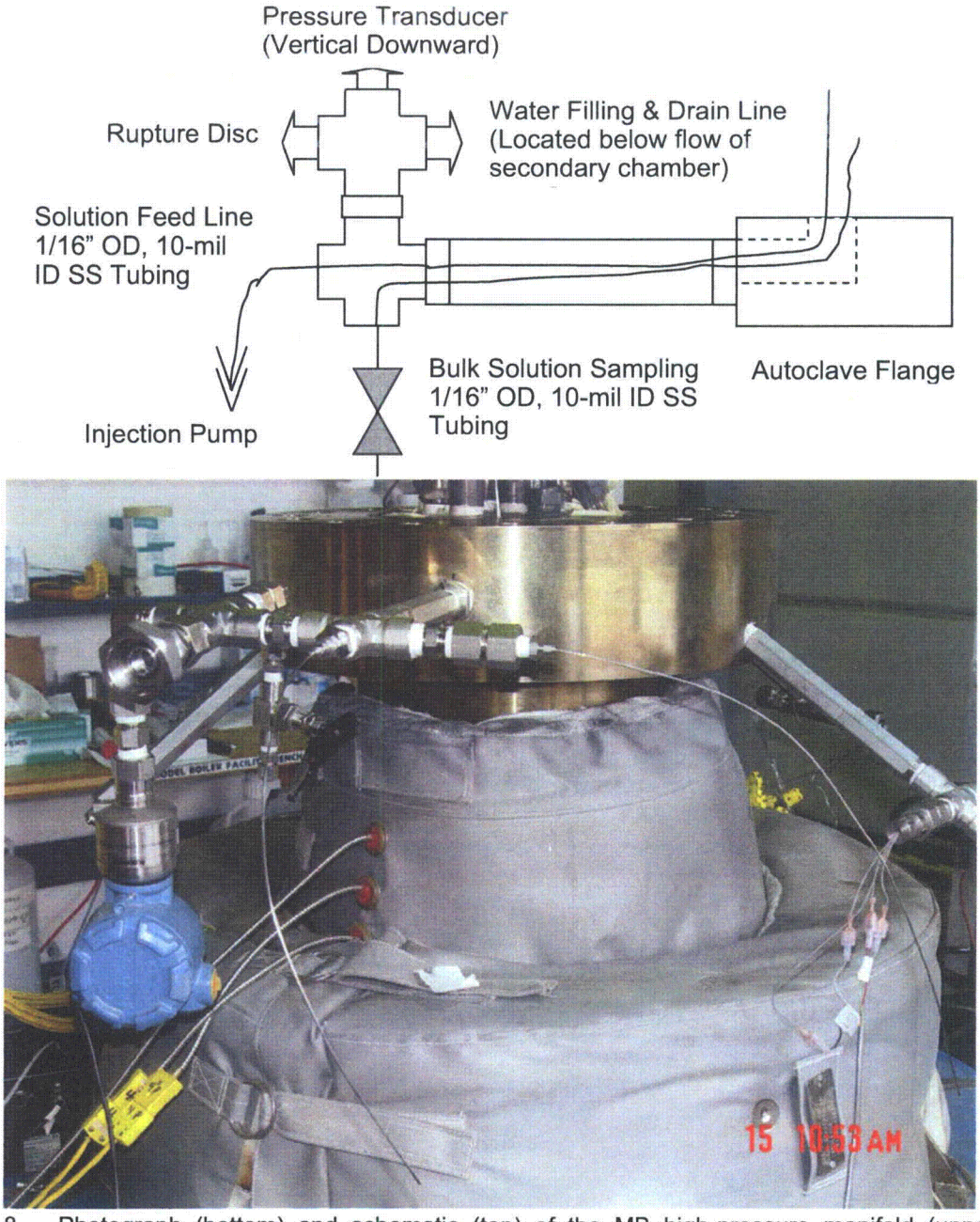

Figure 8. Photograph (bottom) and schematic (top) of the MB high-pressure manifold (upper left) access for secondary-chamber bulk-solution feed/sampling lines, overpressure safety rupture disc, pressure transducer, and filling/drain line.

2.2.2 Instrumentation

Figure 9 shows the MB internal components. To simulate SG tubes, six tubes with 7/8-in. OD are used for heat transfer, and crevice assemblies are mounted on two of them. Two on/off type level sensors are installed to monitor the secondary water level. During normal operation, the water level is located between lower and upper level sensors so that the lower one is always on and the upper one is off. If the lower level sensor indicates loss of water level, the only way to explain such loss of water level could be leaking of the secondary system. If the upper level sensor indicates high water level, that could be explained by a leak from the primary to secondary systems. Therefore, two water level sensors can also be used as a system leak indicator. To measure the bulk environment change *in situ*, various environmental parameters are monitored: temperature, ECP, pH, conductivity, and impurity concentration as determined by solution sampling.

Temperature

The secondary bulk water temperature is monitored with thermocouples located at different levels inside the secondary chamber to ensure temperature uniformity.

ECP, pH, and Conductivity

The thermodynamic stability of a metal or alloy in aqueous solution is primarily controlled by the ECP and pH of the solution. The thermodynamically stable phases of a certain metal or alloy are typically indicated on an ECP versus pH diagram. It is known that the SCC resistance of alloy 600 tubing in SGs depends on ECP and pH. In these tests, the ECPs of platinum (Pt), nickel (Ni), and alloy 600 are monitored with respect to an Ag/AgCl reference electrode. The solution pH can be monitored with various electrochemical tools. In these tests, metal-to-metal oxide electrodes are introduced. The general equation for the reduction of a metal having a charge valence number of 2, and at a certain temperature T, can be written as:

$$MO + 2H^+ + 2e^- \Leftrightarrow M + H_2O \tag{1}$$

The electric cell potential of the reaction in Eq. (1), E is described by a form of the Nernst equation for the cell:[26]

$$\begin{aligned} E &= E^o - \frac{RT}{2F}\ln\frac{a_M a_{H_2O}}{a_{MO}a_{H^+}^2} \\ &= E^o + \frac{RT}{F}\ln a_{H^+} \\ &= E^o - 2.303\frac{RT}{F}pH \end{aligned} \quad , \tag{2}$$

where R, F, and a_{H^+} represent the universal gas constant, Faraday constant, and the activity of the hydrogen ion, respectively. Based on Eq. (2), the metal-to-metal oxide electrode potential is linearly proportional to pH at a given temperature. This relationship enables us to estimate crevice and bulk pH changes from the measured electrode potentials. The slope representing the dependency of the electrode potential on pH $-2.303RT/F$ is called the "Nernstian slope," which is only dependent on temperature and is -106 mV/pH at 500°F.

Figure 10 shows the bulk ECP electrode assembly and the tip of a pressure-balanced external Ag/AgCl (0.01M KCl) reference electrode. Initially, the bulk ECP electrode assembly was composed of 20-mil (0.5-mm) diameter Pt (99.9 % purity), Ni (99.98 % purity), and two alloy 600 wires. For the later tests, tungsten (W, 0.5-mm dia, 99.95 % purity) and tantalum (Ta, 0.5-mm dia, 99.9+ % purity) wires replaced the two alloy 600 wires for monitoring the bulk pH. Figure 11 is a close-up photograph of the ECP electrode assembly and its electrode wires used for measurement of bulk water chemistry. All wires are covered with heat-shrinkable Teflon tubing for the electric insulation, except the tip length of 5 mm. Teflon is not expected to have creep issues at testing temperature of 260°C (500°F). Four Teflon-sheathed wires are assembled into a Teflon-sealed compression fitting. The Pt electrode provides oxidation/reduction potentials. The Ni and alloy 600 wires are used to measure their own ECP in the secondary test environment. The W and Ta wires are used to measure the bulk solution pH. A tungsten/tungsten oxide (W/WO_x) electrode has been studied and used as a pH electrode at room temperature[27,28] and high temperature (up to 300°C).[29] The tungsten/tungsten oxide electrode showed a Nernstian pH response within the pH range of 2 to 11 at temperatures from 200 to 300°C.[29] Based on this reported high-temperature performance, the tungsten electrode was selected as a pH electrode. The tantalum/tantalum oxide (Ta/TaO_x) electrode was introduced as a pH electrode in later tests, but the W/WO_x electrode was used as a main pH sensor. Following earlier work[29], a 0.5-mm (20-mil) dia tungsten wire was oxidized in air with a propane torch for 1-2 min. The Ta/TaO_x electrode preparation procedures are the same as for the W/WO_x electrode. White Ta oxide film is formed easily on the Ta wire tip as soon as exposed to a propane torch. A relatively thick oxide layer is formed. By comparing the results of two electrodes, we are able to evaluate if there is any problem in the W/WO_x electrode itself. The design of the external pressure-balanced Ag/AgCl (0.01 M KCl) reference electrode is based on earlier work.[30,31] The calibration curve of the reference electrode at high temperature is taken from the earlier experimental data of Macdonald et al.[30]

Electrolytic solutions obey Ohm's law accurately once the effect of the electrolysis products is eliminated by using high-frequency alternating current.[32] If direct current is applied continuously, two electrodes used for conductivity measurement become anode and cathode, respectively. Certain chemical products can be formed by oxidation and reduction reactions at each electrode surface which may affect the conductivity measurement (for example, hydrogen and oxygen for electrolysis of water). The conductivity of a solution can be composed of separate contributions from each ion; this is known as Kohlrausch's law of the independent migration of ions.[32] The conductivity of a mixture of several electrolytes is

$$\kappa = \sum_i c_i \lambda_i \,, \tag{3}$$

where c_i is the molar concentration of each ion, and the ionic molar conductivity $\lambda_i = z_i F u_i$, in which F is Faraday's constant, and z_i and u_i are charge number and ionic mobility, respectively. The ionic mobility depends on temperature, ion concentration, and each ion characteristic. Therefore, as shown in Eq. (3), the solution conductivity is dependent on concentration, temperature, and ion species in the solution.

The secondary water conductivity is monitored with Pt parallel plates. The lead wires of two parallel plates are connected to a conductivity meter (MYLON L Company, Model #: 750II). The secondary fluid conductivity probe, which is mounted near the inner wall of the secondary chamber, is shown in Figure 12. Because of its greater surface area than exposed wires, the conductivity probe has a greater sensitivity in tracking changes in bulk water chemistry. The probe was explored as a means for tracking the movement of chemicals into and out of the bulk solution, as an indirect indicator of crevice

behavior. Comparing conductivity changes in the bulk and crevices allows one to monitor the movement of chemicals from the bulk solution to the crevices.

Solution Sampling

The bulk secondary fluid is sampled by use of a micro-bore tube (1/16-in. OD, 0.010-in. ID 316 SS) with the inlet positioned at the mid-fluid level in the secondary chamber, as shown in Figure 13. At the end of the sampling tube, a micro-control valve is adjusted to sample bulk solution. The volume of the bulk samples is typically about 1000 μL, which is much larger than the dead volume of the bulk-solution sampling line of about 90 μL. The impurity concentrations of the samples are analyzed by inductively coupled plasma/optical emission spectroscopy (ICP/OES) and ion chromatography (IC) for Na and Cl, respectively. If desired, the concentrations of Fe, Ni, and Cr can also be analyzed by ICP/OES. The chemical forms of impurities in samples might change during cooling. However, since ICP/OES analyze total concentration of each element regardless of chemical forms unless impurity forms significant precipitates, total concentration of each element should be conserved even after cooling. Some samples are additionally analyzed by a Na ion selective electrode (Accumet, Model #13-620-503) and a Cl ion selective electrode (Orion: Thermo Electron Corp., Model #9617BN).

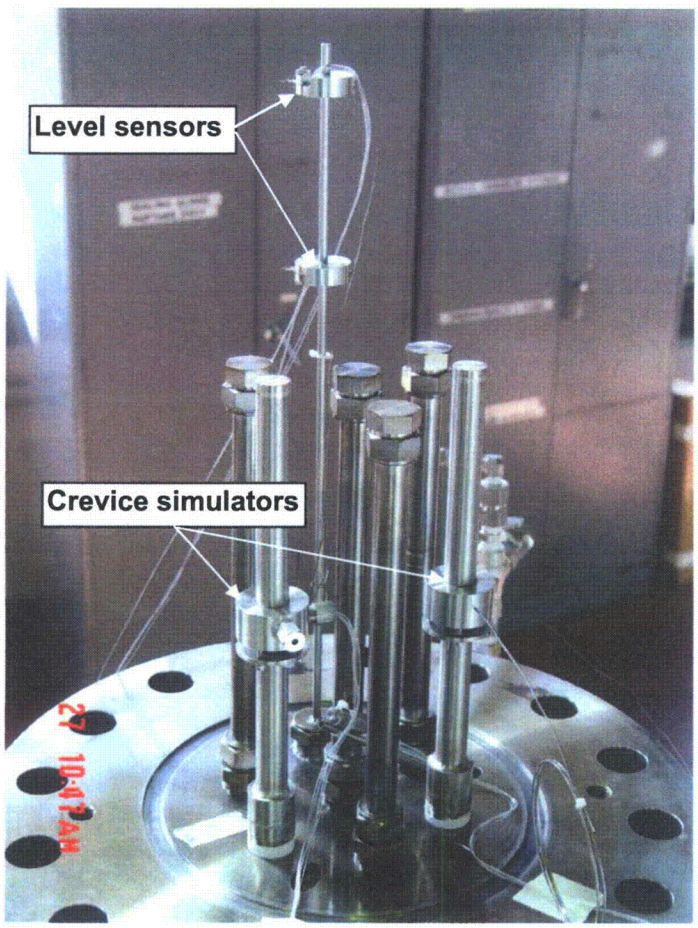

Figure 9.
Photograph of internal model boiler.

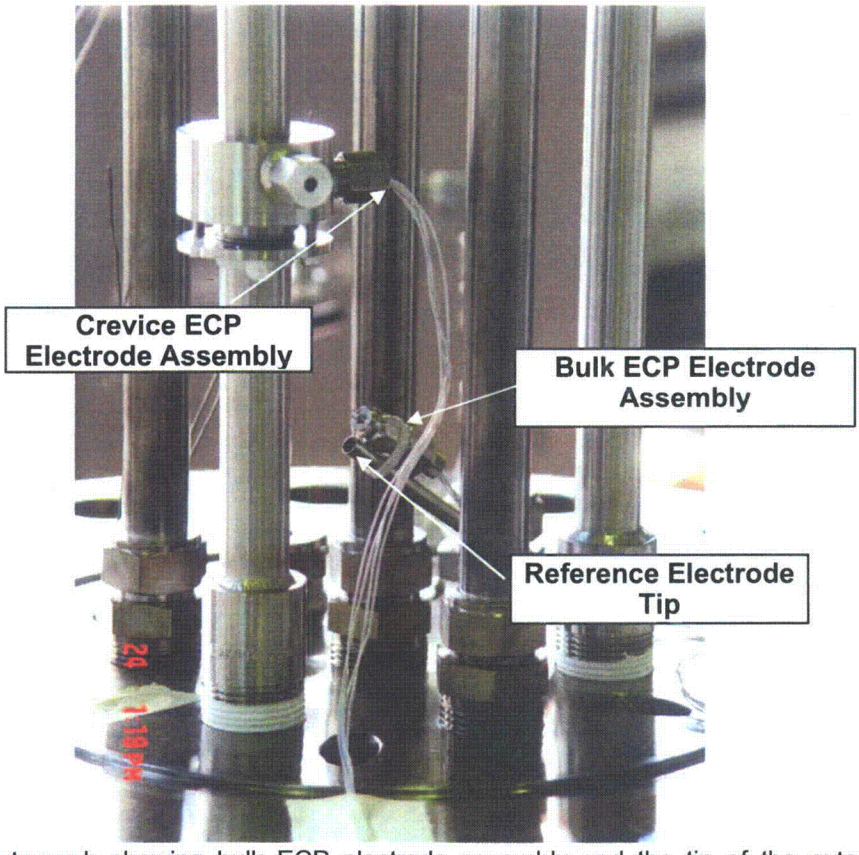

Figure 10. Photograph showing bulk ECP electrode assembly and the tip of the external pressure-balanced Ag/AgCl (0.01M KCl) reference electrode.

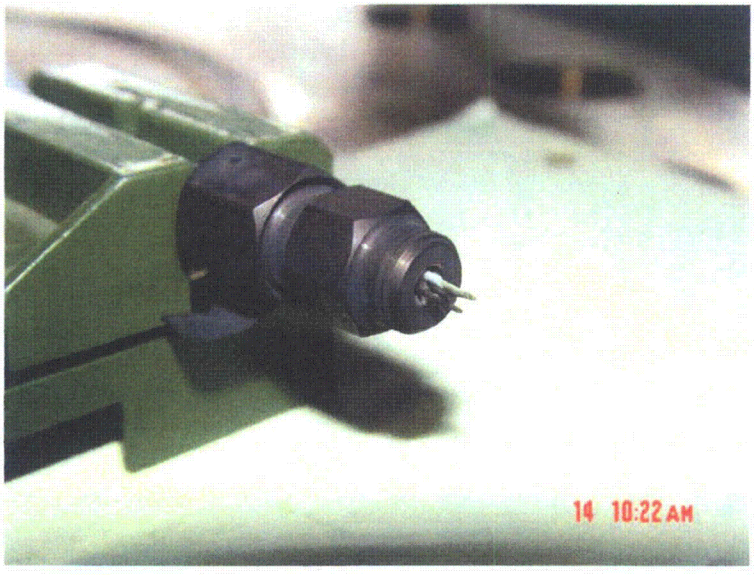

Figure 11.
Close-up photograph of an ECP electrode assembly for bulk water chemistry measurement.

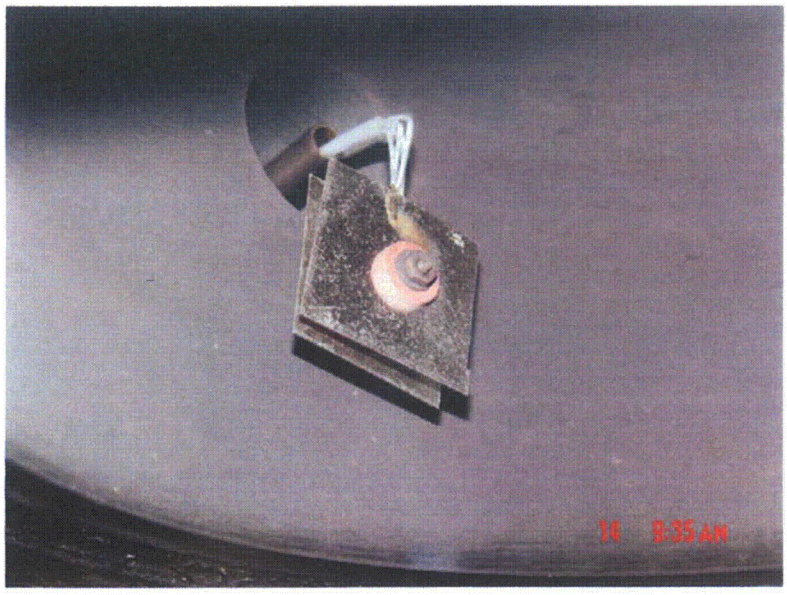

Figure 12.
Secondary chamber parallel-plate fluid conductivity probe for measuring changes in bulk water chemistry of MB.

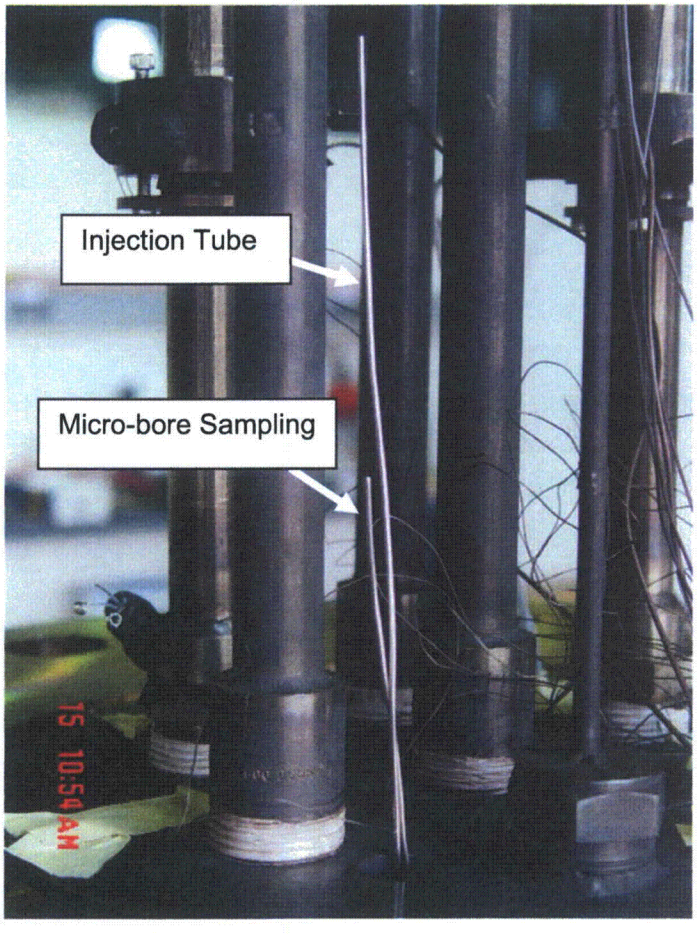

Figure 13.
Photograph of bulk secondary micro-bore sampling (shorter 1/16-in. OD tubing at center) and injection tube (longer 1/16-in. OD tubing at center).

2.3 Crevice Simulator

2.3.1 Design

The MB has two crevice simulators with radial gaps of 0.25 and 0.51 mm (10 and 20 mil). The crevice is open on the top and closed on the bottom and is nominally 7/8-in. deep. Figure 14 shows a schematic of the crevice simulator design. A crevice ring is machined so that the crevice simulator has a radial gap size of 10 or 20 mil. The crevice ring is mounted on the SG tube by a 316 SS cone ring and a 316 SS back ferrule. The SS cone ring is used to seal the bottom of the crevice and hold the simulator on the tube. It resulted in occasional SCC of the SG tubing and, along with the packing, made it difficult to remove the crevice simulator from the tube. Hence, the SS cone ring was replaced with a Teflon seal cone ring to reduce SG tube stressing and facilitate crevice simulator removal, as shown in Figure 15. Because the Teflon is not as robust in holding the simulator on the tube as the 316 SS, especially at elevated temperatures, three narrow 316 SS straps were spot welded on the simulator and extended downward onto the SG tube and welded, as shown in Figure 15. The post-test investigation confirmed the water tightness of the Teflon cone ring.

A nickel foam mesh having 43 pores/cm (110 pores/in.) is located on the top of the crevice mouth to retain the diamond or magnetite powder filling the crevice. A cover plate is placed on the top of the nickel foam mesh and tightened to the crevice simulator by three screws. Inspection of the crevices upon completing acidic tests showed that the nickel foam had been badly corroded by the acidic environment having Na-to-Cl MR of less than one. After that, a Ni-Cr-Mo alloy foam mesh was introduced because it is more inert to acidic bulk water than Ni.

To ensure concentricity of the crevice ring mounted on the SG tubes, three wire shims equally spaced around the circumference are spot welded on the top of the crevice ring. Alloy 600 tubing (Sandvik Heat No. NX8527) was mill-annealed for 3 min at 940°C.[33] Since the carbon concentration in this tubing is 0.023-0.025 wt%, this tubing can be considered to have been mill-annealed at low temperature. Generally, low-temperature mill-annealed alloy 600 has less resistance to corrosion than thermally treated (TT) alloy 600. The alloy 600 SG tubes were replaced with 7/8-in. OD alloy 690 TT (Sumitomo Metal Industries, Heat No. D1A1801) because post-test investigations revealed that the alloy 600 tube surfaces were gouged and cracks were developed in the crevice region. Alloy 690 TT is usually known to be more corrosion resistant than mill-annealed alloy 600.

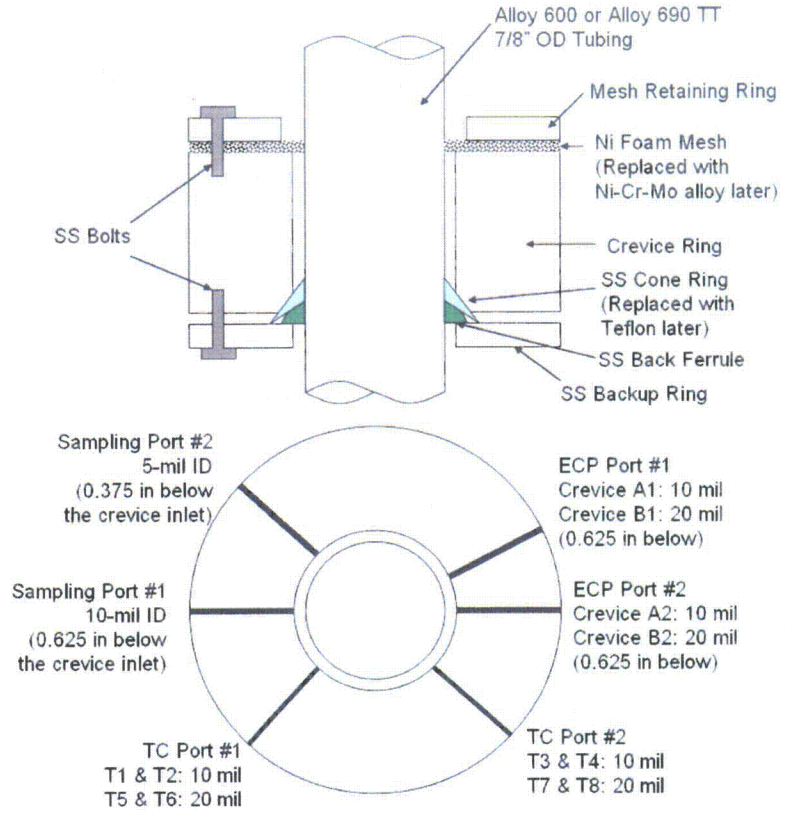

Figure 14.
Schematic of crevice simulator design.

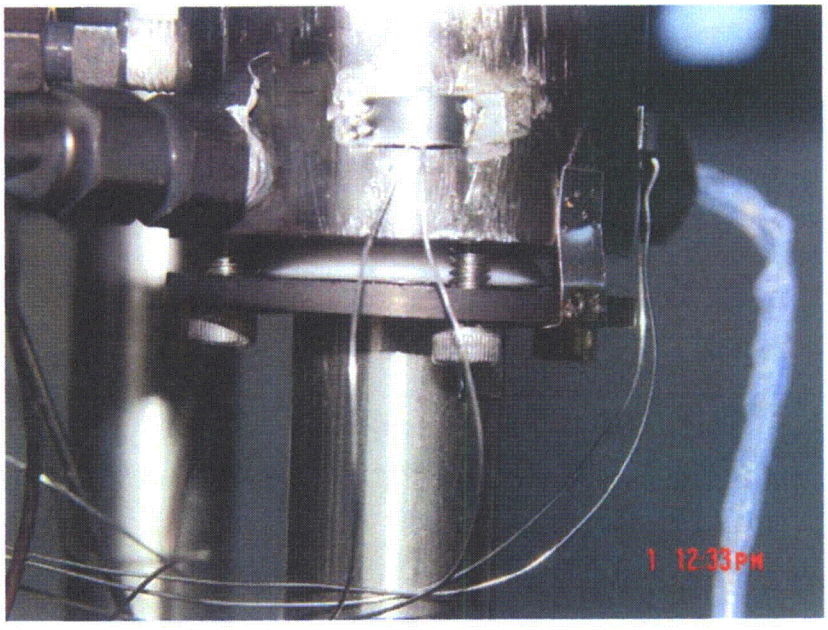

Figure 15.
Close-up of 10-mil gap crevice showing new Teflon seal ring on bottom of crevice to reduce SG tube stressing and facilitate crevice removal.

2.3.2 Instrumentation

To measure the crevice environment change *in situ*, various environmental parameters are monitored: temperature, ECP, pH, conductivity, and impurity concentration as determined by solution sampling. Figure 16 shows the crevice simulator with various instrumentation ports. Figure 17 shows a fully assembled crevice simulator having two ECP electrode assemblies, thermocouples, and sampling lines.

Temperature

Each crevice simulator has four radial ports for crevice thermocouples, which are located at two circumferential locations, 90 degrees apart, as shown in Figure 16. The top and the bottom thermocouples are located 0.442-in. and 0.567-in. below the crevice inlet, respectively. The radial position of the thermocouples is adjusted to be at the mid-radial gap. As shown in Figure 16, thermocouples in the 10-mil gap crevice simulator are named T1, T2, T3, and T4. In the 20-mil gap crevice simulator, thermocouples located at the same positions as those of the 10-mil gap crevice simulator are named T5, T6, T7, and T8, respectively. However, since post-test examination revealed that crevice thermocouples have slipped during the test, high-pressure fittings were welded outside of the crevice ring, and the thermocouples were swaged and fixed by soft Teflon ferrules to prevent the thermocouple slippage. Only two thermocouples were installed through the radial holes in the crevice ring; T2 and T4 are located 0.57-in. below the crevice top opening. Due to the welded fittings, the radial holes for T1 and T3 were not available. In some tests, one more thermocouple was installed touching the tube wall labeled "TW." This thermocouple is not shown in Figure 14 but it is located at the opposite direction of 'TC port #1.' In later tests a 20-mil OD thermocouple sheathed with alloy 600 was introduced as the crevice electrode assembly to measure the electrode tip temperature.

The measured crevice solution temperature can be related to the concentration of impurities in the crevice if the identity of the impurities is known. The boiling point of a solution elevates as the concentration of impurities increases at constant pressure.[6] If the solution is dilute in all solutes, the crevice impurity concentration is linearly proportional to the temperature difference between the measured and bulk saturation temperature, i.e. the boiling point elevation (BPE). The proportionality constant of each species depends on temperature and concentration. The BPE as a function of impurity concentrations can be predicted by MULTEQ.

ECP, pH, and Conductivity

Each crevice has two ECP ports, but in some tests only one ECP port is used. The ports are located at the same elevation in the crevice but are separated by 30 degrees. The ECP port is located 0.625-in. below the crevice inlet, which is the lowest level that facilitates the welding of a compression fitting. The crevice ECP electrode assembly is composed of four 20-mil dia wires. Initially, like the bulk ECP electrode assembly, Pt, Ni, and alloy 600 wires are used, but later W and Ta wires replaced alloy 600 wires as pH electrodes. Like the bulk ECP electrode assembly, all wires are covered with heat-shrinkable Teflon tubing for electric insulation, except the tip length of 1-2 mm. Four Teflon-sheathed wires are assembled into a Teflon-sealed compression fitting. The preparation procedures for W/WO_x and Ta/TaO_x electrodes are the same as those of the bulk ECP electrode assembly, described in Section 2.2.2. For ECP measurements, an electrochemical interface system (Solartron 1287) and a multiplexer with 8 channels (Solartron 1281) are used. Platinum and alloy 600 wires are connected to a crevice conductivity meter (MYLON L Company, Model #750 II). In some tests, two alloy 600 wires are used as the crevice

conductivity probes. As discussed before, one alloy 600-sheathed thermocouple is installed in a crevice ECP electrode assembly, which is used to act as an alloy 600 electrode.

Sampling

There are two sampling lines for the crevice solution: 5- and 10-mil inner dia (ID) 316 SS tubes. The two sampling lines are located 0.375- and 0.625-in. below the crevice inlet, respectively. In most tests, the 10-mil dia sampling line was used for the crevice solution extraction because the 5-mil dia sampling line was clogged. Both crevices have the micro-bore solution extraction lines with a micro-bleed valve used to meter the samples on a two- or three-drop basis, which is roughly varied at 40-90 μL. The crevice sampling frequency is varied over time. In earlier tests, the crevice solution was extracted once or twice a day for analysis. However, after crevice sample analysis showed a time-delay effect due to the dead volume of the sampling lines, the crevice samples were taken only before changing the temperature. Since the dead volume of the solution sampling line, 90 μL, is comparable to the crevice sample's volume, a crevice sample taken at a certain time does not really represent the actual crevice chemistry at the sampling time. Instead, it represents the crevice chemistry at the previous sampling time. Crevice sample analysis should be analyzed considering this time-delay effect.

The samples were analyzed by ICP/OES and IC for Na and Cl concentrations, respectively. Like bulk samples, Fe, Ni, and Cr concentrations were also analyzed, if desired, by ICP/OES. To prevent the diamond or magnetite powders from plugging the entrances of the sampling tubes, an SS porous frit disc is mounted on the entrance of each of the sampling tubes, as shown in Figure 18.

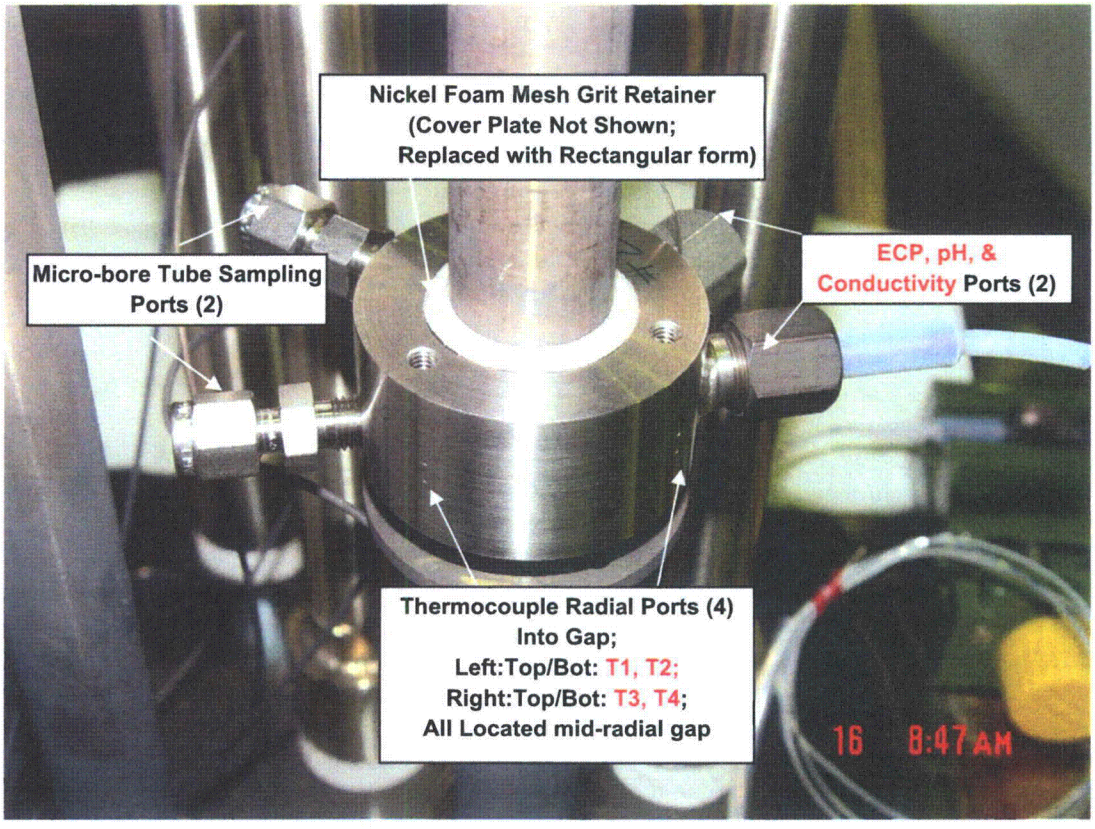

Figure 16. Photograph of 10-mil gap crevice simulator showing various instrumentation ports.

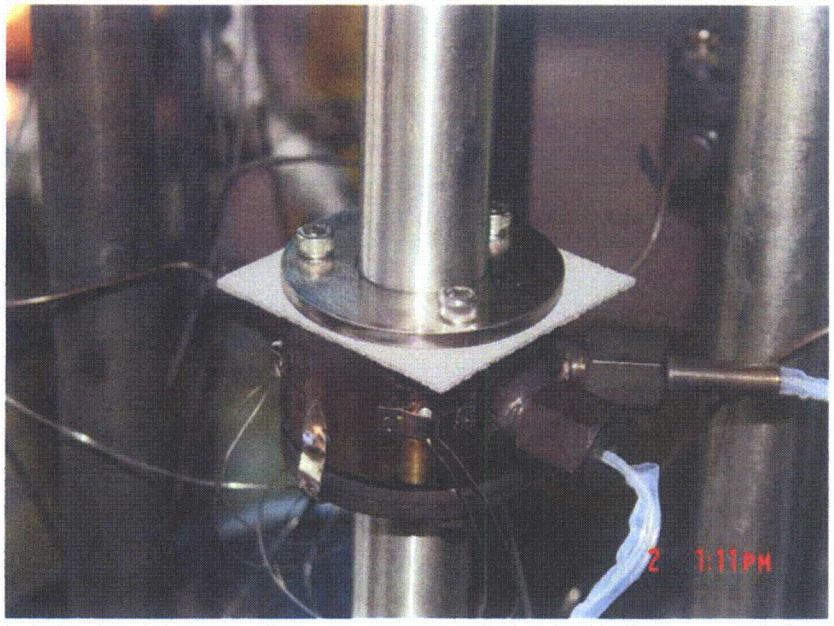

Figure 17.
Assembled diamond-packed crevice with 0.010-in. radial gap. Photograph shows two ECP electrode probes (right), four installed mid-crevice gap thermocouples, and Ni-Cr-Mo alloy porous foam mesh for retaining packing.

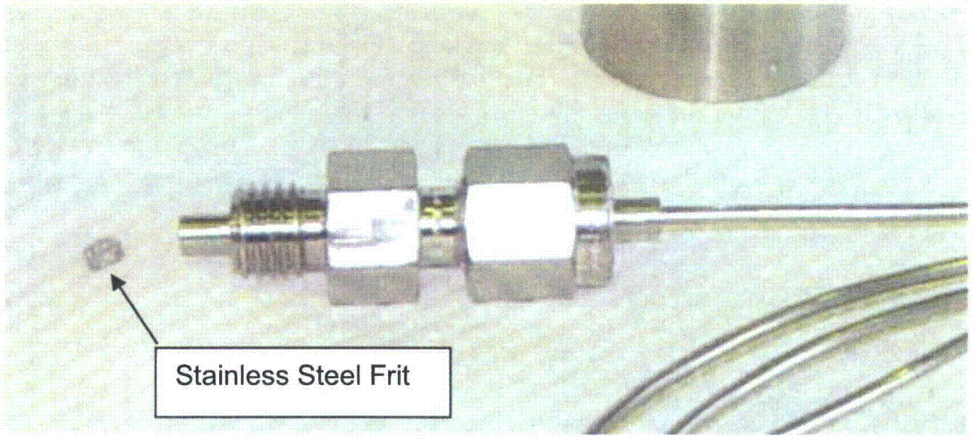

Figure 18. Micro-bore crevice sampling tube assembly and SS frit used to prevent plugging of the tube.

2.3.3 Packing Materials

As packing materials, synthetic diamond powders are introduced first. Diamond is known to be chemically inert even at acidic or caustic environments, and this means diamond itself will not react with the crevice chemistry. Since the effect of packing materials on the crevice chemistry can be excluded, chemically inert diamond is a convenient packing material. However, since magnetite is known as the main deposit in actual SG crevices of nuclear power plants, magnetite powders are also used in later tests. Table 2 shows the thermal conductivity and density of diamond and magnetite. As compared with magnetite, diamond has around 600 times higher thermal conductivity at room temperature, which may drastically change the heat transfer characteristics in a packed crevice. The test results with diamond powder should be carefully evaluated by considering the higher thermal conductivity of diamond compared with magnetite.

Table 2. Physical properties of diamond and magnetite at room temperature and high temperature.[34]

Properties	Diamond		Magnetite	
	27 °C	127 °C	Room Temp.	260 °C (500 °F)
Thermal Conductivity (W/m-K)	2320 (IIA)	1540 (IIA)	3.8[35]	3.5[35]
Density (10^3 kg/m^3)	3.51	-	5.17	-

Some crevices were packed with diamond grit ranging in size from 127 to 165 μm (Diamond Innovations, Model #MBG-660). To increase packing density, two sizes of diamond powders were used: 127-165 μm and 75-97 μm. However, no significant change in packing density was observed. Packing density which is inversely related to porosity for each crevice was estimated from the weight of the diamond powder used and the estimated total crevice volume. The highest packing density possible for filling space by stacking equal-sized hard spheres is 74 % regardless of the diameter of the sphere.[36] The measured values were close to the ideal packing density, considering that the diamond powders are non-spherical and vary in size. In one test, the crevice porosity was significantly lower than other tests. The post-test investigation revealed that one idle ECP port had not been completely plugged, and this condition created an unexpected crevice volume. In some tests, the crevices were packed with magnetite (Fe_3O_4) powder (Alfa Aesar, 99.997 % purity). Even though fine magnetite particles were used as packing materials and were expected to provide tight packing, the measured packing porosity was very high in the first use. In the next magnetite-packed crevice test, a highly packed crevice was achieved by pushing down powders with a thin metal plate shim. The magnetite is not inert to the hideout chemicals like diamond. It can become involved in chemical reactions, but this represents more realistic crevice environments than diamond-packed crevices. Figure 19 shows the top of a crevice ring packed with diamond powder. It also shows three equally spaced wire shims, the micro-bore sampling tubes, the thermocouples, and the ECP electrode assembly port. Figure 20 shows the top of a crevice ring packed with magnetite powders. The introduction of magnetite allows an initial assessment of the influence of the two types of packing on hideout.

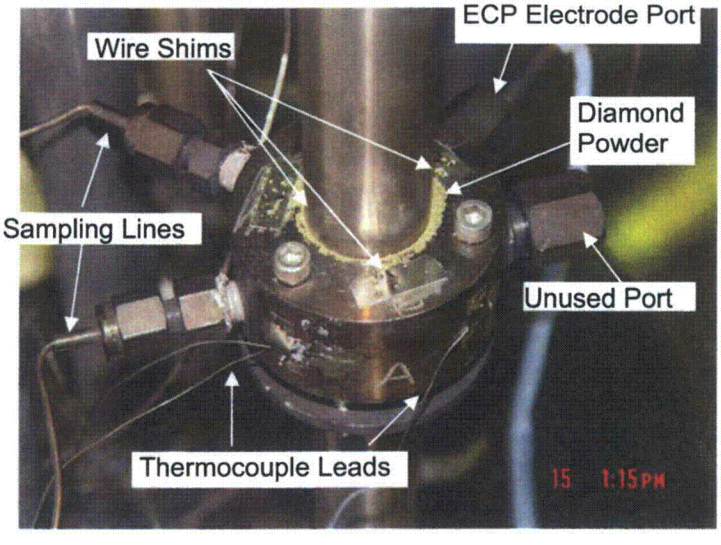

Figure 19.
Photograph of crevice A (0.010-in. radial gap) showing diamond grit packing, three equally spaced wire shims, two micro-bore sampling lines, ECP electrodes connections, thermocouple leads, and an unused crevice port (right).

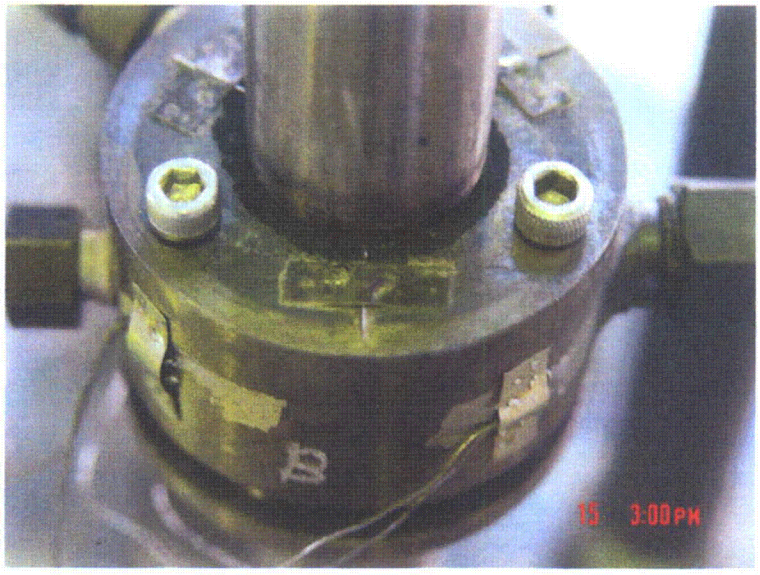

Figure 20.
Photograph of crevice B (0.020-in. radial gap) showing magnetite packing and equally spaced wire shims.

2.4 Test Procedures

The secondary chamber was closed and cleaned by flushing it with pure water several times until the effluent had conductivity < 1 μS/cm. Then, the secondary chamber was loaded with 39 lb (17.7 L at room temperature) of high purity water and began heat-up to the desired initial primary/secondary test temperatures, for example, 282/260°C (540/500°F). During the heat-up, when the MB primary and secondary chambers reached 149°C (300°F), non-condensables were purged from each chamber by venting steam. The heating was then continued to the desired temperatures. Between test inspections we discovered that the SG tube initially built with a Swagelok fitting on its upper end for filling the primary heater chamber and also for purging non-condensable gases during test startup would not seal tightly. This SG tube was replaced with a tube having a welded cap into which was welded a high-pressure SS tube for bleeding gases from the primary chamber. The bleed tube exits from the pressure vessel for purging primary non-condensable gases during the start of a test without having to open the secondary chamber. Figure 21 shows the primary chamber bleed line and valve exiting from the pressure vessel. Figure 21 also shows two high-pressure fitting ports used for two crevice ECP electrode assemblies. This arrangement has greatly facilitated the bleed/gas-purge operation and also allows monitoring of the purging process of the non-condensable gases in the primary-side water. The valve on the bleed line was opened with the primary chamber heated to 149°C (300°F). The flow rate through the bleed line was slow and steam was cooled easily to the ambient temperature so that no steam reached the tube at the exit. Thus only water or air exited the tube. At the early stages of non-condensable gas purge from the primary chamber with the tube immersed in a beaker of water, mainly air bubbles purged. Later in the purge no air bubbles were evident, and the purging was complete.

The temperature of the MB secondary chamber for all tests was kept at 260°C (500°F), while the primary-side temperature was varied from 282°C (540°F) to 327°C (620°F). In earlier tests, the primary-to-secondary temperature difference, ΔT was 100 or 120°F but in later tests, three ΔT conditions (40, 60, and 80°F) were used. For each test, reference data were generated for the primary/secondary temperatures of 540/500°F with only high purity water in the secondary chamber. The generated reference data allowed us to compare crevice thermal distributions for the case of no hideout with that for hideout after a chemical was added, as well as for a packed and unpacked crevice. After achieving steady state and obtaining the pure water data, we injected a solution with impurities into the secondary chamber using a

high-pressure metering pump. Changes in crevice temperatures and secondary bulk and crevice chemistry conditions were tracked by ECP electrodes and micro-bore sampling lines as hideout occurred. In earlier tests where the high-pressure metering pump was not used, a chemically adjusted secondary test solution was injected by a pump before heat-up. For each test we allowed several days for the crevices and bulk solution to adjust and allowed hideout to develop in response to the temperature or chemical changes. Sometimes, after crevice and bulk thermal and chemical stability were achieved, the solution on the secondary side was altered to match the initial test conditions and assess its influence on crevice behavior.

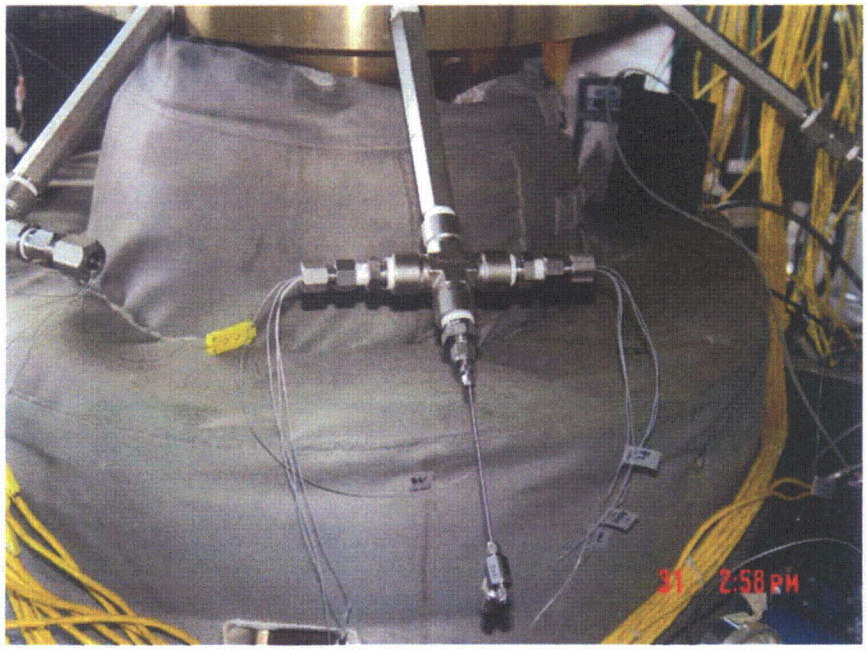

Figure 21.
Primary chamber bleed line and valve which exits the pressure vessel and purges primary non-condensable gases.

2.5 Test Matrix

In the initial crevice tests, reference data were obtained for unpacked conditions with NaOH bulk water chemistry. Then, packed crevice tests were conducted. Table 3 shows the test matrix of the MB tests with packed crevices, which is listed chronologically. Each test has its own ID, as shown in Table 3. For simplicity of the bulk water chemistry, NaOH solution was introduced first (NaOH-01 and NaOH-02). Two diamond-packed crevices were installed and tested simultaneously. The NaOH tests were followed by the tests with NaCl bulk water chemistry having an MR of 1.0 (NaCl-01 and NaCl-02). To evaluate the effect of MR on the crevice hideout behavior, the bulk solution's MR was changed from 1.0 to 0.3 (NaCl-03) and then 0.7 (NaCl-04). Packing materials were not changed between the NaCl-03 and the NaCl-04 but the secondary system was flushed with high purity water. When lowering the bulk MR, the larger gap crevice was packed with magnetite powders. The pH electrodes at the crevice and bulk and a crevice conductivity probe were introduced from the NaCl-03 test. The crevice hideout tests with two crevices provided a large amount of data in a short time, but it was difficult to analyze the partition of the bulk impurity hideouts between each crevice. Therefore, to simplify the test conditions and maximize the use of bulk solution data for the evaluation of crevice chemistry, a single crevice was introduced instead of double crevices. Another NaOH test, NaOH-03, was conducted before the single-crevice tests with NaCl bulk water chemistry (NaCl-05 and NaCl-06) in order to confirm the functionality of the crevice instrumentation under relatively simple bulk water chemistry. Then, the effect of packing materials on the

crevice hideout was explored in NaCl-05 and -06 tests. As shown in Table 3, for each crevice test, ΔT stays constant or varies stepwise. The minimum and the maximum ΔT are 40°F and 120°F, respectively. The actual ΔT at normal operating SG conditions is plant-specific but would be close to 60°F.

Table 3. Test matrix of MB tests with packed crevice conditions.

Test ID	Bulk Water Chemistry	ΔT Variation (°F)	Measuring Parameters	Crevice A (10-mil)		Crevice B (20-mil)	
				Packing Materials	Porosity	Packing Materials	Porosity
NaOH-01	20 ppm NaOH	100	Sampling, Temperature	Diamond	30 %	Diamond	30 %
NaOH-02	20 ppm NaOH	100	Sampling, Temperature	Diamond	40 %	Diamond	29 %
NaCl-01	10 ppm Cl (MR=1.0)	100→120	Sampling, Temperature, Bulk Conductivity	Diamond	3 %[a)]	Diamond	32 %
NaCl-02[b)]	10 ppm Cl (MR=1.0)	100 →60 →80 →40	Sampling, Temperature, Bulk Conductivity, ECP	Diamond	3 %[a)]	Diamond	32 %
NaCl-03	10 ppm Cl (MR=0.3)	40 →60 →80 →40	Sampling, Temperature, Bulk & Crevice Conductivity, ECP, pH	Diamond	33 %	Magnetite	78 %
NaCl-04[c)]	10 ppm Cl (MR=0.7)	40 →60 →80 →60 →40	Sampling, Temperature, Bulk & Crevice Conductivity, ECP, pH	Diamond	33 %	Magnetite	78 %
NaOH-03	20 ppm NaOH	40 →60 → 100	Sampling, Temperature, Bulk & Crevice Conductivity, ECP, pH	Diamond	35 %	Open	100 %
NaCl-05	10 ppm Cl (MR=0.7)	40 →60 →80 →50 →40	Sampling, Temperature, Bulk & Crevice Conductivity, ECP, pH	Diamond	40 %	Crevice Ring Removed	N/A
NaCl-06	10 ppm Cl (MR=0.7)	40 →60 →80	Sampling, Temperature, Bulk & Crevice Conductivity, ECP, pH	Magnetite	54 %	Crevice Ring Removed	N/A

a) Since one idle electrode port was not completely plugged, actual crevice porosity should be higher than this value.
b) This test was continued after NaCl-01 without opening the MB.
c) This test was continued after NaCl-03 without opening the MB.

3. Preliminary Crevice Tests

3.1 Unpacked Crevice Tests

Unpacked crevice hideout tests were conducted as a reference. The tests were performed on three unpacked crevice simulators having a closed bottom and open top and drilled symmetric holes and having 0.25-, 0.38- and 0.51-mm (0.010-, 0.015-, and 0.020-in.) radial gaps. In later tests the crevice having a 0.38-mm radial gap was not used any more. The primary bulk temperature was 316°C (600°F) but, in one test, it was increased to 329°C (625°F) to examine the effect of the primary-to-secondary temperature difference. The secondary bulk temperature was maintained at 260°C (500°F). The depth of the crevices was nominally 21.6 mm (0.85 in.). The secondary chamber was filled with 11.5 ppm Na solution (20 ppm as NaOH) having a conductivity of 113.8 μS/cm at 22.1°C (71.8°F).

Crevice hideout was determined from samples drawn periodically by using micro-bore sampling tubes. The micro-bore-extracted fluid samples from the crevices were analyzed by ICP/OES. Concentration factors are plotted as a function of time in Figures 22 and 23 for most of the tests. The concentration factor was defined by the crevice-to-bulk Na concentration ratio. The hideout concentration for these crevices varies with time, gap size, and ΔT, and the maximum concentration factor was around 30. The largest concentration occurred for the smallest radial gap crevice of 0.25 mm (0.010 in.) in a test with ΔT=56°C (100°F). This test was repeated as a check on experimental reproducibility, and similar concentration behavior was obtained, as shown in Figures 22 and 23. When the smallest gap crevice was tested under ΔT=69°C (125°F), the concentration factor was only 3. The maximum concentration factors were 3.6 and 7 for the 0.5- and 0.38-mm (0.020- and 0.015-in.) radial gap crevices under the 56°C (100°F) temperature difference, respectively. For all tests, a steady-state crevice concentration buildup was reached within 2-3 days. The smallest gap crevice of 0.25 mm (0.010 in.) exhibited the highest concentration, which is compatible with greater flow resistance in the smaller crevice gap that retards the boiling-induced expulsion and ingress of fluid. For some crevice gaps smaller than the current tested sizes, the flow resistance to boiling-induced fluid expulsion out of the crevice and ingress of bulk refreshing liquid will increase to a level that is conducive to higher hideout.

The crevice thermocouples for these tests showed no increase of superheat in the crevice. The crevice temperature elevation from the secondary bulk temperature of 260°C (500°F) was within 0.28°C (0.5°F), which suggests no significant Na hideout in the crevice. This observation is also supported by the very low Na concentration observed in the crevice samples. No significant large-amplitude oscillations in crevice temperature were detected. These observations imply that, for the range of geometries and thermal conditions tested, the crevices do not undergo intermittent periods of steam blanketing that would cause transient hot spots. Thus, for these unpacked crevices, the mixing between crevice and bulk appears to be so active that significant hideout does not occur, and the hideout is kinetically limited. The boiling occurring in the crevices, which creates an expulsion and ingress of fresh bulk fluid, is robust enough to limit hideout. The 0.25-mm (10-mil) gap crevice also shows that merely increasing ΔT, in this case from 56 to 69°C (100 to 125°F), does not necessarily increase hideout. Our data showed the concentration factor to be reduced from 30 to 3. The liquid penetration depth, i.e., how deep the liquid phase can penetrate into a heated crevice, decreases with the increase of heat flux or ΔT. Because of higher ΔT and resultant shorter liquid penetration depth, the area around the sampling line in the crevice became a steam-dominant region. The sampling solution picked up more steam rather than concentrated liquid. If crevices are not filled with deposits and the gap size is larger than 0.25-mm (10 mil), the impurity hideout in the crevice can be limited. However, in actual SGs, crevices tend to be packed with magnetite and less

soluble precipitates, except for new SGs. Crevice hideout studies with packed crevices will permit evaluating and estimating the actual crevice conditions in SGs.

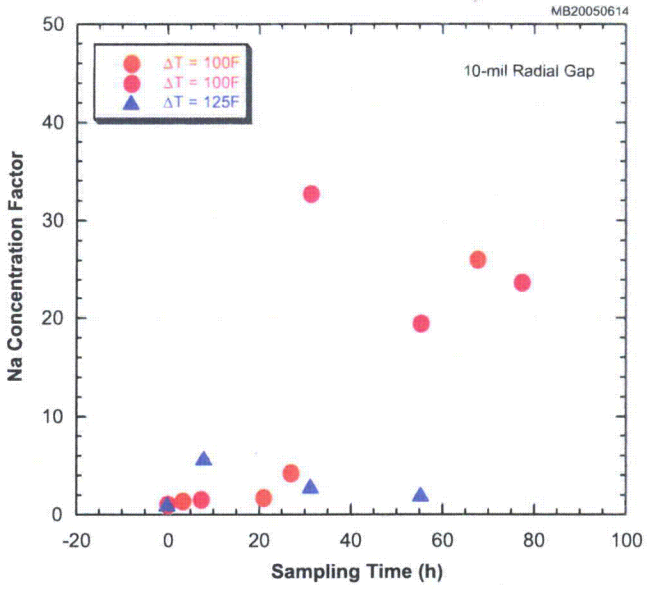

Figure 22.
Concentration factors vs. time for 0.25-mm (0.010-in.) radial gap unpacked crevice and primary-to-secondary temperature differences of 56°C and 69°C (100°F and 125°F).

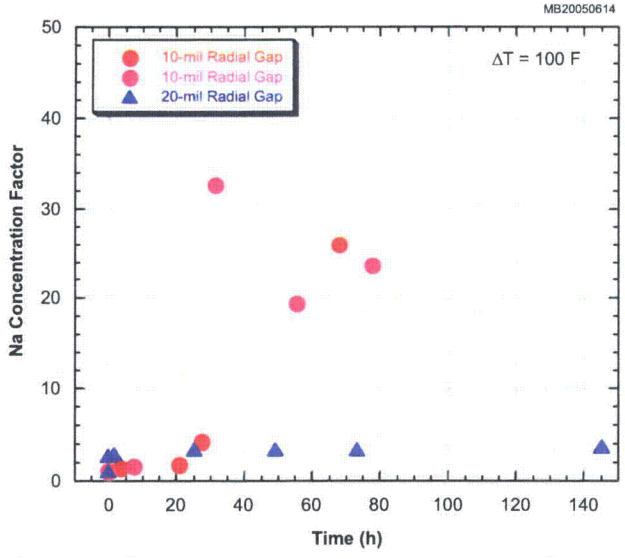

Figure 23.
Concentration factors vs. time for 0.25- and 0.51-mm (0.010- and 0.020-in.) radial gap unpacked crevice and a 56°C (100°F) primary-to-secondary temperature difference.

3.2 Packed Crevice Test with NaOH

Two packed crevice tests (NaOH-01 and NaOH-02) were conducted for two crevice simulators with radial gap sizes of 0.25 mm (10 mil) and 0.51 mm (20 mil). Each crevice was filled with synthetic diamond powders. The secondary bulk solution was 11.5-ppm Na solution as NaOH, the same as for the unpacked crevice test. Two NaOH tests were basically conducted under the same chemical and thermal-hydraulic conditions, and the NaOH-02 was a duplicate test of the NaOH-01. The NaOH-01 had longer

test duration than the NaOH-02 because the NaOH-02 had to be shut down due to a leak. More details on the test results and analysis for the preliminary packed crevice tests with NaOH are described in Appendix A.

3.2.1 Packed Crevice Test: NaOH-01

Four initial series of tests were conducted. The first test involved about 2 days of testing, after which the MB was shut down and allowed to cool over a weekend. The second test involved 4.5 days of testing and was performed as a check on the reproducibility of test data from the first test and the possibility of achieving increased concentration with longer time. The third test extended for 14 days to explore the ultimate crevice concentration achievable. The fourth test involved, without interrupting the third test, raising the primary temperature from 316 to 329°C (600 to 625°F), as was done for the unpacked crevices, to see if crevice hideout increases or decreases.

Inspection of the two crevices revealed that most of the diamond packing in the 0.51-mm (20-mil) radial gap crevice was blown out because a tear in the nickel foam membrane placed over the crevice exit had resulted in a failure to seal the gap. For the 0.25-mm (10-mil) radial gap crevice, the nickel membrane was intact, and the crevice retained its packing. This explained why substantial crevice superheating, approaching 27°C (49°F), was observed in the 0.25-mm (10-mil) crevice while only minor superheat occurred in the 0.51-mm (20-mil) gap crevice, similar to our previous result for the unpacked crevice of the same radial gap size. The inspection also showed that the tube wall for the 0.25-mm (10-mil) radial gap crevice had undergone considerable outer-wall gouging of the tube at the end of NaOH-01, as shown in Figure 24. Gouging means that the depth of the dimple is comparable to the diameter of the dimple or less, i.e., a roughening of the surface. This crevice exhibited a NaOH hideout factor approaching 8,600, and the total time under these conditions was 490 hours. The gouging seems to be developed by the strong caustic chemistry. Considering that the diamond particles might vibrate or be agitated by the boiling on the tube surfaces, the abrasion of hard diamond particles may enhance this gouging. Based on the IGA growth rate data for mill-annealed (MA) alloy 600 at the crevice pH of 11 and temperature of 315°C,[37] the estimated IGA attack depth during the 490-hour exposure is around 25 μm (1 mil). The actual depth of gouging was not measured but the order of magnitude seems to be comparable with the prediction result. No gouging/pitting occurred on the larger 0.51-mm (20-mil) gap crevice where the hideout factor is only 5 and where the packed diamond powders were blown out of the crevice.

An estimate of crevice hideout using the MULTEQ code predicts a maximum concentration factor of 45,000 and pH of 11.07, with the neutral pH being 4.88 at the maximum available superheat of 100°F. The estimated concentration factor at the observed maximum boiling point elevation of 49°F is 43,000. The observed maximum concentration factor of 8,600 among crevice samples is less than the MULTEQ predicted value by a factor of five. This discrepancy may be attributed to that the crevice samples were mixed and diluted by the secondary solution during the sampling process which resulted in less concentrated crevice samples. The MULTEQ code cannot account the kinetic effect like mixing between crevice and secondary solution.

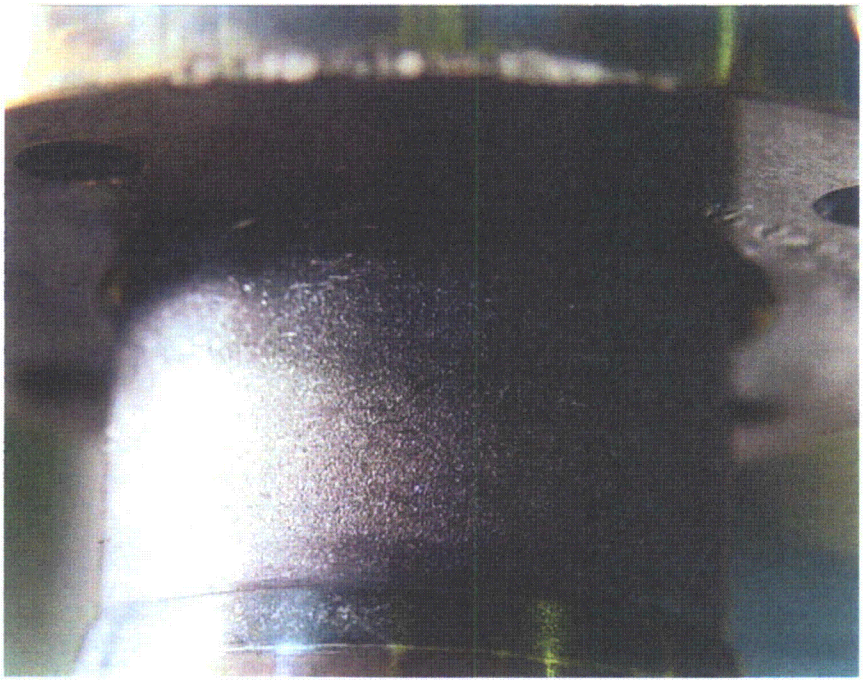

Figure 24.
Photograph of gouging in tube wall in the vicinity of the 0.25-mm (0.010-in.) radial gap crevice.

3.2.2 Packed Crevice Test: NaOH-02

After the NaOH-01 test, the two crevices were repacked, and new nickel-foam grit retention membranes were installed. The 0.25-mm (10-mil) radial gap crevice was packed with 50:50 mixture of two mesh sizes of diamond grit (127-165 μm and 75-97 μm), and the 0.51-mm (20-mil) radial gap crevice was packed with the same grit size (127-165 μm) as used in the NaOH-01 test to obtain data for this grit and crevice size that were not obtained previously because grit was blown out of the crevice through a faulty retention membrane. The estimated crevice porosity was 40 % and 29 % for 0.25-mm (10-mil) and 0.51-mm (20-mil) gap crevices, respectively.

Under the primary and secondary chamber test temperatures of 316°C and 260°C (600°F and 500°F), respectively, the pressure differential across the tube was 5.7 MPa (827 psi). The alloy 600 tube of the 0.25-mm (10-mil) gap crevice failed after about 590 hours of testing accumulated over the two consecutive series of diamond-packed crevice testing during which the crevice hideout factors reached 8,600. The post-test investigation revealed that axial through-wall cracks developed in the 0.25-mm (10-mil) gap crevice. The bulk Na concentration for all tests was initially 11.5 ppm Na (20 ppm as NaOH) in deionized water, but it decreased to 4.2 ppm. Since sodium ion usually does not adsorb on oxide surface and there is no other heat-transfer surfaces than the two crevices, Na ions that left the bulk are expected to hide out in the crevices. Considering the SCC growth rate data of alloy 600 MA under the crevice pH of 11 at 315°C[37], the estimated crack length during the 590-hour exposure is about 67 mils, which is comparable to the tube wall thickness of 50 mils. Because the flaw was very tight, dye penetrant was applied to allow it to be seen and photographed. As shown in Figure 25, the OD axial SCC flaw developed from the bottom to top of the crevice region.

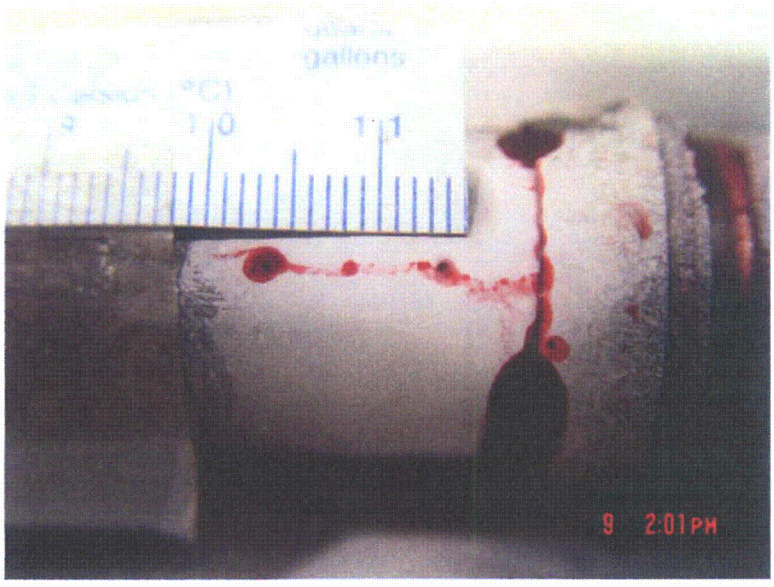

Figure 25.
Crevice SCC flaw photographed using dye penetrant to enhance visualization. The flaw is longer than 18 mm (0.71 in.).

The MB not only appears to be a good facility for studying chemical hideout induced by heat transfer in a prototypic SG tube crevice, but also determining, in a reasonable length of time, the actual cracking potential for various types of hideout chemicals as a function of crevice geometry, thermal hydraulics, and tube materials. There is the possibility that, in the presence of corrosive chemicals concentrated by crevice hideout, the vigorous nucleate boiling at an SG tube outer surface accelerates the growth of SCC above that which takes place in the absence of heat transfer and nucleate boiling.

4. Sodium Chloride Tests with Two Crevices

Based on the preliminary crevice test results with the NaOH solution, crevice hideout tests with NaCl solutions were conducted. The Na-to-Cl MR was varied at each test to determine the effect of the molar ratio on the crevice hideout and chemistry changes. All tests described in this section had two crevices with radial gaps of 10 mils and 20 mils. Each crevice was packed with diamond or magnetite powder.

4.1 NaCl-01: NaCl (MR=1.0) Test

4.1.1 Test Conditions

The first crevice hideout test was conducted with 10-ppm Cl solution as NaCl and MR=1.0. Both crevices were packed with a mixture of two sizes of diamond grit (127-165 μm and 75-97 μm). The estimated porosities for the 10- and 20-mil gap crevices are 3 % and 32 %, respectively. While 32 % is very similar to that in the NaOH-02 test, 3 % cannot be a real value. From the post-test examination, we discovered that one unused ECP port had not been completely plugged, which resulted in unexpected space in the crevice. Based on previous test experiences, the actual crevice porosity for the 10-mil gap crevice should be similar to that of the 20-mil gap crevice. Prepared test solution is injected through a pump before heating up the MB.

4.1.2 High Purity Water Test

As a reference, a test was performed in high purity water first. Five and four thermocouples were installed at the 10- and 20-mil gap crevice, respectively. Their locations are described in Section 2.3.2. Figure 26 shows the normalized temperature variation for the 10-mil crevice gap. To normalize the temperature, the temperature difference between the crevice temperature and secondary saturation temperature are divided by the primary-to-secondary temperature difference. Temperature remained constant for the test period except for the initial heatup and stabilization period. There was no indication of a temperature rise by impurity hideout. The thermocouple labeled "TW" showed a higher value than others because it was installed to touch the outer wall of the alloy 600 tubing. Figure 27 shows the bulk conductivity variation with time. The bulk conductivity value kept constant except for the initial heat-up period.

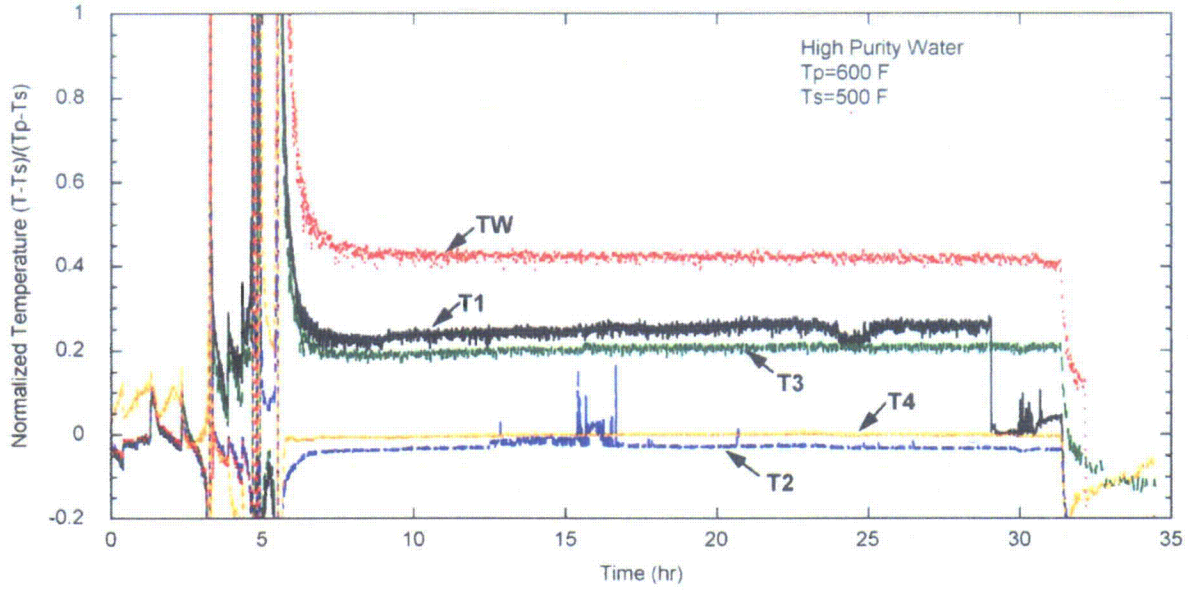

Figure 26. Normalized temperature variation at 10-mil-gap crevice with high purity water in the bulk (NaCl-01).

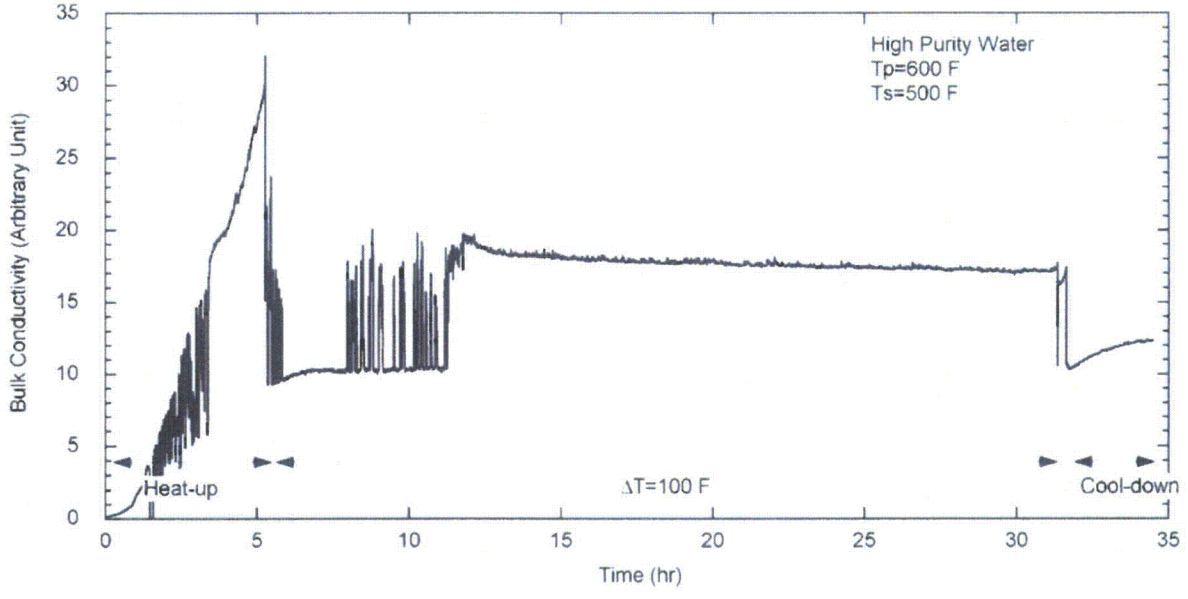

Figure 27. Bulk conductivity variation with time in high purity water (NaCl-01).

4.1.3 Temperature and Conductivity

Figure 28 shows the crevice temperature variation with time in the 10-mil gap crevice packed with diamond powder. The temperature varied with the location of thermocouples and hideout processes. For the 10-mil gap crevice, temperatures increased gradually for the initial test period, followed by stabilization after about 80 hours. The gradual temperature increase over a few tenths of hours is

interpreted as meaning that the Na and Cl ions accumulate in the crevice, causing the boiling point elevation. Since the primary water temperature stabilized within a few hours, the gradual crevice temperature increase cannot be attributed to the primary water temperature variation. The temperature labeled "TW" decreased instead, probably because this thermocouple touched the wall of the alloy 600 tubing. As shown in Figure 28, the amplitude and time constant of the boiling point elevation for each thermocouple varied, mainly because of the different radial distances from the wall of the primary tubing. Based on this interpretation, T4 appears to be the farthest from the wall. After increasing the primary temperature from 600 to 625°F, additional boiling point elevation was not observed at any thermocouple location. NaCl would remain in a dissolved state until its concentration reaches the solubility limit. Since a boiling point elevation is related to the dissolved impurity concentrations, the boiling point elevation equivalent to the NaCl solubility limit under crevice conditions can be predicted thermodynamically. Based on MULTEQ® prediction, the maximum boiling point elevation with NaCl is 46°F; the NaCl precipitation would start if measured temperature is higher than 546°F. At ΔT=125°F NaCl precipitation probably occurred over almost the entire crevice except the location labeled T4 where the measured boiling point elevation was lower than 46 °F. Figure 29 shows the normalized temperature variation in the 10-mil gap crevice. The initial temperature behavior is the same as that in Figure 28, but the normalized temperatures did not change after the increase of ΔT. This finding means that the conduction heat transfer is dominant in the crevice rather than boiling heat transfer before and after the ΔT change. It appears that the boiling rate was decreased by the boiling point elevation and NaCl precipitation.

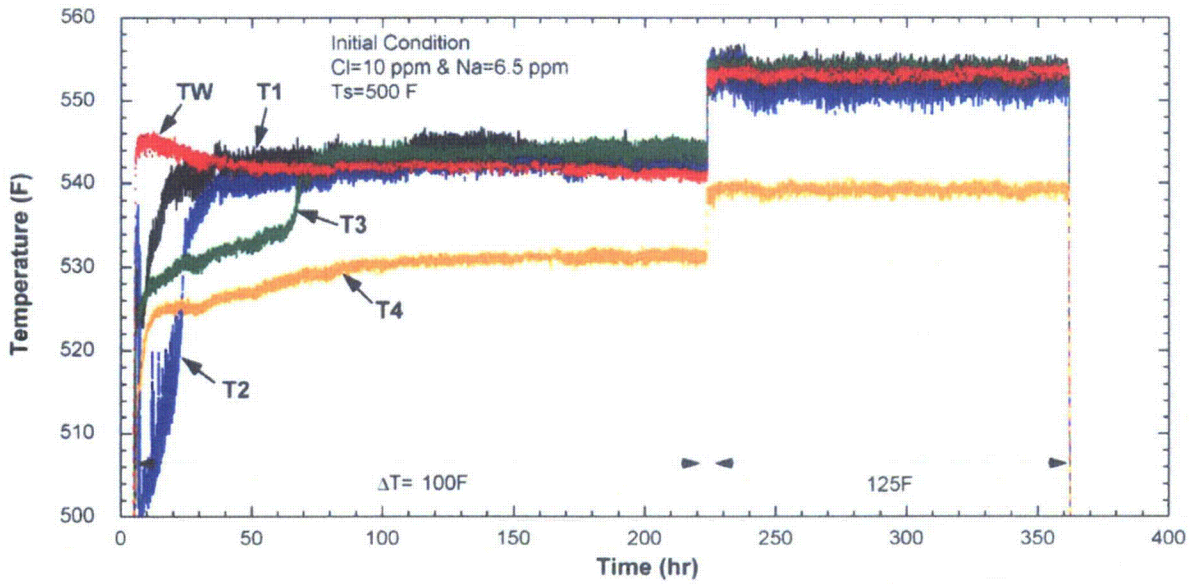

Figure 28. Crevice temperature variation with time in the 10-mil radial gap crevice packed with diamond powder and with NaCl in the bulk solution (NaCl-01).

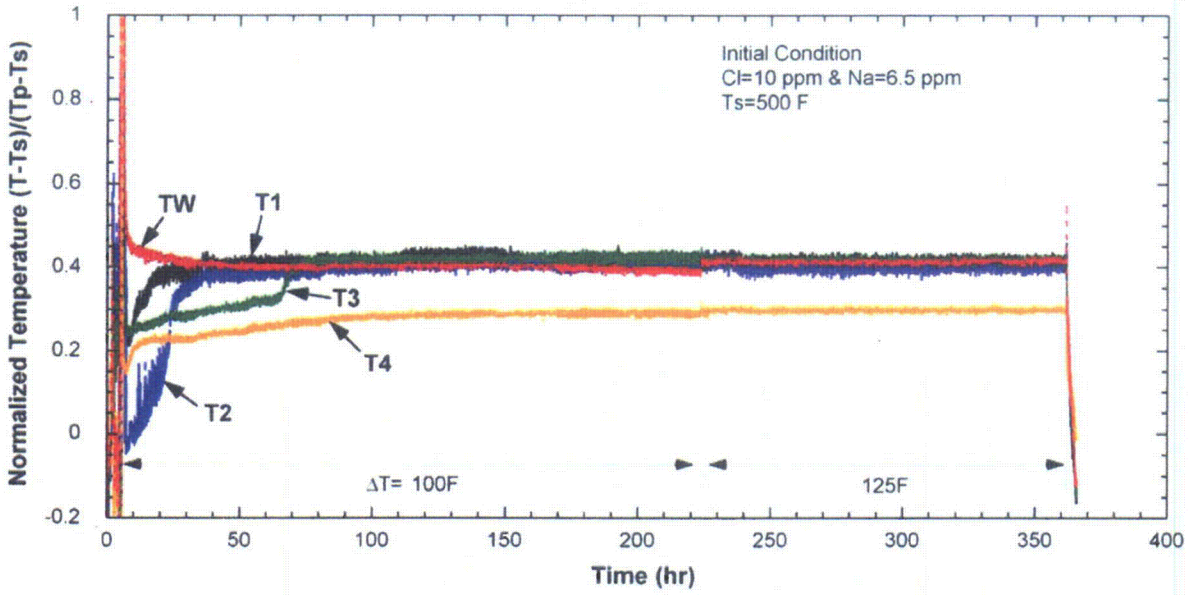

Figure 29. Normalized temperature variation at the 10-mil gap crevice with NaCl in the bulk solution (NaCl-01).

Figure 30 shows the crevice temperature variation in the 20-mil gap crevice. The crevice temperatures varied depending on the thermocouple locations, and the temperature was much lower than that in the 10-mil gap crevice, except for the thermocouple labeled T7, which might be closer to the alloy 600 tubing wall than the others. The noisy temperature signal appears to indicate boiling heat transfer in the crevice as well as conduction. The alternation of a liquid film and dry spot can cause such a temperature oscillation, as described in earlier work[6]. Gradual boiling point elevation was not significant as compared with the 10-mil gap crevice. T6 and T5 appear to indicate a slow boiling point elevation by impurity hideout after the ΔT increase from 100 to 125°F, but the value is less than 6°F. Figure 31 shows the normalized temperature variation as a function of time and thermocouple location. If overall heat transfer coefficient is the same at each ΔT, the normalized temperature should remain constant regardless of ΔT. However, the normalized temperatures showed a shift immediately after the ΔT change, which might indicate that overall heat transfer coefficient became less.

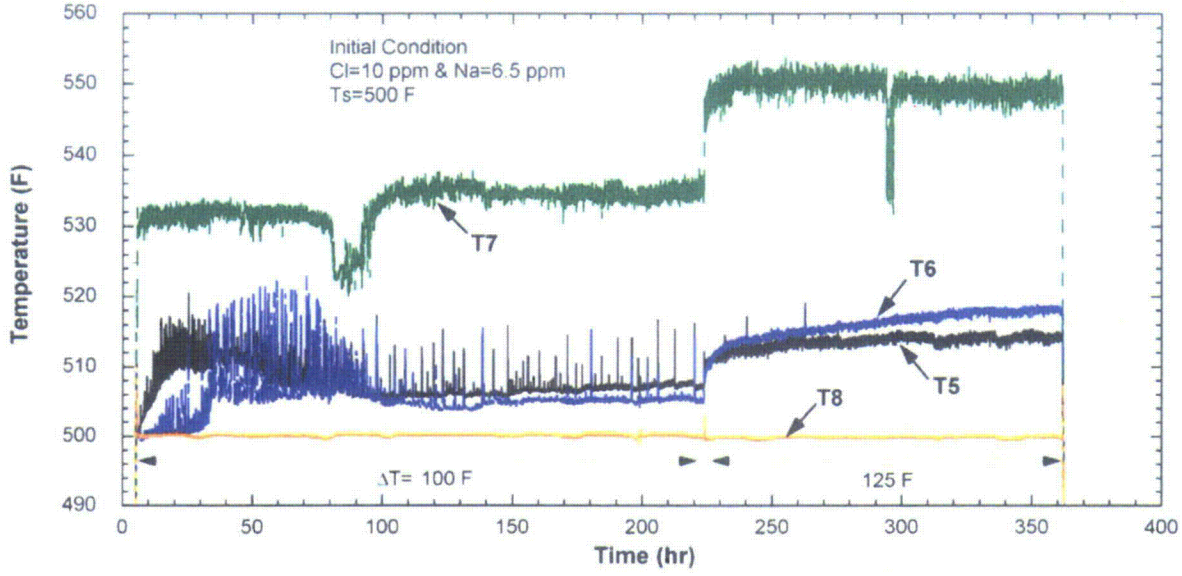

Figure 30. Crevice temperature variation with time in the 20-mil radial gap crevice packed with diamond powder (NaCl-01).

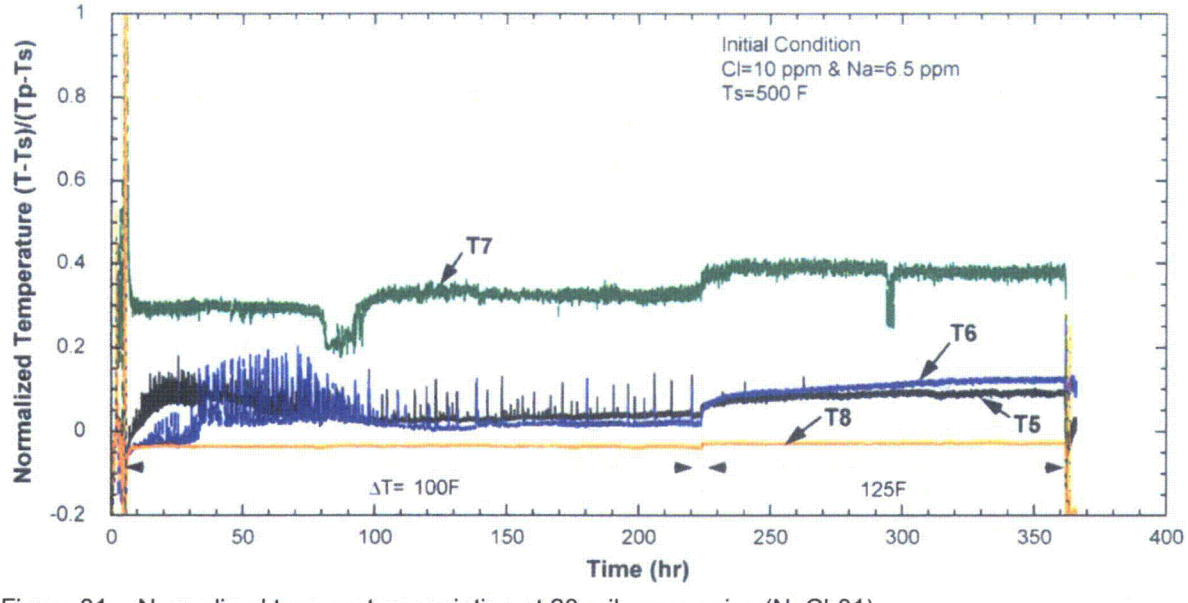

Figure 31. Normalized temperature variation at 20-mil gap crevice (NaCl-01).

Figure 32 shows the bulk conductivity variation and Cl ion concentration in bulk water samples measured by an ion selective electrode (ISE). The bulk conductivity started to decrease right after the primary temperature stabilization. The reduction rate in the bulk conductivity was not much changed after the ΔT increase from 100 to 125°F. At the end of the test, bulk conductivity decreased to 10 % of the initial value, indicating very significant impurity hideout in the crevice. Quick hideout return was observed after the primary temperature reduction. It is hypothesized that the diamond powder packing was not so restrictive that the impurities in the crevice could easily return to the bulk solution. This is also evidence that mixing between crevice and secondary solutions can be significant. Reduced ΔT allowed

liquid penetration into the crevice and dissolution of the precipitated NaCl. The bulk conductivity decrease after the shut-down is attributed to the temperature decrease. The measured Cl ion concentrations in bulk samples were consistent with the bulk conductivity data before the change of ΔT. However, even though the measured data points are limited, the Cl ion concentration did not appear to change significantly after the change of ΔT. The Na ion concentration was also measured by the ISE, but the uncertainty of the measurements was too large to be of value. In the next tests, the bulk and the crevice samples were analyzed by analytical equipment in addition to the ISE to obtain more accurate ion concentrations.

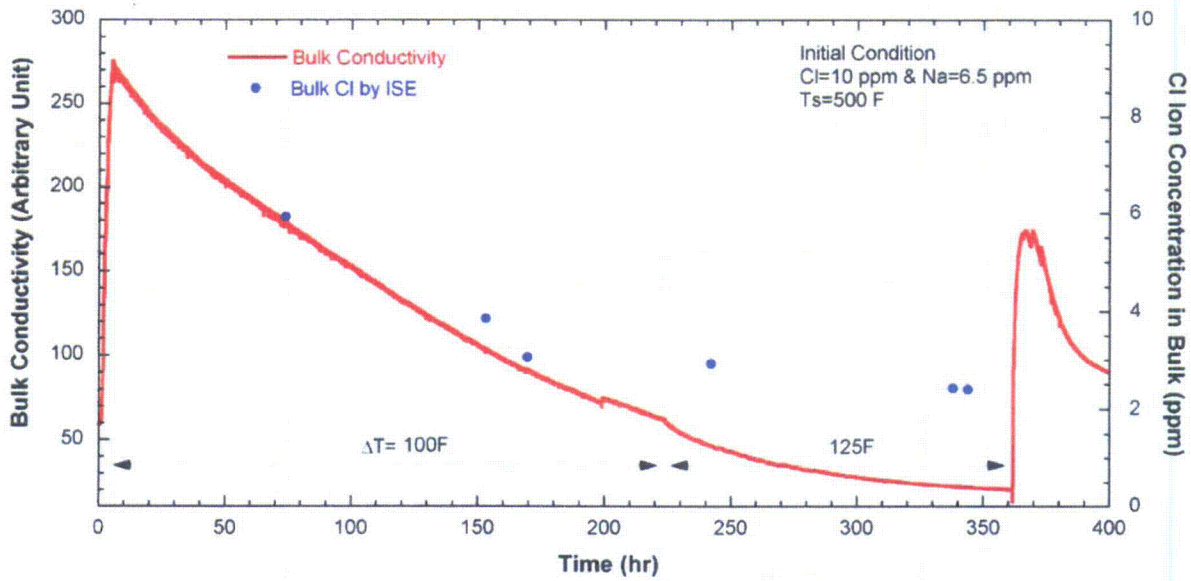

Figure 32. Bulk conductivity variation and Cl ion concentration versus time in bulk water samples measured by an ISE (NaCl-01).

4.1.4 ECP Measurement

Figure 33 shows the variation in Ni electrode potential in the crevice with respect to the Ag/AgCl (0.01 N KCl) reference electrode in the bulk solution. Because of the potentiometer problem, other ECP data are not available. Assuming that the Ni electrode serves as a hydrogen electrode in deaerated alkaline and neutral environments, rough estimation for crevice pH variation may be possible from Figure 33. This assumption may be reasonable because Kawamura et al.[14] experimentally showed that the ECP versus pH slope of alloy 600 was close to that of hydrogen electrode at high temperature and pH ranging 3-10. The Ni ECP initially decreased and stabilized at -650 mV over the first 20 hours. However, the Ni ECP started increasing and stabilized at -610 mV at ΔT=100°F. If the ECP decreases, that correlates to an increasing pH or hydrogen fugacity in crevice, but hydrogen is not supposed to concentrate in the crevice. A pH variation can be a result of the variation of Na and Cl concentrations in the crevice. The initial decrease of the Ni ECP indicates the crevice pH increased as a result of preferential Na concentration and a Cl volatility effect. The following Ni ECP increase and stabilization at ΔT=100°F might be interpreted as a crevice pH decrease caused by preferential Cl hideout following the initial preferential Na hideout. The delayed Cl hideout is discussed and experimentally supported in single crevice tests (NaCl-05 & -06).

At ΔT=125°F, the Ni ECP gradually decreased. This decrease might indicate an increased Cl volatility effect caused by the increased boiling rate at higher ΔT. Note that the crevice temperature data indicated NaCl precipitation at ΔT=125°F so that the ECP might not be measurable under the

precipitation condition. Therefore, the tip of the Ni electrode appears to be located far enough from the tube wall not to be dry. The measured Ni ECP may represent the chemistry far from the tube wall rather than the chemistry near the tube wall. The effects of the radial location of the electrode tip are discussed in Section 4.2.3. The Ni ECP variation from the beginning of a test at constant ΔT, as shown in Figure 33, is typical ECP behavior under NaCl bulk water chemistry. In other NaCl tests, where a tungsten electrode was used as a pH electrode, the electrode potentials are similar.

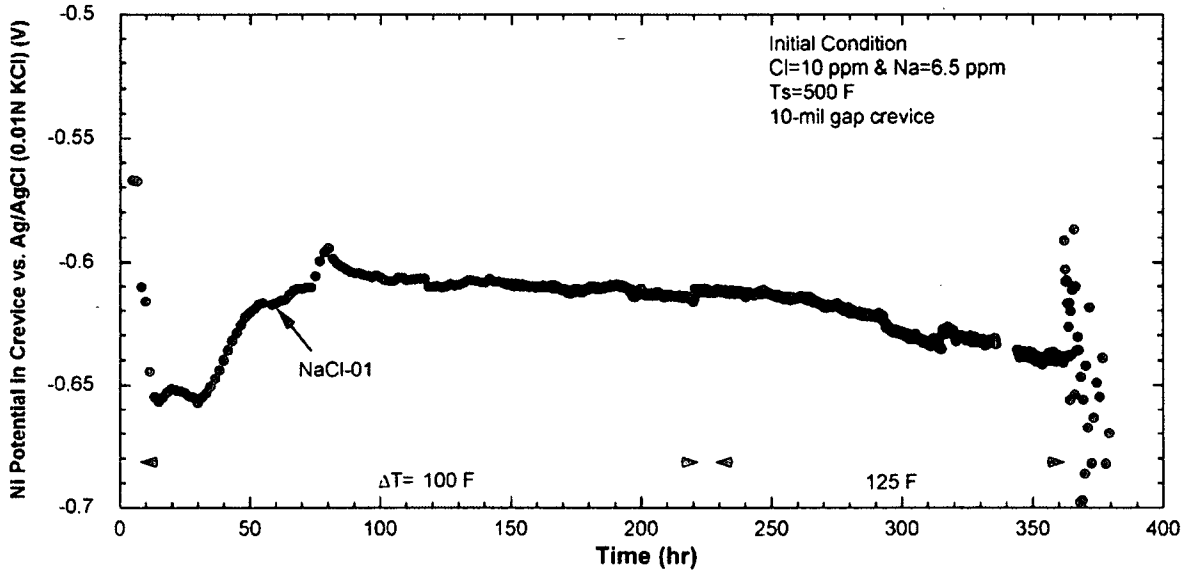

Figure 33. Ni electrode potential variation in crevice with respect to Ag/AgCl (0.01 N KCl) reference electrode in bulk (NaCl-01).

4.2 NaCl-02: NaCl (MR=1.0) Test

After the NaCl-01 test, the MB was heated up again without opening the secondary chamber and changing the bulk solution. This next test was done to evaluate the reproducibility of the NaCl-01 test results. The secondary-side temperature was kept at 260°C (500°F), while the primary-side temperature was set at 282, 293, 304, and 316°C (540, 560, 580, and 600°F) because ΔT=100 or 120°F is higher than the normal operating differential temperature between the primary and secondary sides in actual SGs. The NaCl-02 test results are summarized as below.

4.2.1 Temperature Data

The NaCl-02 test was performed with the primary superheat variation ranging from 40 to 100 °F. The secondary test solution contained 10 ppm Cl as NaCl. Figure 34 shows the crevice temperature variation measured at various crevice locations in a 10-mil gap crevice. As observed in the NaCl-01 test, the amplitude and time constant for the temperature increase caused by impurity hideout depended on the location of each thermocouple at ΔT=100°F. The crevice temperatures decreased instantaneously after decreasing ΔT from 100 to 60°F. After increasing ΔT again from 60 to 80°F, the crevice temperatures started to increase gradually. The TW thermocouple touching the tube wall showed the highest temperature elevation. From this observation, we concluded that impurity hideout kinetics is fastest at the tube wall, and the resultant temperature elevation is the most sensitive on the tube wall at least when ΔT is 60°F or 80°F. When ΔT dropped to 40°F, crevice temperatures decreased instantaneously and did not

show any temperature elevation. But TW indicated a small temperature elevation of about 6°F. The tests at ΔT=60°F and 40°F followed the tests at 100°F and 80°F, respectively. The transition from higher to lower ΔT resulted in the impurity movement out of the crevice, a dilution by drawing in the secondary solution to the crevice, and possible dissolution of the precipitated NaCl. These are the reasons why temperature elevation was not observed at ΔT=60°F and 40°F. With decreasing ΔT, the crevice would reach a new steady-state condition at lower ΔT in a short time due to relatively fast diffusion in the diamond powder pack. Figure 35 shows the normalized crevice temperatures as a function of time. As shown in Figure 35, the crevice temperature appears to be relatively independent of the primary superheat ΔT. However, the temperature increased at the beginning of the test with the primary superheat of 100°F. The normalized temperatures labeled as T2 and T3 increased when ΔT was decreased from 100°F to 60°F and from 80°F to 40°F, while the tube wall temperature labeled TW decreased when the ΔT was decreased. It is concluded from the normalized temperature variation that the concentrated solution on the tube wall is diluted when ΔT decreases but the area away from the tube wall is affected by NaCl precipitates formed at higher ΔT so that the nucleate boiling rate is reduced because of the concentrated solution formation by the dissolution of NaCl precipitates at that area when ΔT decreases.

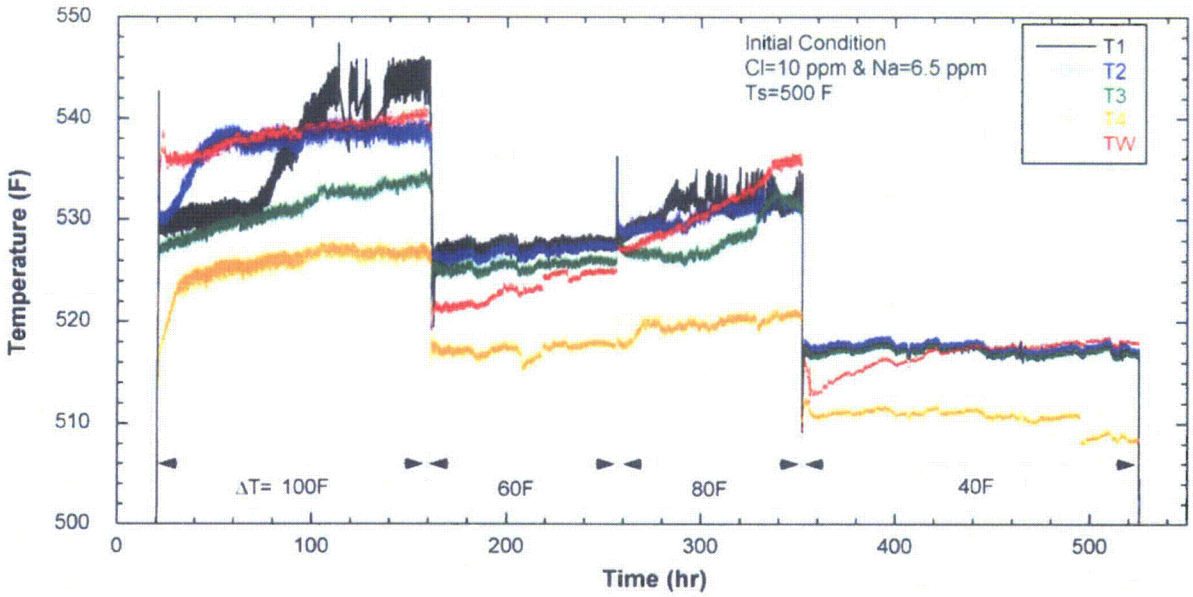

Figure 34. Crevice temperature variation with time and ΔT in a 10-mil radial gap crevice packed with diamond powder (NaCl-02).

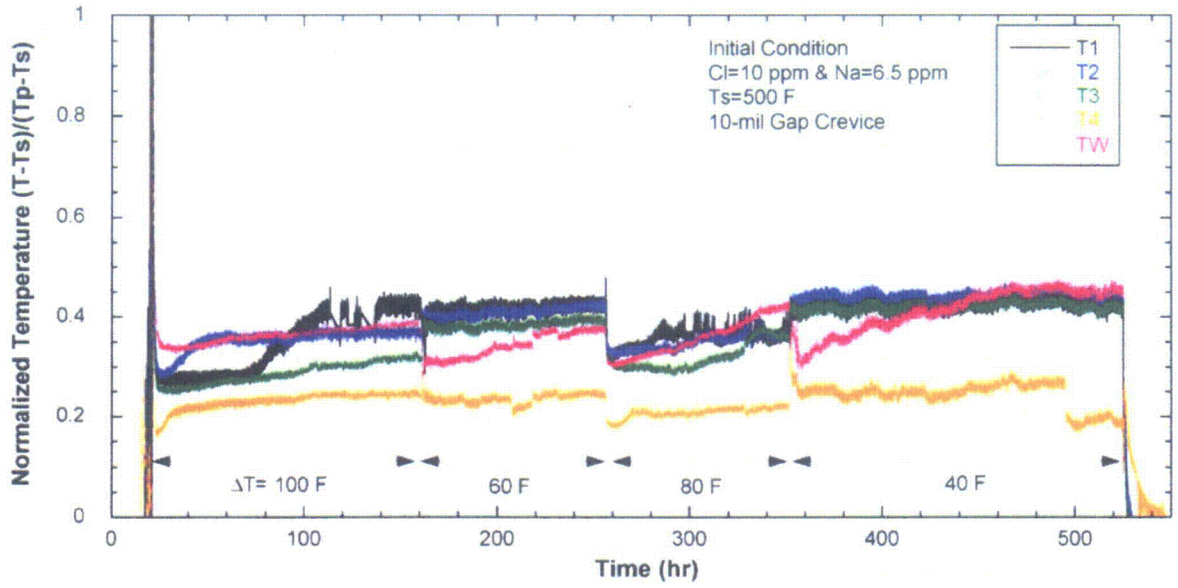

Figure 35. Normalized temperature variation at 10-mil gap crevice (NaCl-02).

Figure 36 shows the crevice temperatures in the 20-mil radial gap crevice. As observed in the NaCl-01 test and shown in Figure 30, the temperature elevation is not significant except at T7. Some noisy temperature signals might indicate presence of both steam and liquid phases in near the thermocouple. As shown in Figure 37, the normalized temperature is relatively independent of ΔT except at T7; this finding is interpreted as the effect of the thermocouple's location. As compared with the temperature data in 10-mil gap crevice, the normalized temperatures in the 20-mil gap crevice are lower. In the wider gap crevice, liquid penetration into the crevice and mixing between bulk and crevice appear to be easier, and this condition causes a higher heat transfer coefficient and lower normalized crevice temperatures.

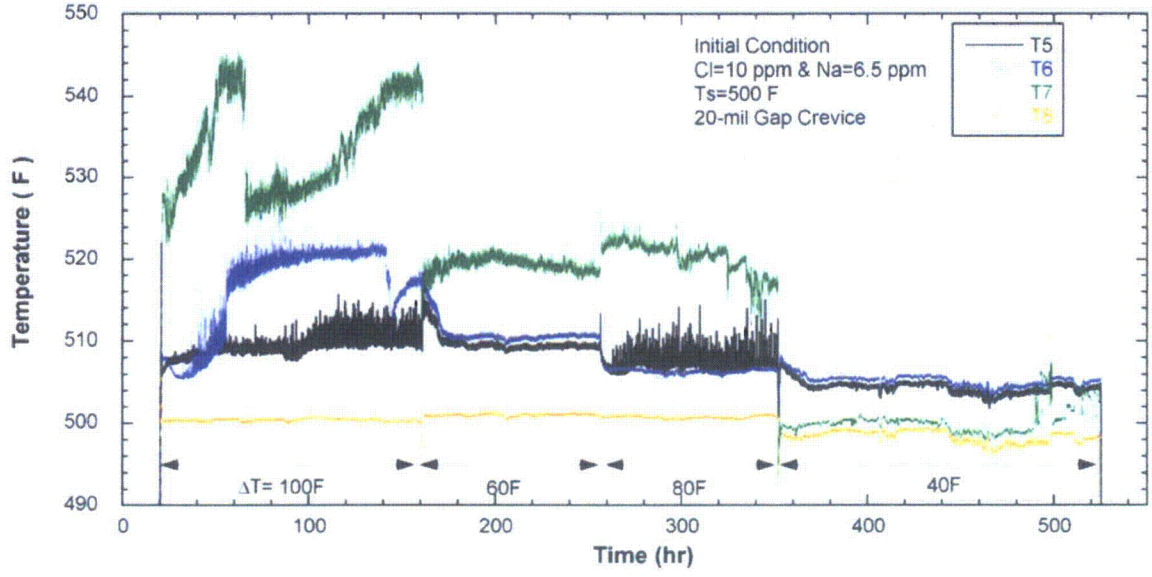

Figure 36. Crevice temperature variation with time and ΔT in a 20-mil radial gap crevice packed with diamond powder (NaCl-02).

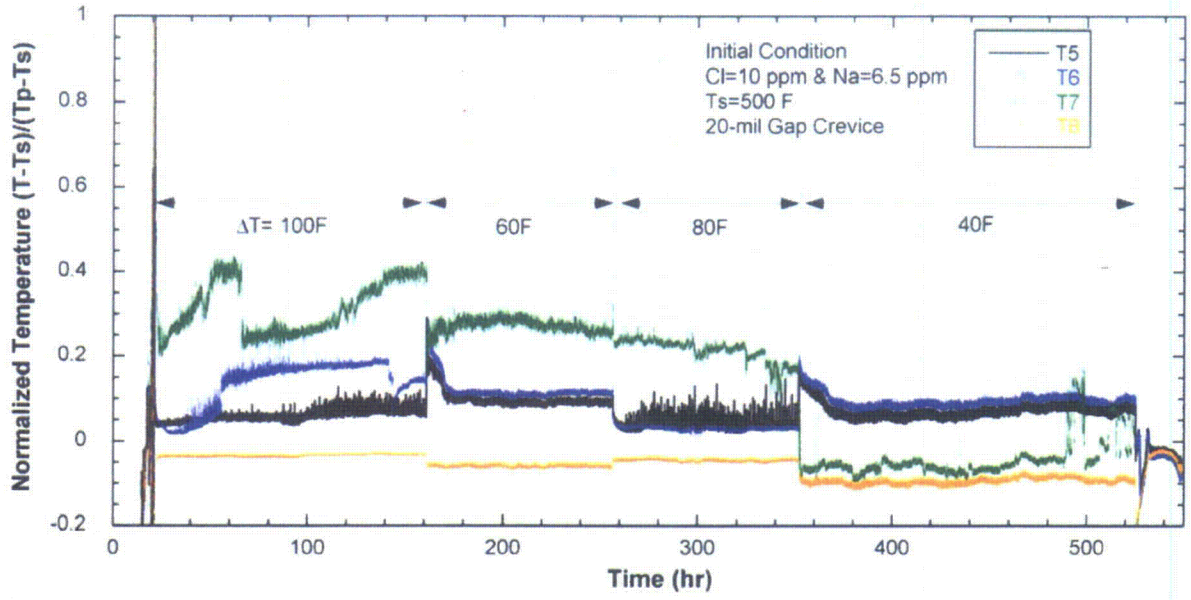

Figure 37. Normalized temperature variation at 20-mil gap crevice (NaCl-02).

4.2.2 Bulk and Crevice Chemistry

Figure 38 shows the bulk conductivity and the bulk impurity concentration measured by solution sampling. The bulk conductivity reduced gradually, but the conductivity reduction rate was dependent on ΔT. Hideout return was observed after ΔT decreased from 100°F to 60°F and from 80°F to 40°F. The Cl and Na concentrations measured by IC and ICP/OES are consistent with the bulk conductivity variations. The Na data determined by ICP/OES at 400 hours deviate from the general trend. The large fluctuation of Na ion concentration at ΔT=40°F is unexpected because the Cl ion concentration and bulk conductivity kept nearly constant over that time period. This Na data at 400 hrs could be measurement error. The Cl concentration determined by ISE did not correspond to the value determined by IC, but the overall trend seems to be consistent with the bulk conductivity data at least during the first two ΔT periods. These findings verify that the ISE analysis method for Cl determination is appropriate for evaluating the overall trend but not for accurate measurements. The Na concentration determined by the ISE is not reliable because the sampling solution volume of about 1-1.5 mL was too small for the Na ISE.

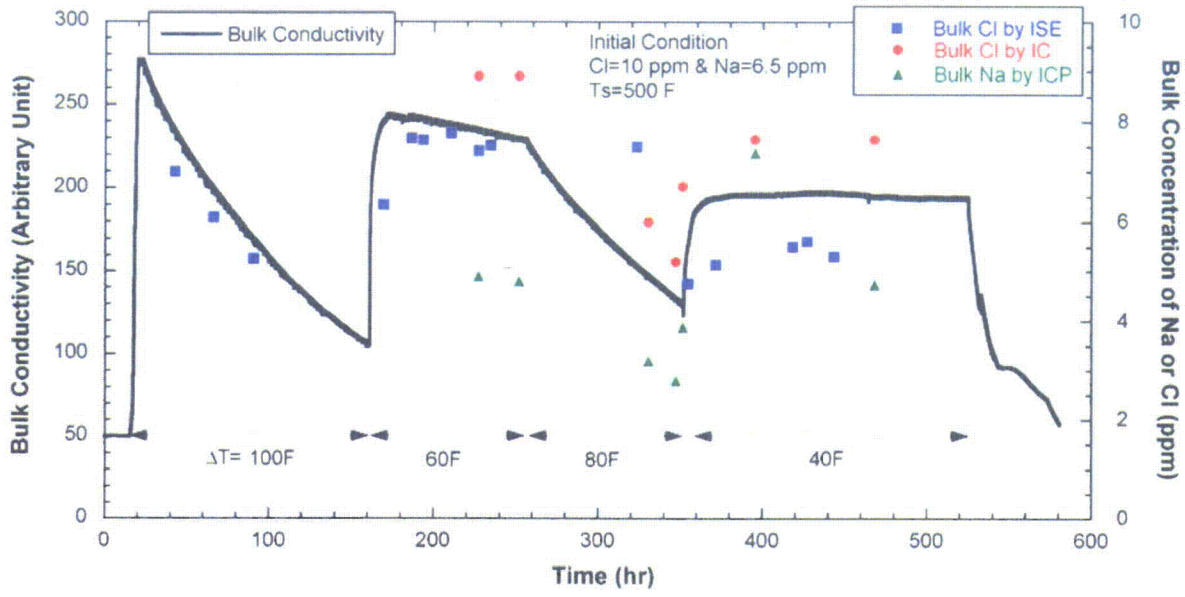

Figure 38. Comparison of bulk conductivity and measured bulk impurity concentration determined by solution sampling (NaCl-02).

The bulk conductivity from the NaCl-02 test was compared with that from the NaCl-01 test over the first 150 hours at $\Delta T=100°F$, as shown in Figure 39. The conductivity excursions showed very similar behavior. Since the experimental conditions for the two tests were exactly the same, this comparison confirmed the data reproducibility at $\Delta T=100°F$. The slopes for bulk conductivity reduction are strongly dependent on the superheat changes, as shown in Figure 40. To remove the dependency on bulk concentration itself, the bulk conductivity data were normalized with the initial bulk conductivity at each ΔT. There is a drastic change in the rate of bulk conductivity reduction between $\Delta T=60°F$ and $\Delta T=80°F$. As discussed earlier, ΔT was not increased monotonically from 40°F to 100°F. In evaluating the data, it should be noted that the excessive hideout occurred before changing ΔT from 100°F to 60°F and from 80°F to 40°F. Because of this excessive amount of hideout prior to decreasing the ΔT, the force to drive ions out of the crevice was large immediately after the decrease of ΔT. Then driving forces to move ions into and out of the crevice were balanced and, at $\Delta T=60°F$, the driving force to move ions into the crevice became dominant because the diffusion flux of ions out of the crevice became negligible. At $\Delta T=40°F$ steady state was achieved based on the data for bulk conductivity and Cl ion concentration. We expect that if ΔT is increased monotonically from 40°F to higher value, the rate of bulk conductivity reduction at $\Delta T=40°F$ and 60°F will be much higher than those in Figure 40 and possibly even close to the rates at $\Delta T=80°F$ and 100°F. This assumption is supported by the test results for a single-diamond-packed crevice test, NaCl-05, discussed in Section 5.3.3.

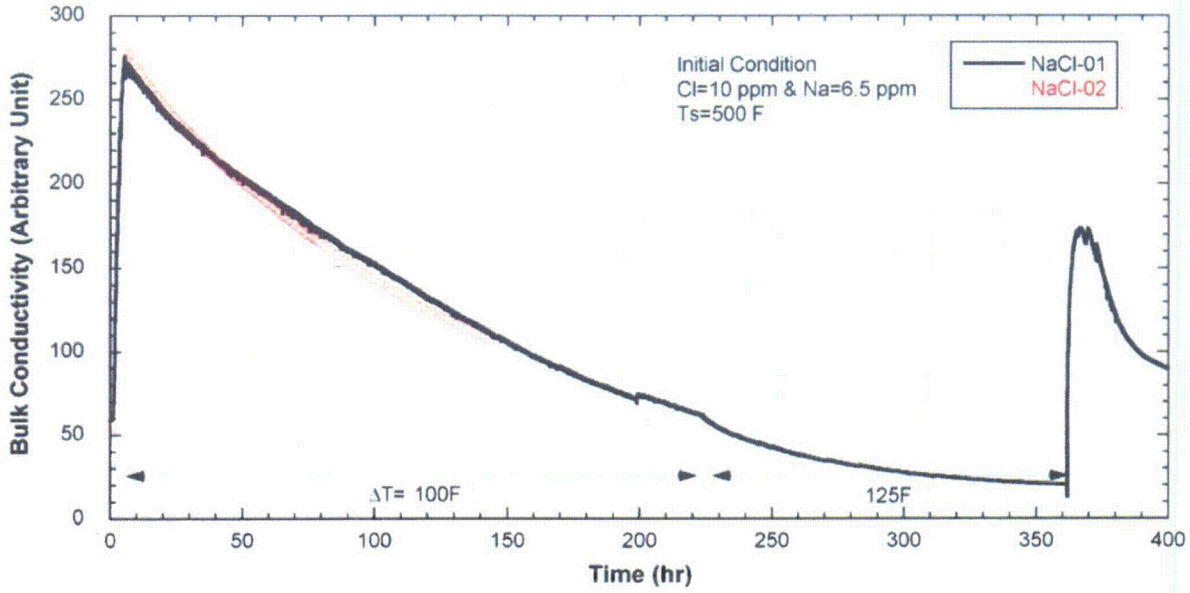

Figure 39. Comparison of measured bulk conductivity in the NaCl-01 test and NaCl-02 test.

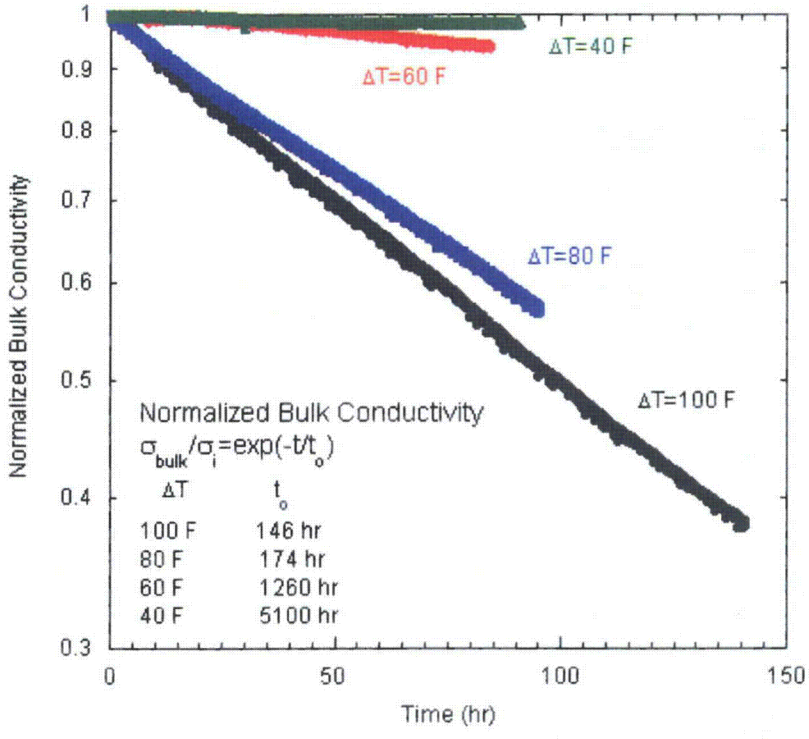

Figure 40.
Normalized bulk conductivity variation as a function of ΔT in the NaCl-02 test comparing the bulk conductivity decreasing rates.

Figure 41 shows the results for crevice-solution analysis by IC for Cl and ICP/OES for Na, as well as some results by ISE. When the ΔT=80 or 100°F, the crevice samples did not show hideout, but significant impurity concentrations were observed at lower ΔT. It is likely that higher ΔT resulted in NaCl

precipitation on the tube surface, and mainly steam is condensed and sampled out of the crevice. However, at ΔT=40°F, the precipitated NaCl dissolved at the beginning of the test, and this dissolution caused the highest concentration in the earliest crevice sample, followed by a gradual decrease and stabilization. In Figure 41, Na and Cl concentrations determined by ISE are shown to be similar to those obtained by IC or ICP/OES. The ISE analysis has better accuracy at higher concentration in the crevice samples compared with the accuracy at lower concentration in the bulk samples shown in Figure 38.

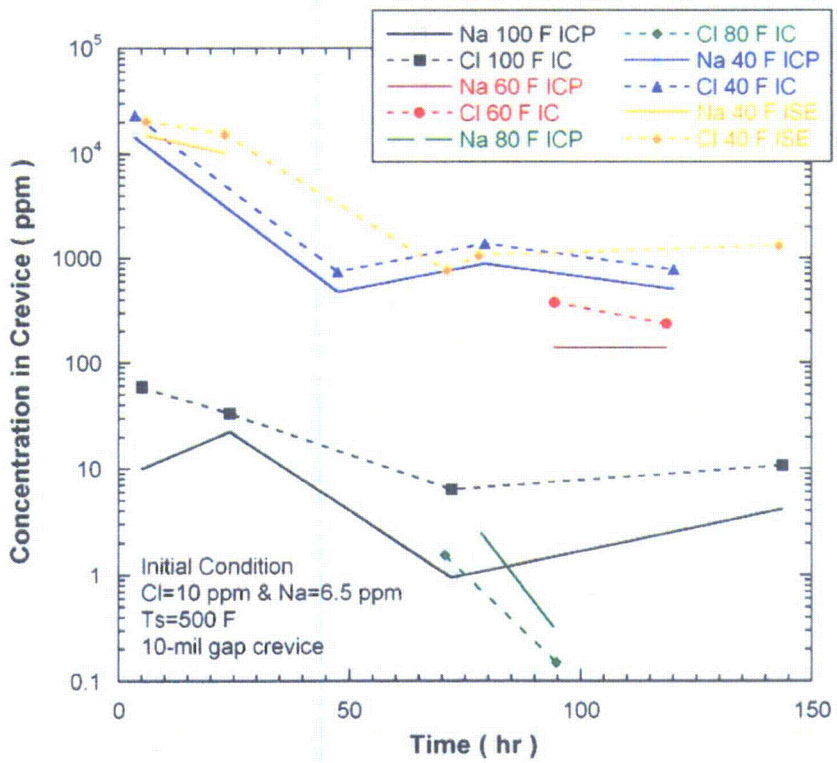

Figure 41. Concentrations from crevice-solution sample analysis as functions of time and ΔT in the NaCl-02 test.

Figure 42 shows the Na-to-Cl molar ratio ([Na]/[Cl]) in a crevice compared with that in the bulk as a function of ΔT for the 10-mil and 20-mil gaps. For the 10-mil gap crevice, as ΔT decreases, [Na]/[Cl] in the crevice increases. This trend indicates that mainly steam is condensed and extracted from the sampling line at higher ΔT, and actual concentrated liquid is extracted at lower ΔT. The variations of the crevice molar ratio at ΔT=100°F is also attributed to the variations of the extracted amount of steam. As compared with the [Na]/[Cl] in the crevice, the variation of [Na]/[Cl] in the bulk is not as large but slightly increases with ΔT. This result appears to indicate a dependence of Cl volatility on ΔT. Since [Na]/[Cl] in the bulk is less than unity, the crevice solution should have higher [Na]/[Cl] than unity. However, only crevice samples at ΔT=40°F tend to have [Na]/[Cl] ratios that are higher or close to unity, because at ΔT=40°F concentrated liquid from NaCl dissolution minimized the steam extraction. For the 20-mil gap crevice, as compared with 10-mil gap crevice, [Na/[Cl] in the crevice is closer to the bulk value. It appears that fluid mixing between the crevice and bulk is easier in the 20-mil gap than in the 10-mil gap.

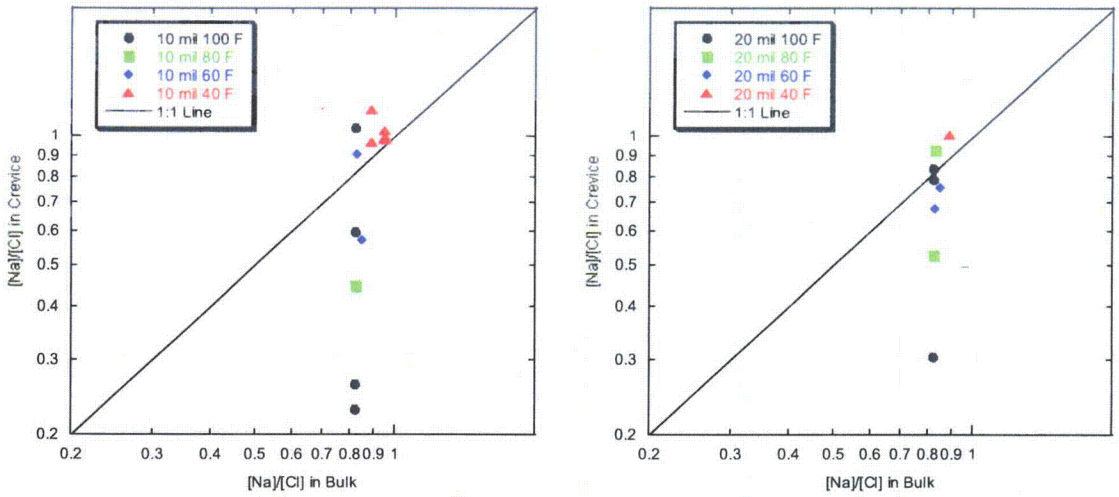

(a) (b)

Figure 42. [Na]/[Cl] ratios in crevice versus bulk as a function of ΔT for (a) 10-mil gap and (b) 20-mil gap crevices in the NaCl-02 test.

4.2.3 ECP Measurement

Figure 43 shows the ECP variation of various electrodes installed in the crevice and the bulk solution with respect to the Ag/AgCl (0.01 N KCl) reference electrode. The bulk Pt electrode potential increased gradually and independently of the primary superheat. If the bulk Pt change was caused by the drift of the Ag/AgCl reference electrode, potential should change toward a negative direction. Assuming the Pt electrode behaves as a pH electrode under the deaerated condition, it is assumed that the bulk pH would gradually move to the acidic direction because of the high volatility of Cl and resultant preferential hideout of Na. Precise bulk chemistry analyses by IC and ICP/OES indicated that the [Na]/[Cl] molar ratio in the bulk solution was always less than unity, a finding that supports the measured bulk Pt potential variation. Figure 44 shows the solution pH variation with molar ratio and ion concentration at 260°C (500°F). For the 10-ppm Cl concentration, the MR change from 1.0 to 0.9 can lower the solution pH by almost one pH unit. However, reduced ion concentration itself can make the solution pH higher. Consideration should be given to both effects when evaluating the bulk solution pH with ion concentration data. Based on the MULTEQ calculations in Figure 44, it is difficult to explain the initial decrease of bulk Pt ECP. The Pt electrode might be affected by residual oxygen, but the Pt ECP decrease suggests that eventually the oxygen becomes consumed by the oxidation of metals. As shown in Figure 43, Ni and alloy 600 electrodes in bulk water show similar behavior to bulk Pt electrode.

Figure 45 shows the electrode potential difference between the crevice and bulk for Pt, Ni, and alloy 600 electrodes. If all conditions are the same for the crevice and bulk, the potential difference should be zero. Assuming Pt behaves as a hydrogen electrode and hydrogen activity in the crevice and bulk are the same or the difference of hydrogen activity between the bulk and crevice is negligible, the potential difference can be interpreted as related to a pH difference. Based on this assumption, it was concluded that the crevice was acidified gradually during the first 50 hours. The crevice solution analysis at ΔT=100°F, as shown in Figure 42, indicated that the crevice sample was acidic. Since the potential difference decreased with time, the crevice pH was gradually increasing. After the primary superheat change from 80°F to 40°F, the Pt potential difference was drastically changed in the alkaline direction. The molar ratio in bulk solution at ΔT=80°F was less than unity, which means Na was preferentially concentrated in the crevice. Preferential Na concentration should make the crevice more alkaline than the

bulk, but the measured Pt ECP in the crevice was higher than that of the bulk Pt. This discrepancy can be resolved with the assumption that at higher ΔT (80°F or 100°F) NaCl precipitation occurred at the tube surface of the deeper crevice region, and around the Pt electrode tip, the steam phase was dominant. The condensed steam would cause the slightly acidic pH signal of the Pt ECP. The drastic change of crevice Pt potential when lowering ΔT is attributed to the fact that the formerly present NaCl precipitation near the tube surface was mixed with penetrating liquid caused by the reduced ΔT, and then the mixed liquid touched the Pt electrode tip. The Pt potential difference slowly came back to near neutral condition, which is caused by the mixing between bulk and crevice solution. The return of excessive Na from the crevice was confirmed by the bulk solution analysis, indicating the molar ratio had become larger and close to unity.

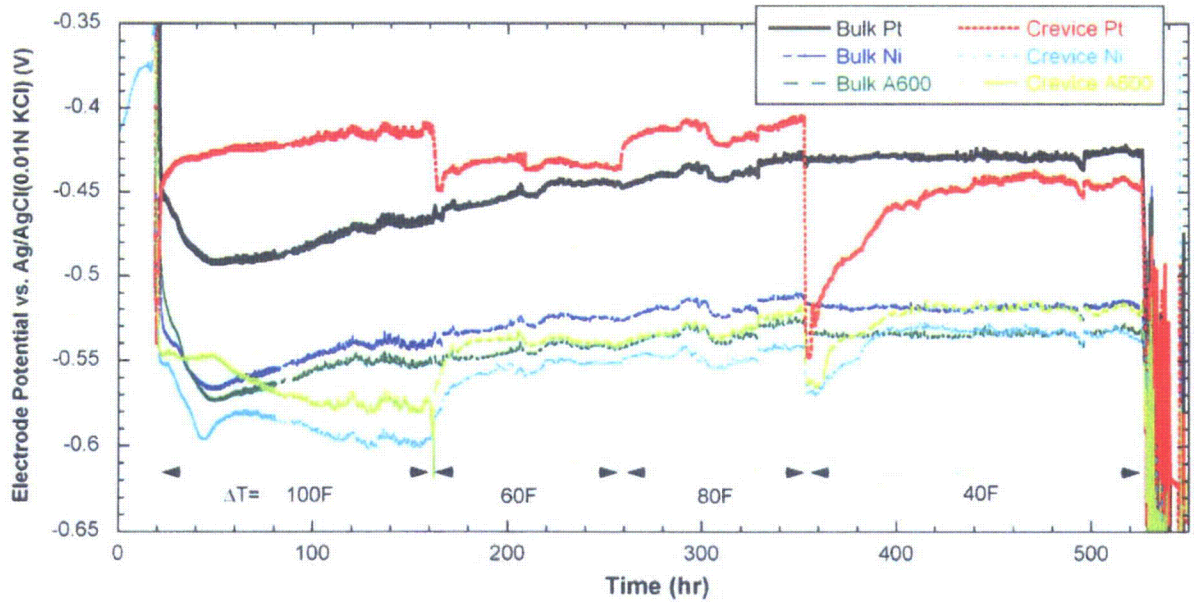

Figure 43. Electrode potential variation with respect to Ag/AgCl (0.01N KCl) (NaCl-02).

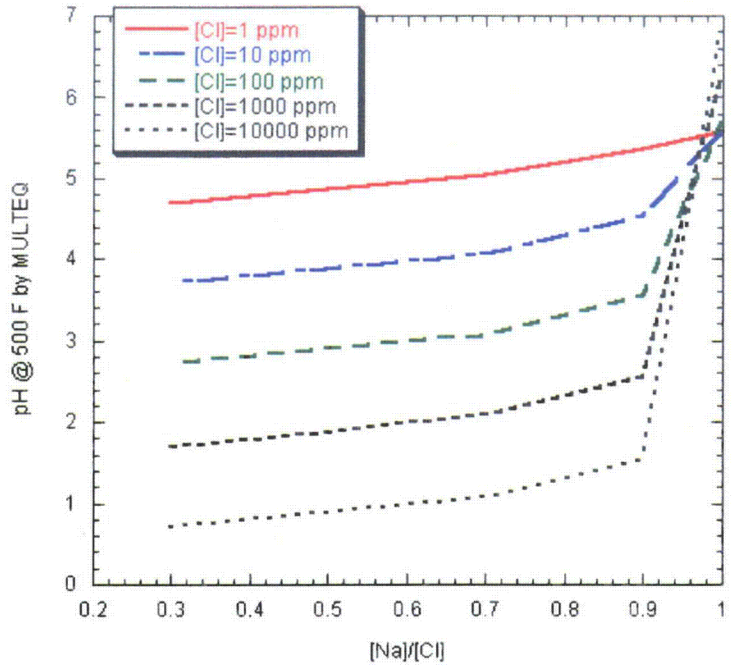

Figure 44.
Predictions of solution pH variation at 260°C (500°F) with Na-to-Cl molar ratio and ion concentration.

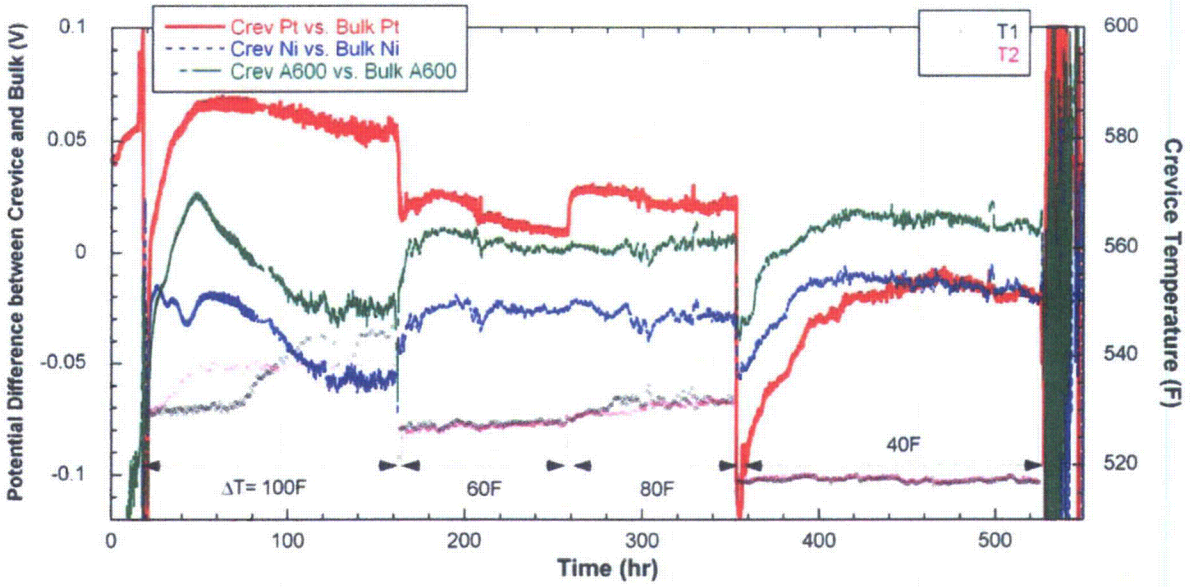

Figure 45. Electrode potential difference between crevice and bulk (NaCl-02).

As shown in Figure 46, the crevice Ni electrode potential of the NaCl-02 test was compared with that of the NaCl-01 test. In general, the NaCl-02 results indicated higher potential. The initial potential decrease was not significant in the NaCl-02 test, probably because the precipitated NaCl in the NaCl-01 test, which might not have been completely dissolved out, affected the crevice Ni electrode potential in the subsequent test, NaCl-02. The potential difference between the two NaCl tests was around 10 mV after 150 hours, which is an acceptable reproducibility for high-temperature ECP measurements.

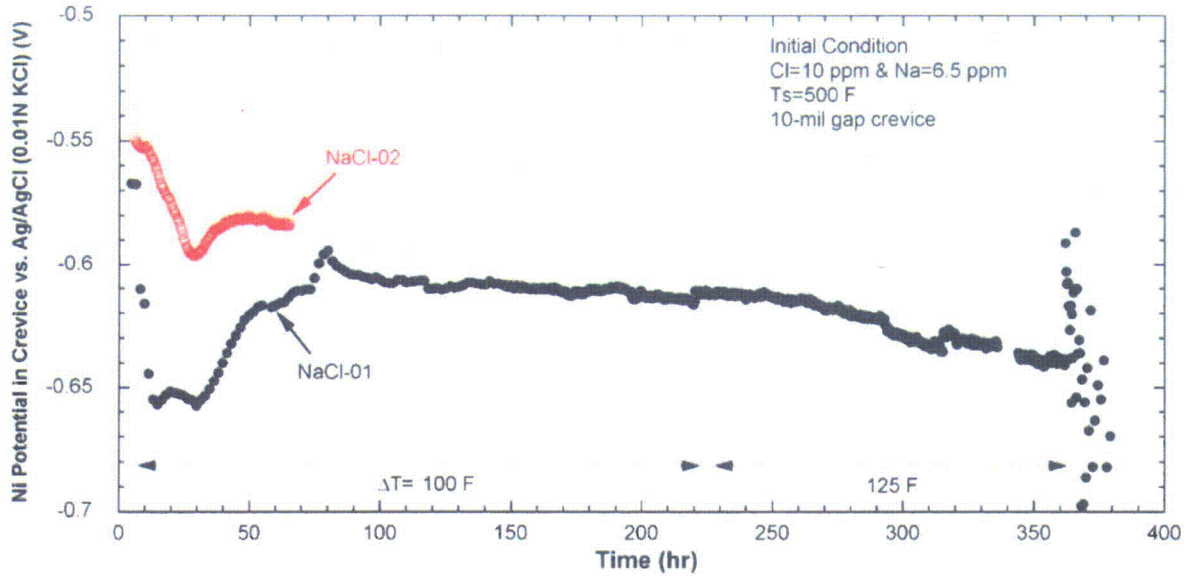

Figure 46. Measured Ni electrode potential in crevice in the NaCl-01 and NaCl-02 tests.

Figure 47 shows the Pt potential difference between the crevice and bulk as a function of pH difference. The sample pH was calculated by MULTEQ, and Pt potential data corresponding to the sampling time were used. If the Pt electrode reaction follows the Nernstian equation, the potential slope with respect to pH should be -106 mV/pH at 260°C (500°F), but the measured slope was only -18 mV/pH. The calculated pH data based on the extracted sample composition predict a larger pH difference between crevice and bulk compared with measured Pt potential. For example, the maximum potential difference is about -120 mV, corresponding to one pH unit difference, but the calculated pH difference was around 5. It is likely that the crevice samples might have been diluted or affected so that they did not fully represent the actual Na and Cl concentrations in crevice. The post-test examination for the tube surfaces in the crevice region revealed no gouging in the 10- or 20-mil gap crevice. Even though the crevice sample indicated the caustic chemistry in a short-time period at $\Delta T=40°F$, the post-test examination suggests that the crevice chemistry was near neutral during the NaCl-01 and -02 tests. Keeping the bulk water chemistry neutral and having the MR=1.0 helped the crevice chemistry stay near neutral.

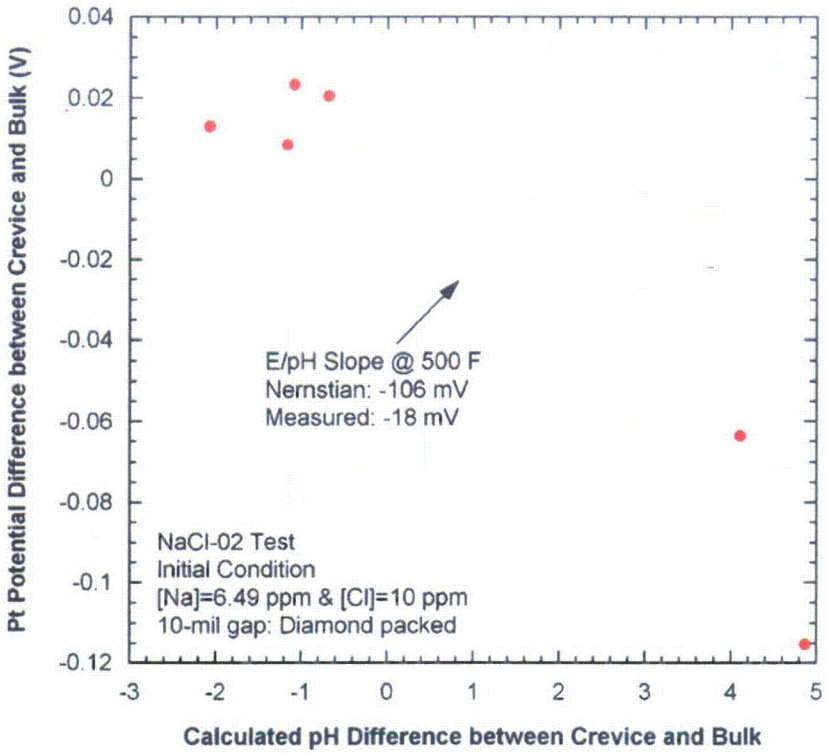

Figure 47.
Pt potential difference between crevice and bulk as a function of pH difference calculated by MULTEQ (NaCl-02).

4.2.4 Summary

Figure 48 illustrates the precipitation and concentrated phenomena in the crevice for (a) higher ΔT and (b) lower ΔT. The gap is filled with diamond powder, and a small pocket exists for signal wires, as shown in Figure 48. For higher ΔT, liquid film that condensed from the steam would exist around the signal wire, which tends to generate signals for acidic condition. On the tube surface there would be NaCl precipitation and/or Na-rich concentrated liquid film. By lowering of ΔT from 100°F to 60°F and from 80°F to 40°F, the bulk liquid would penetrate into the crevice and be mixed with the Na-rich liquid film present. The formerly precipitated NaCl at higher ΔT would be dissolved. Then, the concentrated liquid would touch the signal wire, which makes an alkaline or near neutral crevice signal. Note that this interpretation for crevice hideout phenomena with ΔT is limited to this NaCl-02 test. If ΔT increases monotonically from 40°F to 100°F, the crevice hideout phenomena as a function of ΔT will be different. Nonetheless, the NaCl-02 test has shown the MB to be a good vehicle for studying chemical hideout induced by heat transfer in prototypic SG tubes. Temperature and potential variation with time and experimental conditions were successfully monitored. The effects of crevice gap size and primary-to-secondary temperature differences were explored. The extracted solution samples from both the crevice and bulk solutions were analyzed, and the results were reasonably consistent with the potential data. However, an advanced crevice sampling method and installation of a pH electrode instead of the Pt electrode might provide a better representation of actual crevice chemistry.

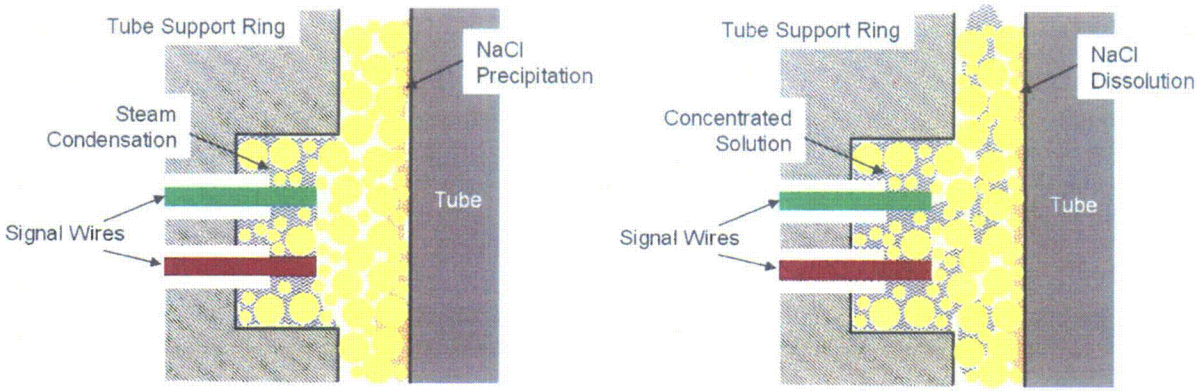

(a) (b)

Figure 48. Schematics of the precipitation and concentration phenomena in the crevice for (a) higher ΔT (80°F and 100°F) and (b) lower ΔT (40°F and 60°F).

4.3 NaCl-03: NaCl (MR=0.3) Test

The influence of [Na]/[Cl] MR on the hideout behavior and Cl volatility was investigated in tests NaCl-03 (MR=0.3) and NaCl-04 (MR=0.7) with 10 ppm Cl. The crevice hideout for MR=1.0 was investigated in NaCl-01 and -02. For the NaCl-03 and NaCl-04 tests, there were major system upgrades and test condition changes: use of magnetite (Fe_3O_4) as packing material, use of tungsten/tungsten oxide electrode as a pH sensor, and installation of a high-pressure injection pump. The experimental setup is described in Sections 2.2 and 2.3. The crevice with a radial gap of 10 mil was packed with diamond grit (127-165 μm-dia), and the crevice with a radial gap of 20 mil was packed with magnetite powder. The measured packing porosities for the 10- and 20-mil gap crevices were 33 % and 78 %, respectively. Only the 10-mil radial gap crevice had ECP electrodes due to the limitation of potential measurement system.

4.3.1 Temperature Data

Figure 49 shows the crevice temperature variation with time in the 10-mil gap crevice packed with diamond powders. Before the first solution injection, all thermocouples indicated about 10°F higher temperatures than the secondary saturation temperature of 500°F. This difference appears to be caused by the diamond powder with its extremely high thermal conductivity surrounding the thermocouple tip area. After the NaCl solution injection, all crevice temperatures started to rise gradually. At ΔT=60°F and 80°F, the temperature elevation was not significant as compared with that at ΔT=40°F. The reference temperature data at these ΔT's with high purity water will permit evaluating the temperature elevation induced by the chemical hideout, but unfortunately only reference data at ΔT=40°F were available. As shown in Figure 49, the second NaCl solution injection to make up depleted bulk ion concentration did not affect the crevice temperatures. Normalized temperatures in the 10-mil gap crevice are plotted in Figure 50 as a function of time. The temperature difference between each crevice temperature and the bulk secondary saturation temperature was divided by the difference between the primary and secondary temperatures. The normalized crevice temperatures show that for ΔT=60°F and 80°F the increase in crevice temperatures was mainly due to the increase in the primary temperature and the temperature difference across the SG tubes; this behavior indicates that the conduction heat transfer by diamond powder is dominant at ΔT=60°F and 80°F as compared with the boiling heat transfer. However, the

normalized crevice temperature data at ΔT=40°F show a different behavior from those of the two higher ΔT cases; hideout is partially responsible for the temperature elevation above the secondary saturation temperature of 500°F.

Figure 51 shows the temperature variation in the 20-mil gap crevice packed with magnetite powder. With high purity water the crevice temperatures are much closer to the secondary saturation temperature as compared with the 10-mil gap crevice, even though T8 shows higher temperature, which appears to be caused by the tip location of the thermocouple. The lower crevice temperature in high purity water with magnetite powder is attributed to the low thermal conductivity of magnetite. After the first NaCl solution injection, all thermocouples indicated a gradual temperature elevation. As observed in the 10-mil gap crevice, the significant temperature elevation did not occur at ΔT=60°F and 80°F compared with that at ΔT=40°F. When decreasing ΔT from 80°F to 40°F, the temperatures returned to the final values of the initial ΔT=40°F test. Figure 52 shows the normalized crevice temperatures in the 20-mil gap crevice packed with magnetite powder. As observed in Figure 50, the normalized temperatures did not vary with time except for ΔT=40°F.

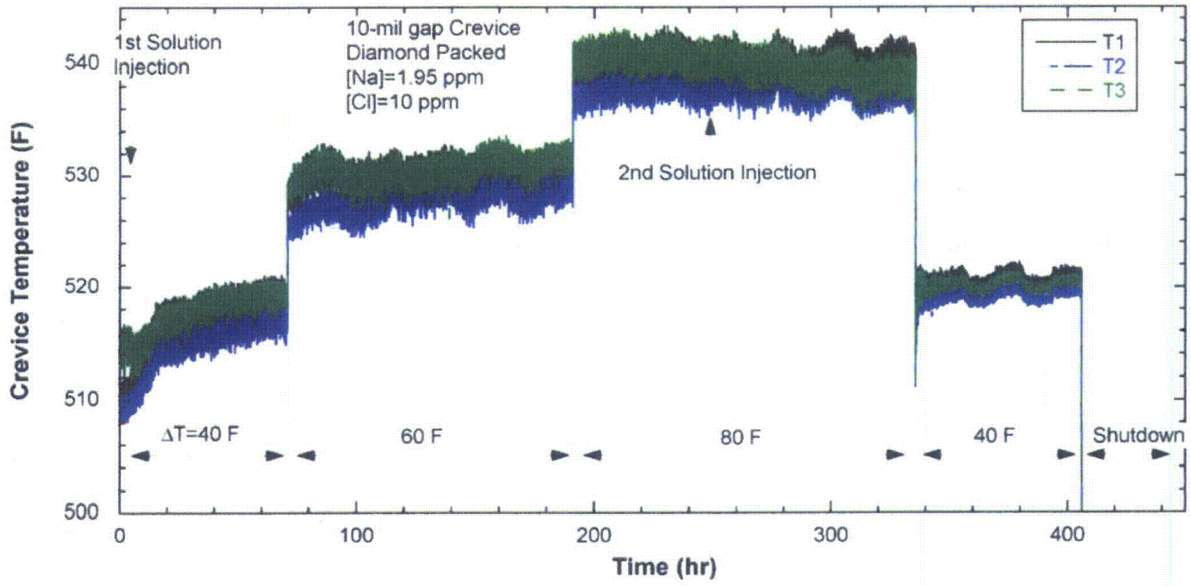

Figure 49. Crevice temperature variation with time in a 10-mil gap crevice packed with diamond powder (NaCl-03).

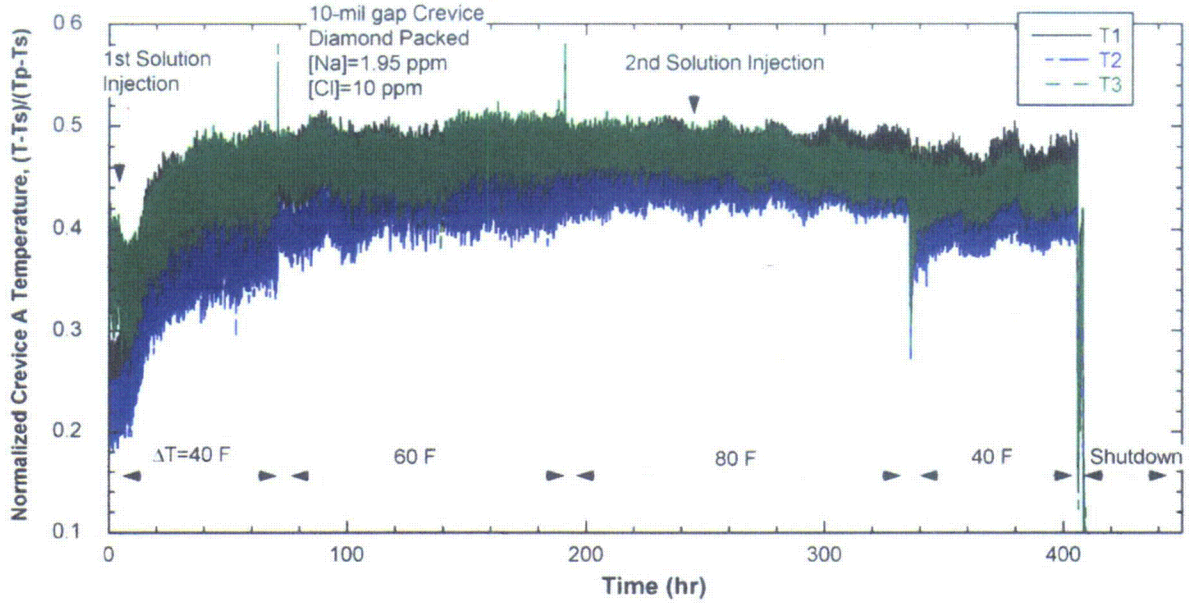

Figure 50. Normalized crevice temperature variation with time in a 10-mil gap crevice packed with diamond powder (NaCl-03).

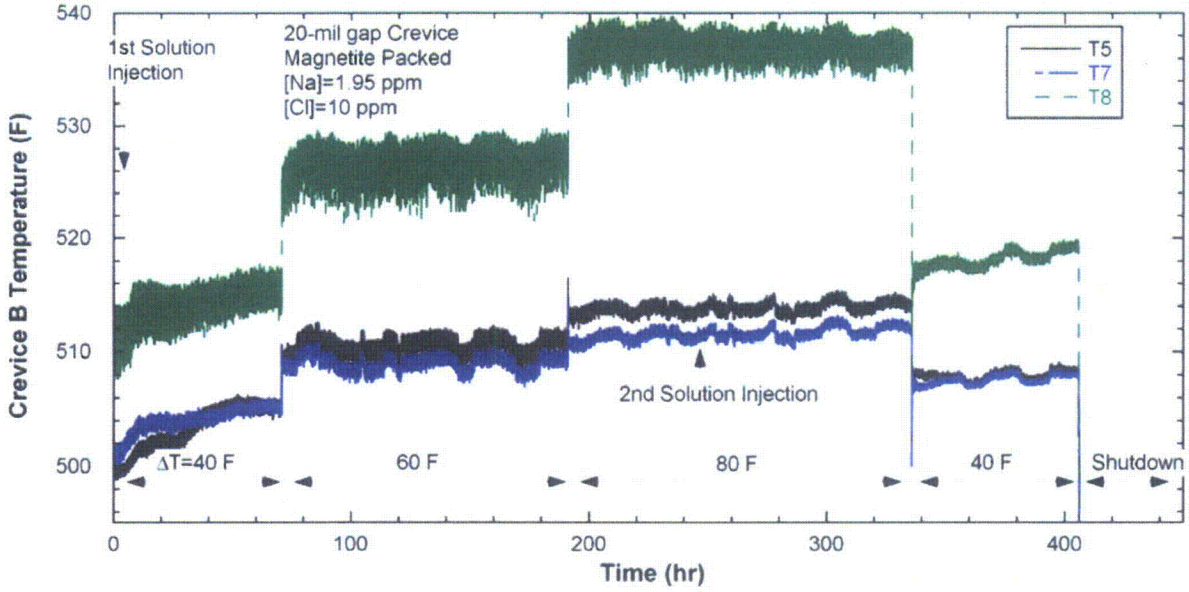

Figure 51. Crevice temperature variation with time in a 20-mil gap crevice packed with magnetite powder (NaCl-03).

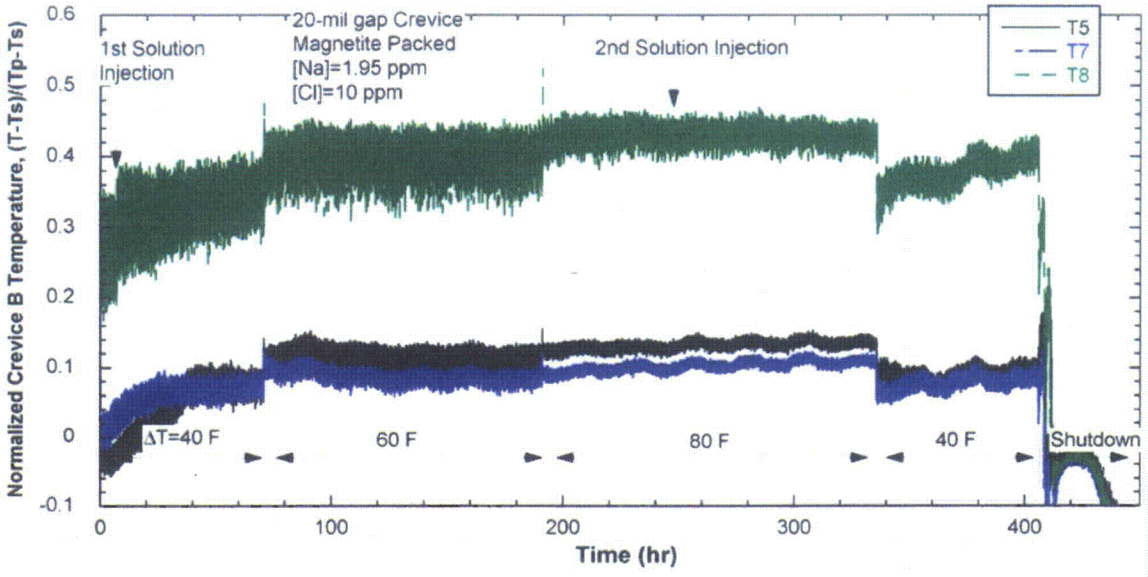

Figure 52. Normalized crevice temperature variation with time in a 20-mil gap crevice packed with magnetite powder (NaCl-03).

4.3.2 Bulk & Crevice Chemistry

The variations in bulk conductivity and the ion concentrations for bulk samples are plotted in Figure 53. The bulk conductivity responded quickly to the change of the bulk solution chemistry. At ΔT=40°F, large hideout was indicated by the bulk conductivity change, which is much greater than that of the previous test NaCl-02 with MR=1.0, but in the NaCl-02 test, ΔT=80°F was followed by ΔT=40°F. The IC analysis for Cl showed better fit to the bulk conductivity variation than the ISE results. The ISE tends to underestimate the Cl concentration. The plateau that occurred after the second NaCl solution injection is attributed to the bulk conductivity exceeding the upper limit of the conductivity meter. The accumulated impurity mass or concentration in crevices can be estimated from the bulk solution analysis. This is discussed in Section 4.3.4.

Figure 54 shows crevice conductivity versus bulk conductivity for the 10-mil gap crevice. The crevice conductivity started to show hideout 40 hrs after introducing the NaCl. We attribute this effect to the fact that, as impurity concentration in the crevice proceeded, the pore between the two conductivity probes became filled with concentrated liquid rather than steam, which caused the conductivity signal to start increasing. The additional increase in crevice conductivity after the ΔT increased from 40°F to 60°F was attributed to the increase of the impurity concentration in the crevice. The plateau of the crevice conductivity at ΔT=60°F (from 90 to 140 hours in Figure 54) occurred because the actual conductivity exceeded the upper limit of the measurement of the conductivity meter. The drop and sudden recovery of crevice conductivity at 120 hours occurred because, at this time, the steam phase was located between the two conductivity probes, which blocked the electric path. The gradual decrease of conductivity at ΔT=60°F could be attributed to several causes. In general crevice conductivity can vary in three ways: a liquid-to-vapor ratio change between the two conductivity probes, an ion composition/concentration change, and salt precipitation. At ΔT=60°F, based on the temperature data, it is not likely that NaCl precipitation occurred because the measured superheat was less than that for the NaCl solubility limit, 46°F. The ion composition and concentration might have changed; metal cations were released by corrosion of alloy 600 tubing and Na diffused out of the crevice, which is called electromigration effect

and is discussed again in Section 6.3.6. The crevice chemistry change at that time is supported by the increase in bulk Na concentration and post-test tube surface examination revealing heavy gouging. After changing ΔT from 60 to 80°F, the crevice conductivity decreased more, which is interpreted as the result of all three possible causes. Precipitation of NaCl might have occurred on the tube surface, and steam phase might have become dominant. But a change in liquid-to-vapor ratio is more likely because higher ΔT brings a higher boiling rate and more steam phase. However, the crevice conductivity variation and scattering after the 2nd solution injection is difficult to be explained by three ways. After the decrease of ΔT from 80°F to 40°F, the conductivity signal becomes noisy again and fluctuates presumably because of the residual chemistry developed during ΔT=80°F test.

Figure 55 shows the analysis results for crevice solution samples. The ICP and IC analyses for the 10-mil gap crevice packed with diamond showed higher Na and Cl concentrations at ΔT=40°F and 60°F than that at ΔT=80°F, probably because at a higher ΔT the steam phase was more dominant so that more steam was extracted from the solution line. For the 20-mil gap crevice packed with magnetite, the Cl ion concentration was much higher than the Na ion concentration, and the molar ratio was less than 0.2 in most samples based on the IC results. These findings suggest that either Cl is preferentially concentrated in the magnetite-packed crevice or the steam phase is more dominant at the same ΔT as compared with a diamond-packed crevice. The absolute concentration of Na and Cl in the magnetite-packed crevice was much lower than that in the diamond-packed crevice. This result suggests that it takes much longer for impurities to be concentrated in the magnetite-packed crevice than in the diamond-packed crevice, and the wider gap results in a higher mixing tendency between crevice and bulk solutions and leads to lower concentration. The ISE ion concentration results are also plotted in Figure 55. The ISE tends to have better accuracy for higher concentration (>100 ppm). At lower concentration, the ISE underestimates the Cl concentration, and the ISE is not consistent with ICP analysis results for Na especially at lower concentrations (<100 ppm).

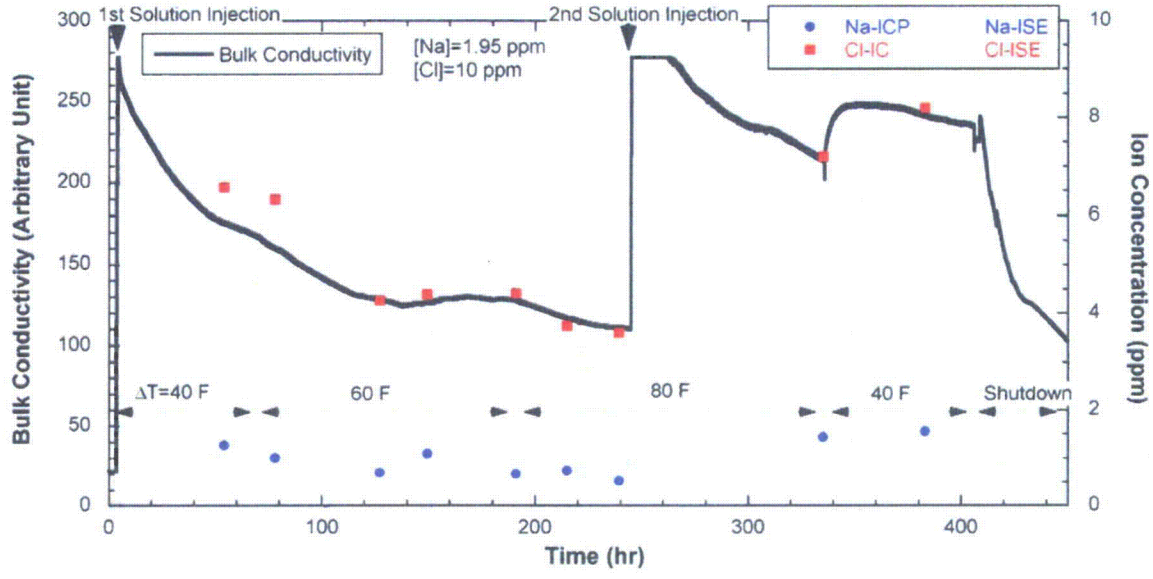

Figure 53. Variation in bulk conductivity and ion concentration with time (NaCl-03).

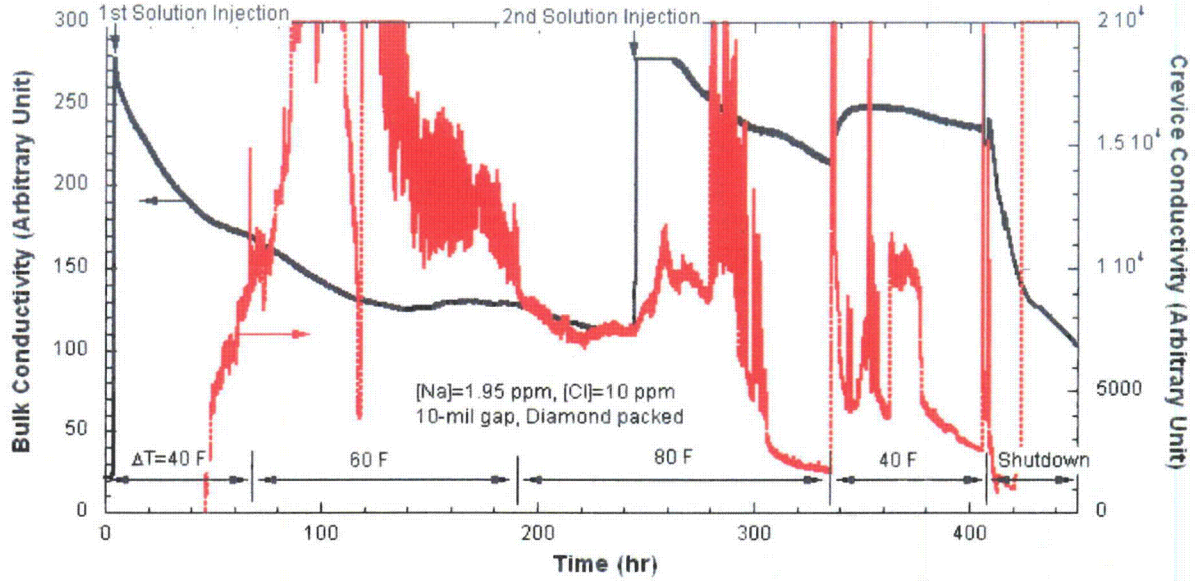

Figure 54. Variation in bulk and crevice conductivity with time in a 10-mil gap crevice packed with diamond powder (NaCl-03).

The sudden drop of crevice concentration in the sample taken at 120 hours was followed by the recovery of concentrations for both Na and Cl. To better understand this unexpected crevice concentration drop and recovery, the crevice concentrations in solution samples were compared with the crevice conductivity variation shown in Figure 56. Taking into consideration the time delay in the crevice solution samples, we concluded that when the sudden crevice conductivity dropped is close to when the crevice ion concentration dropped. The crevice temperature data did not show any significant change at that time, but this result suggests that crevice instability possibly happens for short periods.

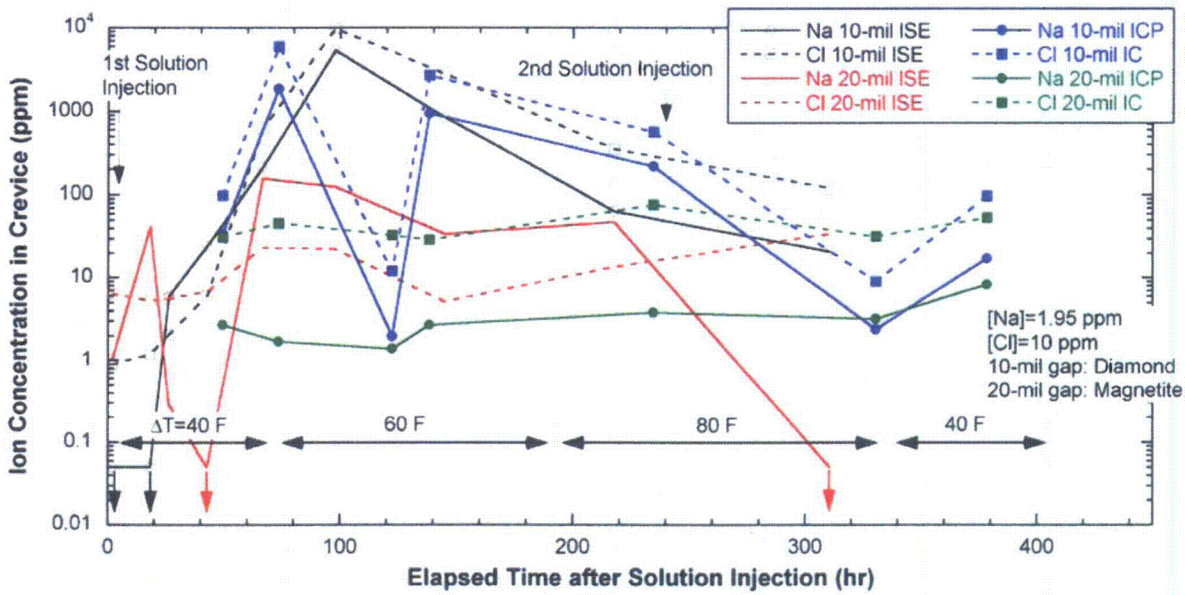

Figure 55. Concentration results for crevice solution samples by using ICP/OES for Na, IC for Cl, and ISE for Na and Cl (NaCl-03).

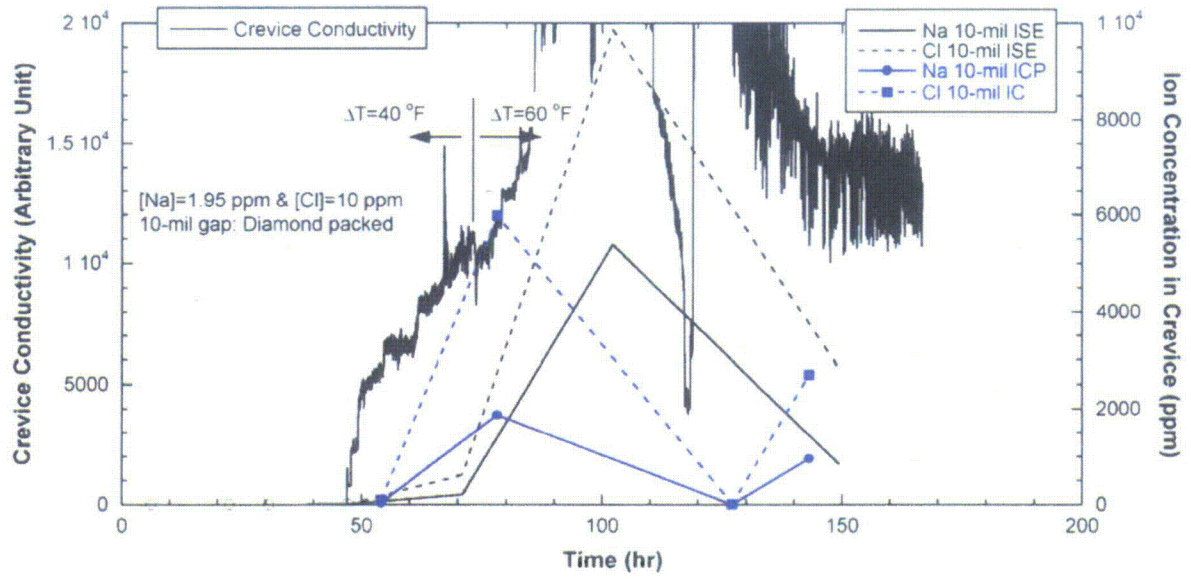

Figure 56. Crevice conductivity variation with time in the 10-mil gap crevice packed with diamond along with analysis results of crevice samples (NaCl-03).

4.3.3 ECP Measurement

The Pt electrode potentials in the bulk and the 10-mil crevice are plotted in Figure 57. Right after the first injection of MR=0.3 NaCl solution, the bulk and the crevice potentials increased because the MR=0.3 NaCl solution is more acidic than pure water. After this test, NaCl-03, the Pt electrode was not used to estimate the solution pH. The crevice Pt potential did not significantly vary with ΔT except for an initial transient period. The oscillation of the Pt bulk electrode potential for the initial 20 hours may be attributed to the dissolved oxygen that originated from the injected solution, which might not have been sufficiently purged. After the second NaCl solution injection, the bulk and crevice potentials increased. Based on the rapid response of the crevice potential to the bulk chemistry change, it is likely that the 10-mil gap crevice was mixed well with the bulk water due to the highly permeable diamond packing. Figure 58 shows the Ni electrode potential variation with time. As was observed in the Pt electrode potential, the Ni electrode potentials in the bulk water and crevice responded quickly to the bulk chemistry change. The crevice Ni potential gradually decreased, probably because Na was preferentially concentrated, and this decrease led to the increase of crevice pH. However, to estimate the crevice pH, the tungsten electrode potentials should be used. The Ni electrodes in the bulk solution and the crevice showed as quick a response to the second NaCl solution injection as the Pt electrodes.

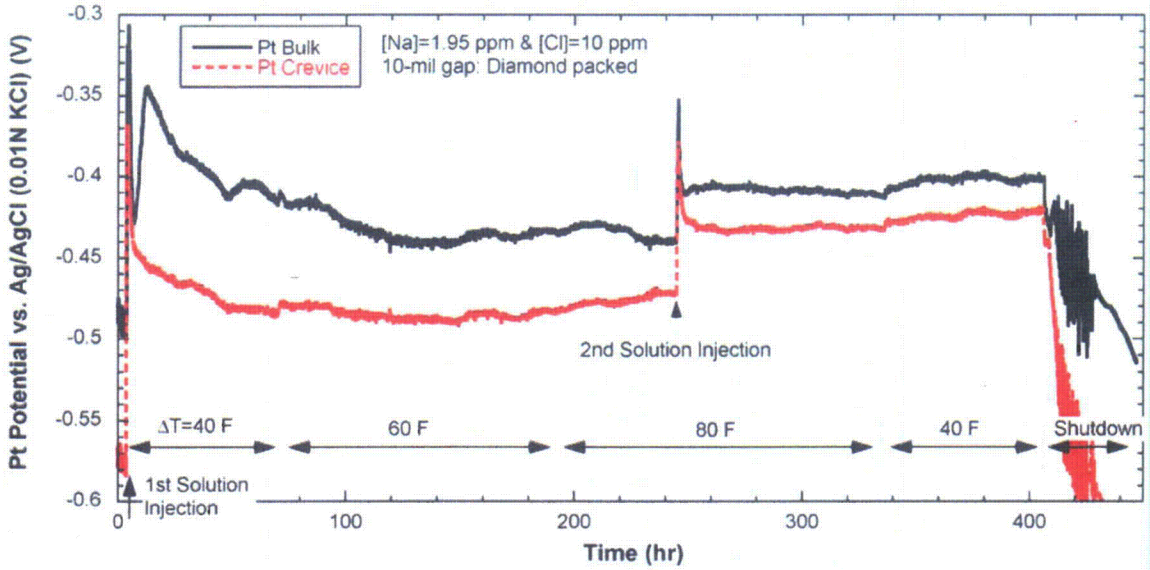

Figure 57. Variations in Pt electrode potential with time in bulk and 10-mil gap crevice packed with diamond (NaCl-03).

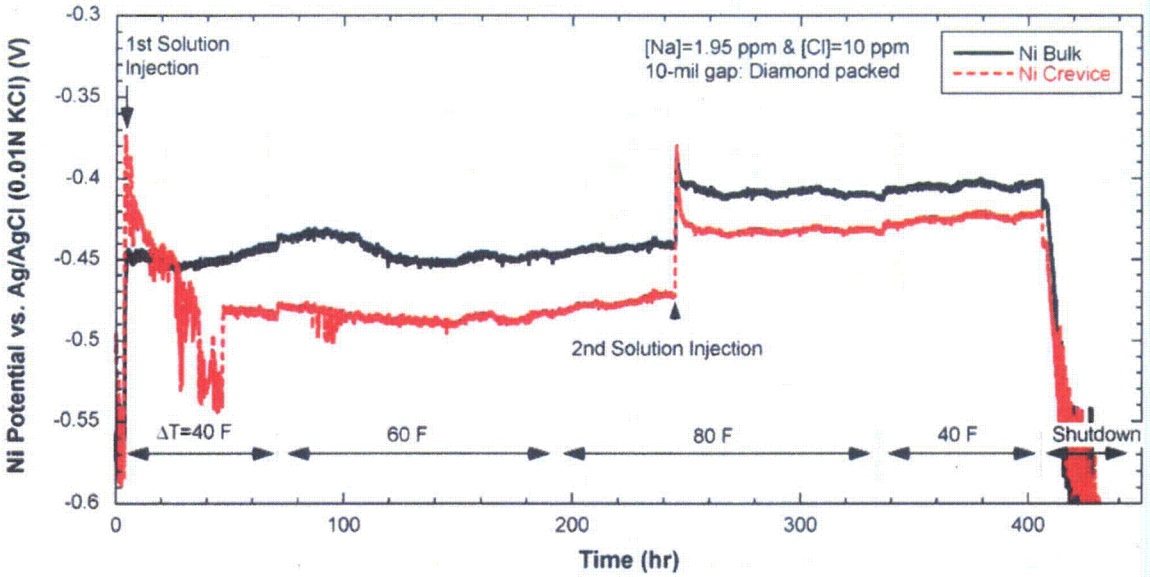

Figure 58. Variations in Ni electrode potential with time in bulk and 10-mil gap crevice packed with diamond (NaCl-03).

The tungsten potentials measured in the 10-mil gap crevice and the bulk solution are plotted in Figure 59. These potentials increased after the first NaCl solution injection because the bulk solution was acidified by the test solution injection from a neutral condition of high purity water. Then, the crevice tungsten potential dropped quickly, followed by a more gradual decrease. This finding might be interpreted as meaning that because of the volatility effect of Cl, less volatile Na was preferentially concentrated. The crevice pH increase associated with the crevice tungsten potential decrease was expected with the increase of ΔT because the volatility effect of Cl becomes more significant at higher boiling rate. However, the crevice tungsten potential slowly moved in a positive direction until the end of

the test even though ΔT was increased, which does not support the expected volatility effect of Cl with ΔT variation. The measured crevice pH based on tungsten electrode potentials tends to reflect the decrease of crevice pH with ΔT. This observation may be attributed to the location of the tungsten electrode tip. As reported by Baum,[3] Na is expected to be preferentially concentrated right on the tube surface. If the tungsten electrode tip is located away from the tube surface, volatilized Cl from the surface would be present around the tungsten tip area and might become dominant with the increase of ΔT.

The bulk tungsten potential showed a gradual decrease with time until the second solution injection. This potential decrease may be interpreted as a bulk solution pH increase. But it should be noted that, as discussed earlier with regard to Figure 44, bulk solution pH can be increased by the dilution of ion concentration itself, even if the Na-to-Cl molar ratio is constant. After the second solution injection, the bulk tungsten potential increased. It was intended to bring the bulk potential to the initial value after the first injection, but the potential value was slightly higher than that because more Cl ion was injected than needed. The potential difference between the bulk and crevice appears to be consistent even after the second solution injection, which is evident in Figure 60. After the ΔT was decreased from 80°F to 40°F, the bulk tungsten potential increased due to the return of Cl and Na to the bulk solution, and it then stabilized. After the MB shut-down, the potential difference between the bulk and crevice increased, and this result might indicate that the crevice had become more acidic during this test.

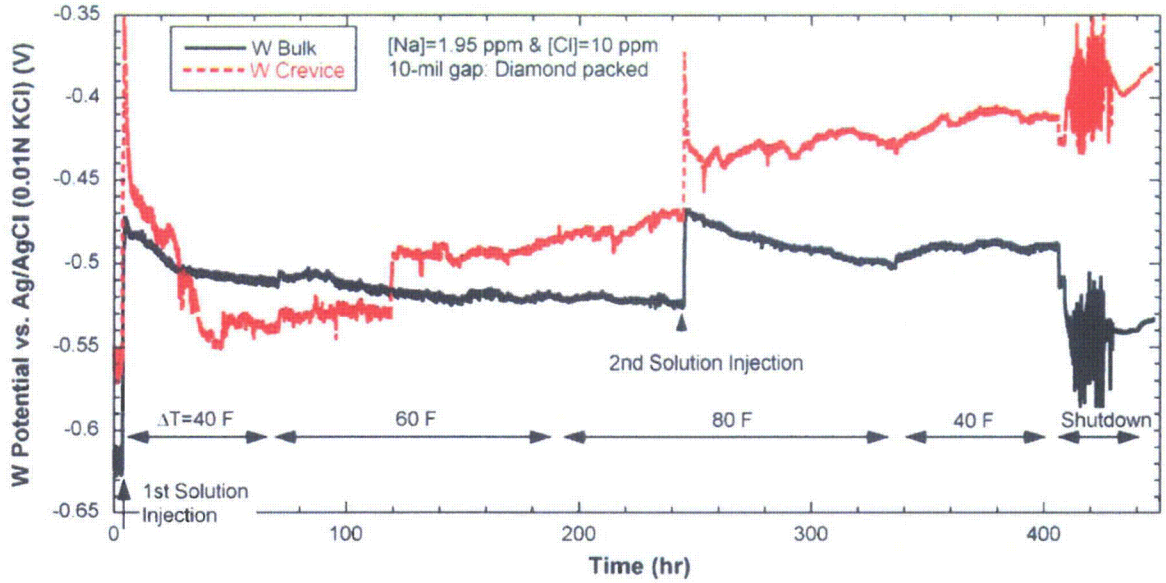

Figure 59. Tungsten electrode potential variations with time in bulk and 10-mil gap crevice packed with diamond (NaCl-03).

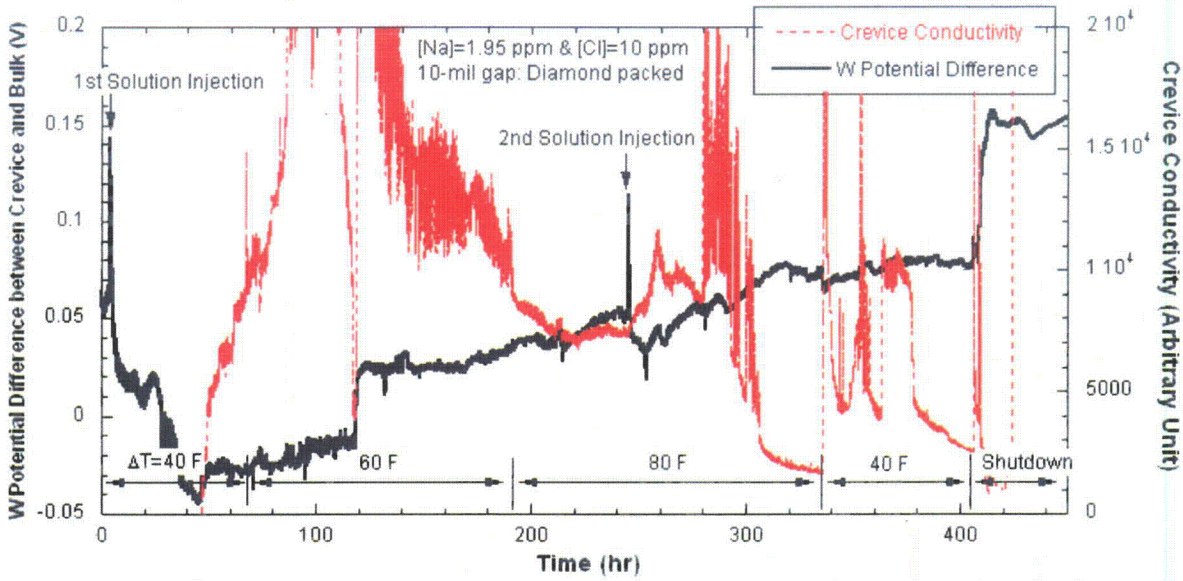

Figure 60. Tungsten potential difference between crevice and bulk compared with crevice conductivity variation in 10-mil gap crevice packed with diamond (NaCl-03).

Figure 60 shows the variations in the tungsten potential difference between the crevice and bulk, as well as the variations in crevice conductivity. The crevice was more alkaline than the bulk during the period of 30-120 hours. The time when the crevice conductivity dropped exactly corresponds to the time when the crevice tungsten potential suddenly jumped. At 120 hours, it is possible that steam was generated near the crevice conductivity probes and this steam also affected the crevice tungsten potential. The higher ΔT and resultant increased steam phase might maintain the increased crevice tungsten potential. The tungsten potential difference did not change significantly after the second NaCl solution injection. The potential difference did not return to the previous value after decreasing ΔT from 80°F to 40°F but maintained a similar value. Since the second ΔT=40°F test had a different operating history from the first one, the tungsten potential difference is not supposed to be the same. Formerly precipitated NaCl or the chemistry that developed at ΔT=80°F would affect the chemistry when the ΔT returned to 40°F.

4.3.4 Discussion

Potentials and pH Analysis

Figure 61 shows the tungsten potential difference as a function of the pH difference between the bulk and 10-mil crevice samples. The sample pH was calculated by using the MULTEQ code based on the solution sample analysis. The tungsten potentials measured at the time when the crevice and bulk samples were taken are used in this figure. The calculated pH difference data indicate that the crevice pH is always lower than the bulk pH. The tungsten potential difference data agreed with the calculated pH difference, except for two data points suggesting that the crevice was more alkaline than the bulk. A trend is not apparent from the data shown in Figure 61. The data in Figure 47 showed at least a linear relationship, even though the slope was far from ideal behavior. Because of the data scattering in Figure 61, the crevice and bulk data were plotted independently. The tungsten potentials measured in the crevice and the bulk are plotted as a function of predicted pH by MULTEQ in Figure 62. The bulk data show

good linear behavior, while the crevice data still do not show any linearity between tungsten potential and solution pH. The measured ECP/pH slope for bulk solution data is -88 mV/pH, which is close to the Nernstian value of -106 mV at 260°C (500°F). The bulk data in Figure 62 confirm that the tungsten electrode can be used as a precise pH electrode at high temperature and in a slightly acidic environment. The data scattering of the crevice data can be attributed to several factors: possible problems during the electrode preparation, the location of the tungsten electrode tip with respect to the tube surface, the total exposed area of the tungsten electrode tip, the accuracy of the MULTEQ calculation, and the representativeness of the crevice solution samples. The bulk and crevice tungsten electrodes were prepared with the same materials and procedures, so that the electrode preparation appears appropriate. The location of the crevice tungsten electrode tip might be far from the tube surface so that the tungsten potentials did not represent the actual crevice pH variation well. The total exposed area of the tungsten electrode tip may be a problem. The bulk electrode has an exposed wire tip that is about 6-7 mm long, but the crevice tungsten electrode has an exposed tip that is only about 1 or 2-mm long, which might decrease the electrode sensitivity. However, the crevice electrode tip cannot be exposed too much if we want to measure the narrow-gap crevice chemistry. The MULTEQ-predicted pH appears to have a reasonable accuracy because the bulk tungsten potentials are well fitted to the bulk sample pH calculated by MULTEQ. The dilution of crevice samples is possible since the crevice and bulk solution interact, but it is difficult to quantitatively evaluate the dilution effect of crevice samples.

One possible correction for the crevice samples data is to consider the time delay effect determined by the dead volume of the sample extraction line and valve, as mentioned in Section 3.2.2. The total dead volume of the extraction line and valve is 90 μL, and the volume of crevice sample varied from 50 to 100 μL. For a simple correction, if the volume of crevice sample is equivalent to that of the dead volume of the extraction line, a crevice sample taken at certain time represents the chemical condition at the time when the very last sample was taken. Crevice tungsten potentials were corrected based on the time delay effect, as shown in Figure 63. Crevice data still show scattering but at least appear to roughly show a decreasing trend with pH. The bulk data did not have to be corrected because there was enough sample volume. The bulk ECP/pH slope after including one more data point measured before chemical injection is much closer to the Nernstian value compared with the data in Figure 62. As discussed in the post-test examination, severe gouging was observed on the tube surface. Therefore, the crevice pH estimation from the crevice samples appears to represent the corrosive crevice chemistry developed in this test.

Figure 64 shows the MR variations as a function of time in the bulk and 10- and 20-mil gap crevices. The MR in the 10-mil gap crevice is always higher than that in the bulk. The MR data cannot specify the solution pH but can suggest the preferential Na concentration in the diamond-packed crevice. The bulk MR was varied within the range of 0.2-0.3, except for one point at 150 hours. At that time the analysis results for bulk samples indicated the return of Na ion from crevices, which increased the bulk MR. The reason for the Na return from crevices is given in Section 4.4.5, but briefly, metal cations generated by the tube corrosion could be driving Na ions out of the crevice. The MR in the 20-mil gap crevice tends to follow the bulk MR variation tendency, and this trend suggests that the extracted sample from the 20-mil gap crevice might contain a significant amount of bulk solution.

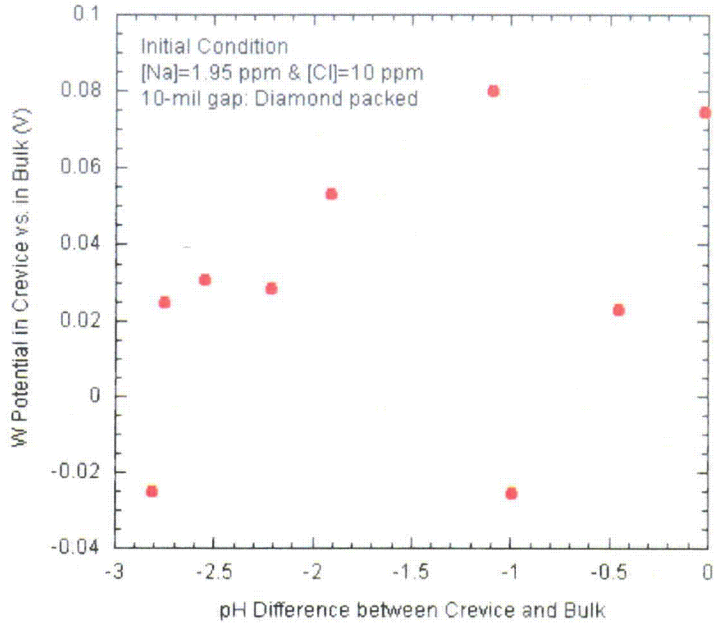

Figure 61.
Plot of MULTEQ-predicted pH difference and tungsten potential difference between bulk and 10-mil gap crevice packed with diamond (NaCl-03).

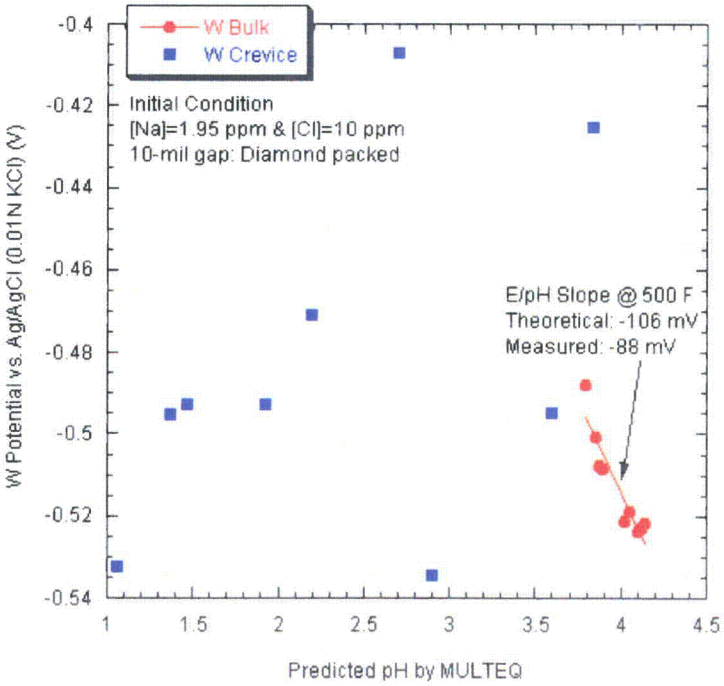

Figure 62.
Tungsten potential measured in crevice and bulk as a function of predicted pH by MULTEQ (initial [Na]/[Cl]=0.3; NaCl-03).

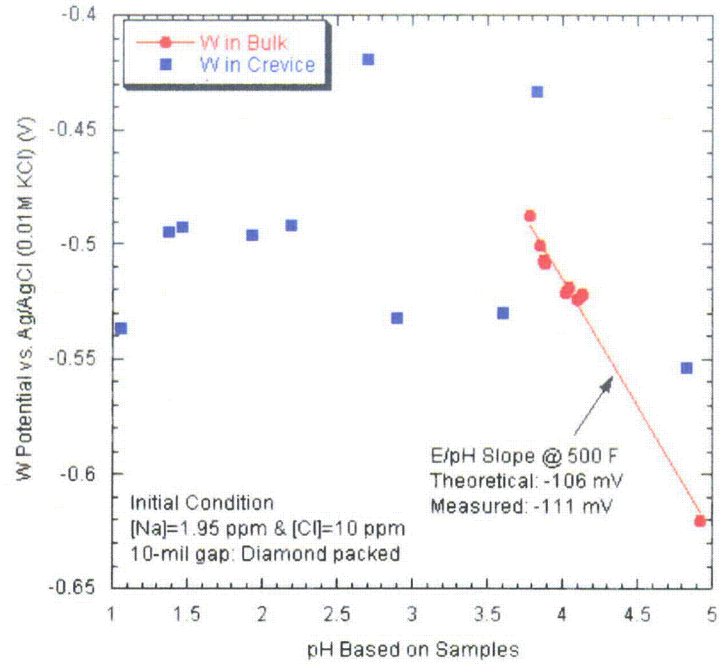

Figure 63.
Tungsten potentials as a function of the calculated pH based on solution samples from crevice and bulk (NaCl-03).

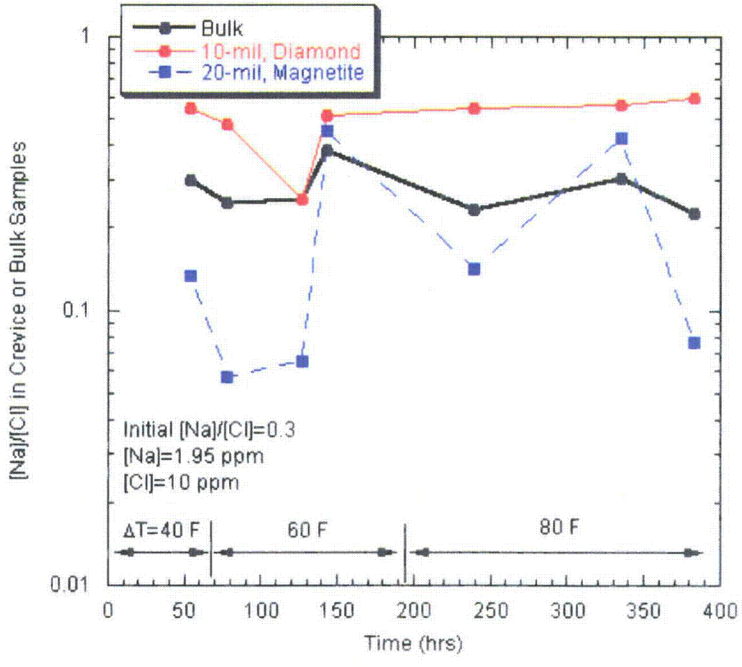

Figure 64.
Molar ratio variations as a function of time in bulk and crevices (NaCl-03).

Mass Balance Analysis

Since the Argonne MB is a closed system, the crevice impurity accumulation can be calculated from the bulk chemical analysis data over time. Figure 65 shows the total accumulated moles of Na and Cl in the crevices as a function of time. The loss of impurity mass by crevice and bulk solution sampling was also considered in calculating the mass balance. The data measured before additional NaCl impurities were injected into the bulk at the elapsed time of 240 hrs were used. Since the atomic weights of Na and Cl are different, a molar unit was used instead of a mass unit. The MR for total accumulated Na and Cl does not correspond to any MR in either diamond- or magnetite-packed crevices. Its value is between the MRs of the diamond-packed crevice and bulk. It appears that Na concentrates preferentially in a diamond-packed crevice and Cl concentrates preferentially in a magnetite-packed crevice. Since, with bulk chemistry data, we cannot distinguish how much impurity hides out in diamond- and magnetite-packed crevices, respectively, a single- rather than a double-crevice test would be more appropriate for the crevice estimation with the bulk data in a closed system like the Argonne MB. As shown in Figure 65, Cl concentration tends to reach a steady state at each ΔT, while the Na concentration does not. The hideout rate into a crevice usually depends on the bulk concentration. Since the MR of the test solution is 0.3, the bulk concentration of Na is much less than that of Cl, and it thus takes longer to reach a steady state. The Na and Cl moles in the crevice vs. ion exposure is shown in Figure 66. The "exposure" is defined by the integration of the variation in bulk concentration with time. We can compare each ion's hideout rate with the exposure unit regardless of the bulk concentration. As shown in Figure 66, the hideout rates of Na and Cl appear to be similar. But, when interpreting these hideout rates, one should note the two different crevice packings used in this test. It is likely that the preferential Na hideout in the diamond-packed crevice and the preferential Cl hideout in the magnetite-packed crevice made a similar contribution to the bulk impurity change. A single crevice test is recommended for estimation of the precise crevice hideout.

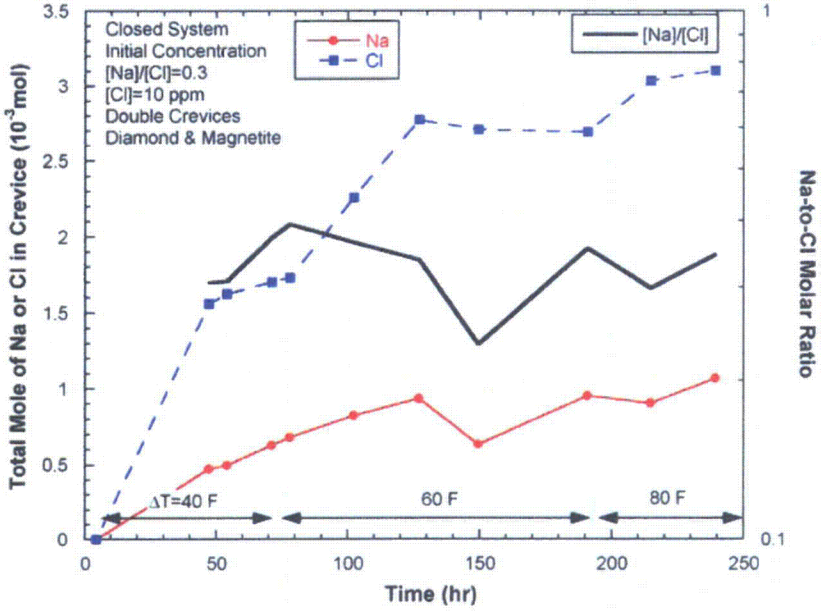

Figure 65.
Total accumulated moles of Na and Cl in crevices as a function of time (NaCl-03).

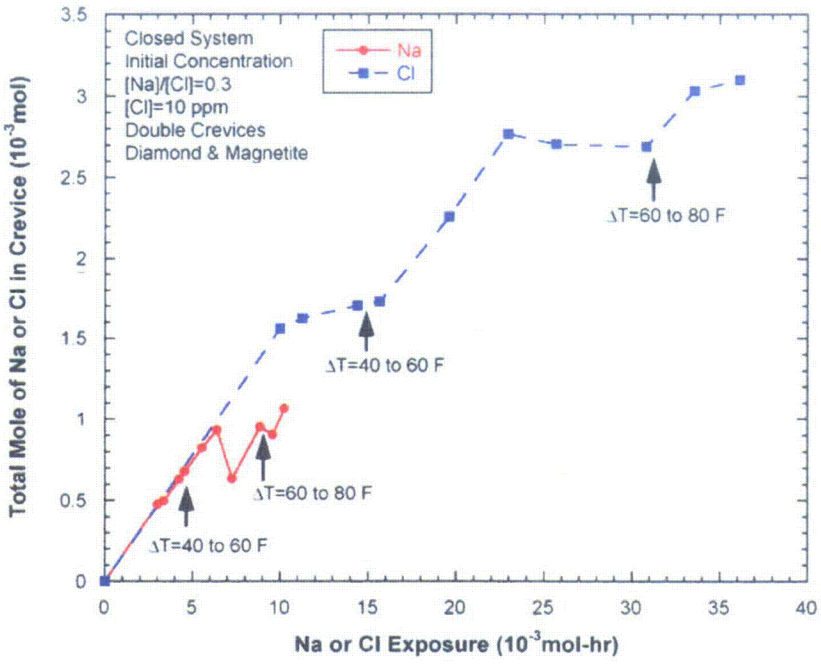

Figure 66.
Total accumulated moles of Na and Cl in crevices as a function of exposure (NaCl-03).

4.3.5 Summary

We introduced W/WO_x electrodes as pH electrodes in the crevice and the bulk water chemistry. In the bulk water chemistry with MR=0.3, the W/WO_x electrode showed a good linearity with respect to the pH variation, and the ECP/pH slope was close to the Nernstian value. The crevice tungsten potential indicated that the crevice was initially alkalinized due to the volatility of Cl, followed by its gradual acidification with time and ΔT. Crevice samples and the post-test examination, which are discussed in Section 4.4.5, indicated that a strongly acidic crevice packed with diamond had developed during the NaCl-03 test. Bulk conductivity variation and bulk samples indicated that Na ions were driven out of the crevice at ΔT=60 °F. This behavior might be caused by the accumulation of metal cations and resultant Na ion's migration to conserve charge neutrality. Molar ratio analysis for crevices and bulk samples showed that the MR in the diamond-packed crevice was always higher than that in the bulk. For the magnetite-packed crevice, Cl appears to be preferentially concentrated as compared with the diamond-packed crevice, probably because of adsorption of Cl to magnetite. In double crevice tests, it is difficult to estimate how much impurity is concentrated at each crevice from bulk concentration data.

4.4 NaCl-04: NaCl (MR=0.7) Test

The NaCl-04 test followed the NaCl-03 test without opening of the MB. The secondary chamber was cleaned with high purity water several times to remove possible residual Na and Cl ions. The test water was prepared with NaCl powders and concentrated HCl solution. The test solution was injected by means of a high-pressure injection pump when the primary and secondary temperatures became stabilized with high purity water. The crevice packing and configurations are the same as those for the NaCl-03 test. The detail test system and instrumentation are described in Sections 2.2 and 2.3.

4.4.1 Temperature Data

The temperature variations with time in the 10-mil gap crevice are plotted for NaCl-04 in Figure 67 . The temperature increased gradually after the solution injection and stabilized after 20 hours. After changing ΔT from 40 to 60°F and from 60 to 80°F, the time-dependent temperature increase was not observed, but the crevice temperature remained nearly constant. As compared with the NaCl-03 test, the crevice temperatures with high purity water were higher. This observation suggests that the NaCl from the previous test, NaCl-03, was not completely returned to bulk water, and the crevice still had some impurities. The steady-state crevice temperatures at each ΔT were almost the same as those in the previous test, shown in Figure 49. Figure 68 shows the variations in normalized crevice temperature with time in the 10-mil gap crevice packed with diamond powder. The crevice temperature elevation is clear at ΔT=40°F. The normalized temperatures do not significantly change after increasing ΔT, indicating that conduction heat transfer is dominant in the crevice. As shown in Figures 67 and 68, the T2 thermocouple read 4-5°F lower temperature than it did in the previous test. This thermocouple was probably not fixed rigidly enough, and its position might have moved slightly out from the tube surface during cool-down or heat-up.

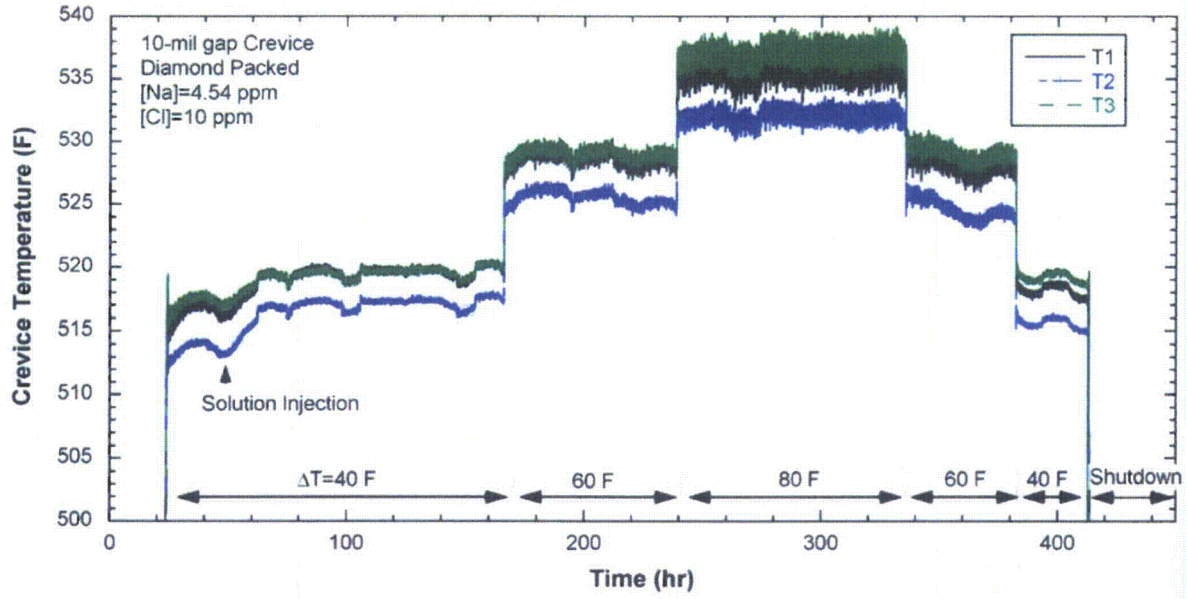

Figure 67. Temperature variation in 10-mil gap crevice with time and locations of TCs (initial [Na]/[Cl]=0.7; NaCl-04).

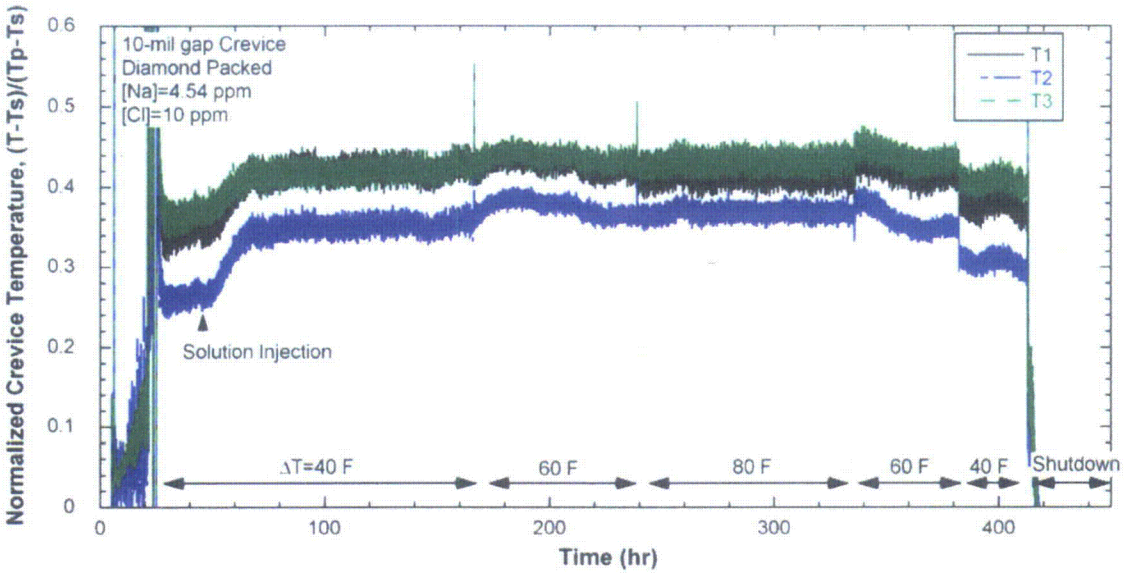

Figure 68. Normalized temperature variation in 10-mil gap crevice (initial [Na]/[Cl]=0.7; NaCl-04).

In Figure 69, the crevice temperature variations with time in the 20-mil gap crevice are plotted. The temperature at T5 only increased after the solution injection and dropped suddenly during ΔT=80°F. However, the other two thermocouples did not show any temperature increase, as they did in the previous test, NaCl-03. Some magnetite powder may have been dislodged from the crevice after the NaCl-03 test. At ΔT=80°F, T5 suddenly dropped to the bulk solution temperature, indicating that the boiling phenomenon in the magnetite-packed crevice is not stable or that the magnetite powder moved around in the crevice. Normalized temperatures in the 20-mil gap crevice are plotted as a function of time in Figure 70. The normalized temperature was relatively independent of the change in ΔT. This behavior indicates that conduction heat transfer is dominant in both the 20- and 10-mil gap crevice.

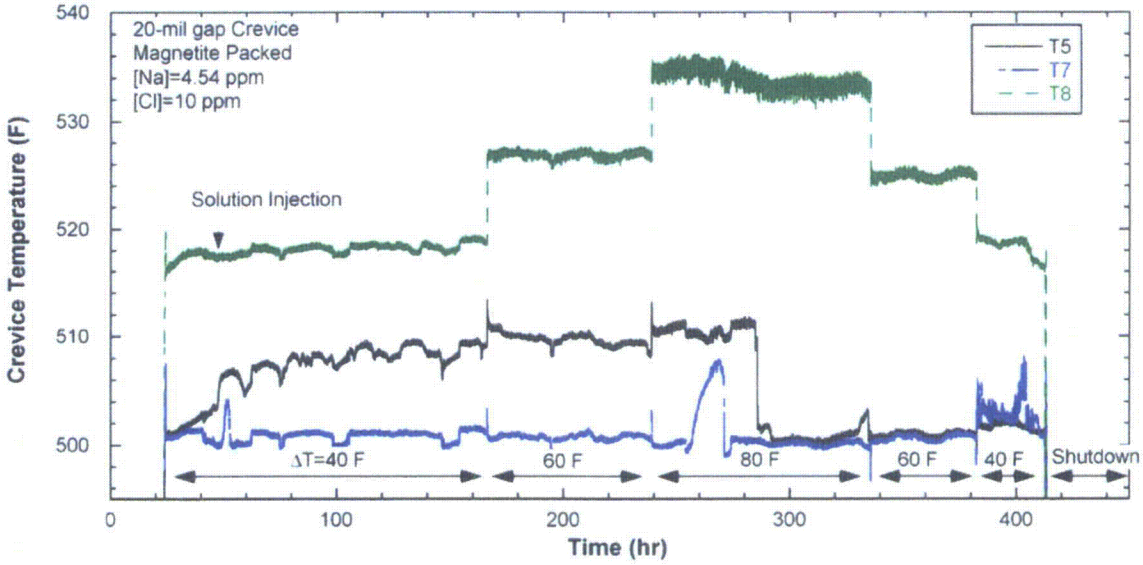

Figure 69. Temperature variation in 20-mil gap crevice with time and locations of TCs (initial [Na]/[Cl]=0.7; NaCl-04).

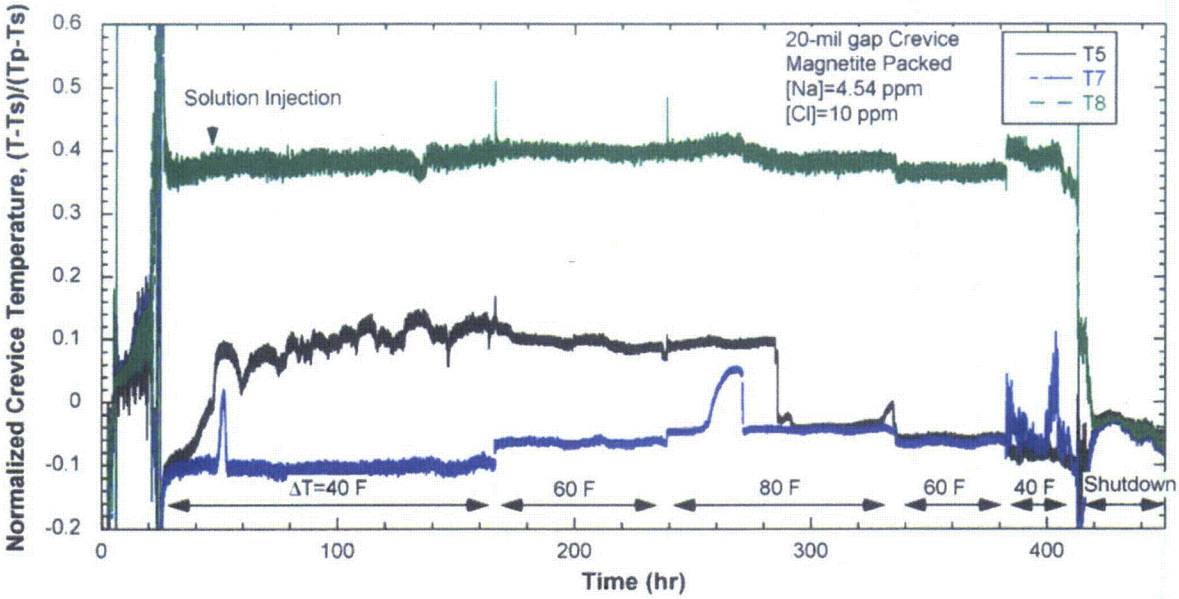

Figure 70. Normalized temperature variation in 20-mil gap crevice (initial [Na]/[Cl]=0.7; NaCl-04).

4.4.2 Bulk & Crevice Chemistry

The variations in the bulk conductivity and the bulk solution analysis are plotted as a function of time in Figure 71,. The ion concentrations are consistent with the measured bulk conductivity. The bulk conductivity did not reach a steady state and increased with decreasing ΔT. In Figure 72, the crevice conductivity in the 10-mil gap crevice packed with diamond is plotted as a function of time. The crevice conductivity increased quickly after the solution injection, but it started to decrease 20 hours later. When increasing ΔT from 40°F to 60°F, the crevice conductivity variation was similar. At ΔT=80°F, the crevice conductivity stabilized at a low value (nearly the same as in high purity water), which means that the steam phase is dominant in the crevice at higher temperature and that possible NaCl precipitation occurred on the tube surface. However, the crevice conductivity did not increase after changing ΔT from 80°F to 60°F and from 60°F to 40°F. After the decrease of ΔT from 80°F to 60°F, the crevice conductivity quickly increased, but it subsided and stabilized at a similar level to that at ΔT=80°F. After the shut-down the crevice conductivity quickly increased then slowly decreased, indicating the hideout return of impurities from the crevice.

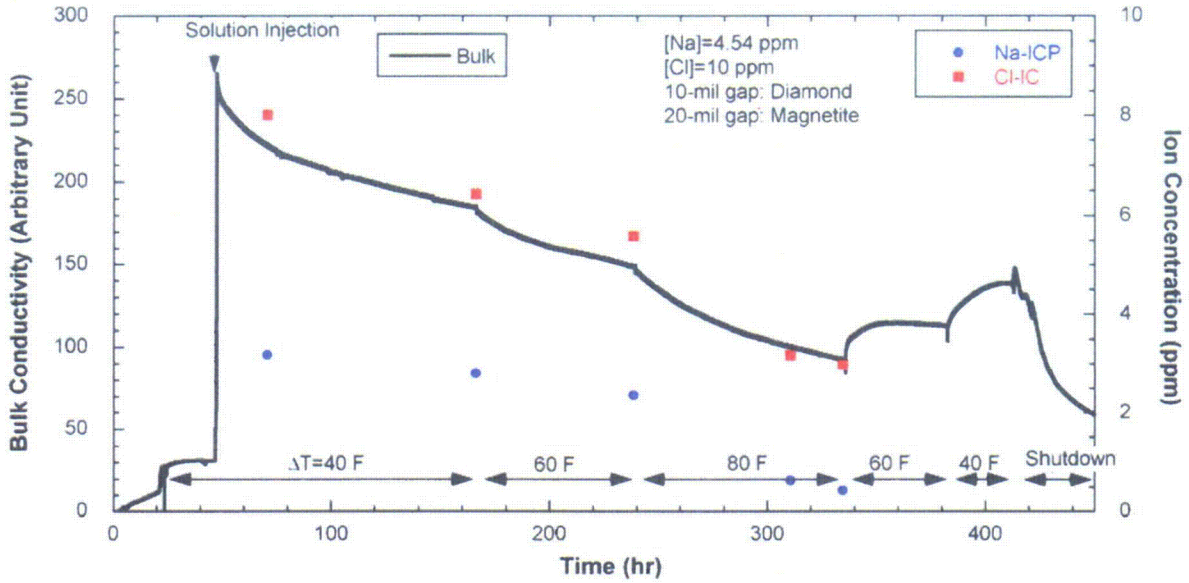

Figure 71. Bulk conductivity variation and measured Na and Cl concentrations in bulk water samples (NaCl-04).

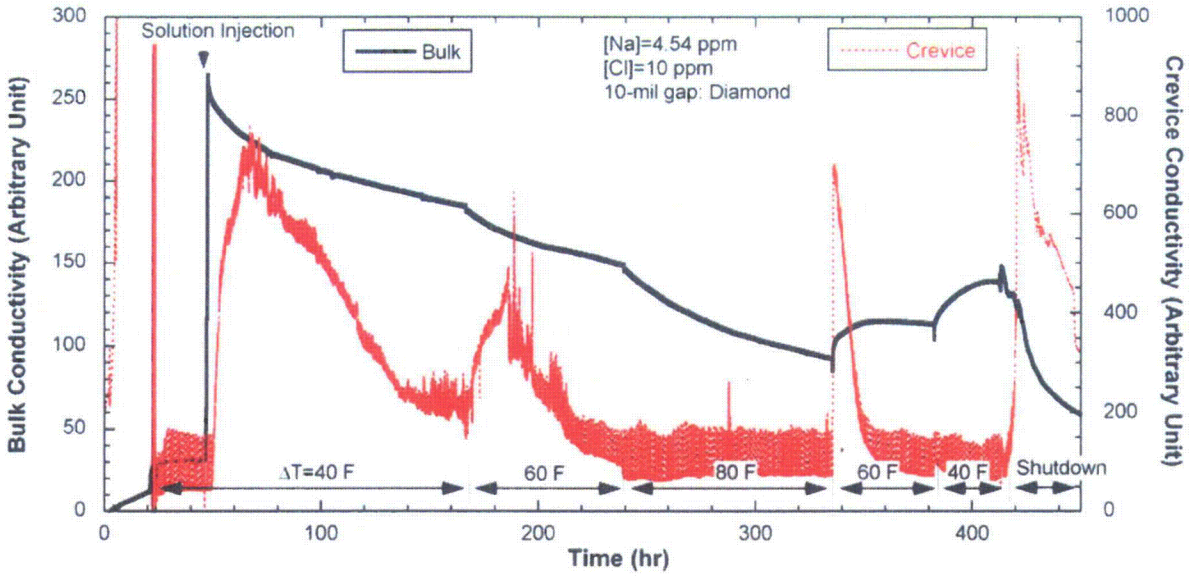

Figure 72. Crevice conductivity variation with time in the 10-mil gap crevice packed with diamond powder (NaCl-04).

Figure 73 shows the chemical analysis results for crevice samples taken from the 10- and 20-mil gap crevices. For the 10-mil gap crevice, the concentration levels are much lower than those in the previous test, NaCl-03 with MR=0.3, as shown in Figure 55. The 20-mil gap crevice packed with magnetite appears to show similar concentration levels to the NaCl-03 test results. One sample taken before the NaCl solution injection had high Cl concentration. This finding indicates that even after flushing the MB several times with high purity water, Cl ions are difficult to remove, probably because of

the adsorption characteristics on the MB internal surfaces. The low ion concentration level in the diamond-packed crevice appears to be caused by the fact that NaCl-04 followed NaCl-03. Some quantity of precipitates or deposits might not be completely removed from the crevice and might remain in the crevice. This hypothesis is discussed again in the post-test examinations (Section 4.4.5).

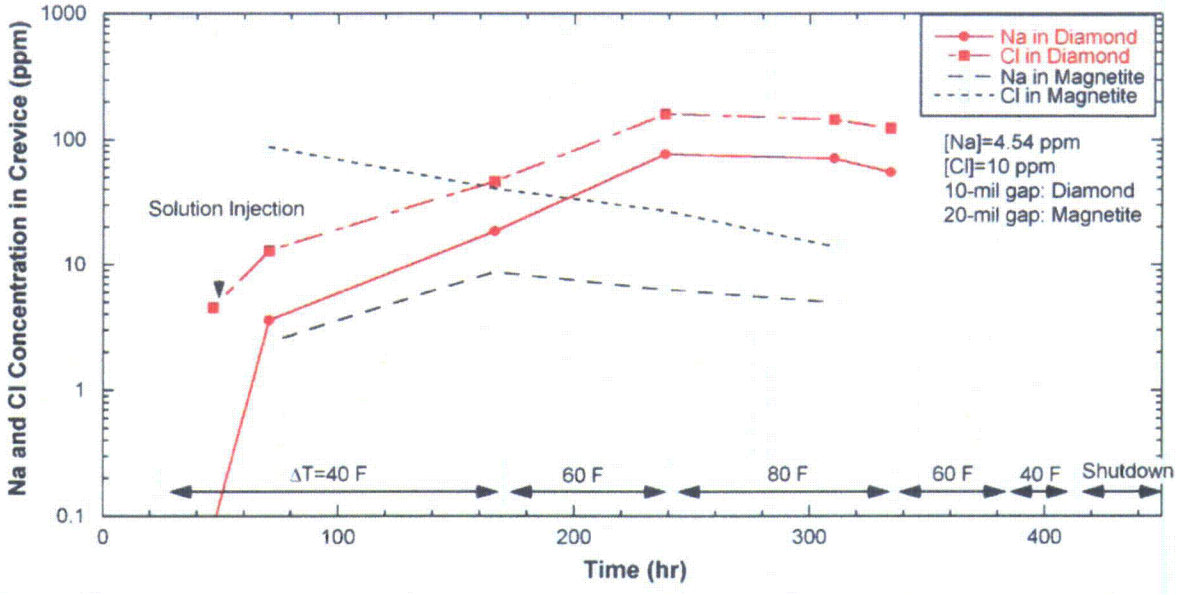

Figure 73. Chemical analysis results for crevice samples from 10-mil gap crevice packed with diamond and 20-mil gap crevice packed with magnetite (NaCl-04).

4.4.3 ECP Measurement

Figure 74 shows the Pt electrode potential variations in bulk and 10-mil gap crevice packed with diamond powder. Bulk and crevice Pt potentials are almost constant regardless of the ΔT. Figure 75 shows the Ni electrode potentials in the bulk and the 10-mil gap crevice packed with diamond. As shown in Figure 74, the bulk Ni electrode potential was almost constant. The tungsten electrode for the crevice and bulk responded quickly to the solution injection, as shown in Figure 76. The crevice tungsten potential before the NaCl solution injection was 140 mV higher than the bulk tungsten potential. It appears that high Cl concentration, as shown in Figure 73, caused the crevice to become acidic and resulted in a higher potential than in the bulk solution. The bulk tungsten potential slowly decreased with the increase of ΔT but seems to have stabilized after the decrease of ΔT because of hideout return from the crevice. The crevice tungsten potential quickly dropped and became stabilized before ΔT was changed from 40°F to 60°F. The initial big spike after the solution injection, which was also observed in the previous test, was caused by the crevice acidification from high purity water followed by the increase in the impurity level. As shown in Figure 44, the solution pH can be decreased by an increase in the ion concentration level, even though the MR remains constant. The tungsten potential in the crevice seems relatively independent of ΔT. The crevice tungsten potentials observed in this test appears to represent actual crevice chemistry, but the crevice tungsten electrode tip might be located too far from the tube surface, such that it might not represent the actual crevice pH change. This issue is discussed further in later sections.

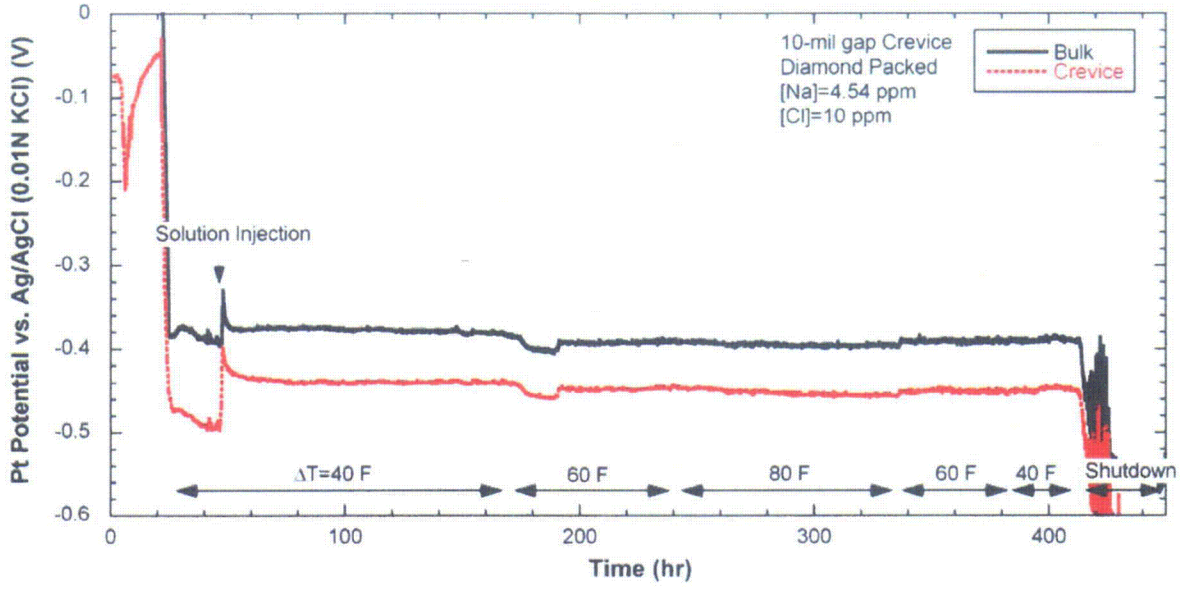

Figure 74. Variations of Pt electrode potential in bulk and 10-mil gap crevice packed with diamond (NaCl-04).

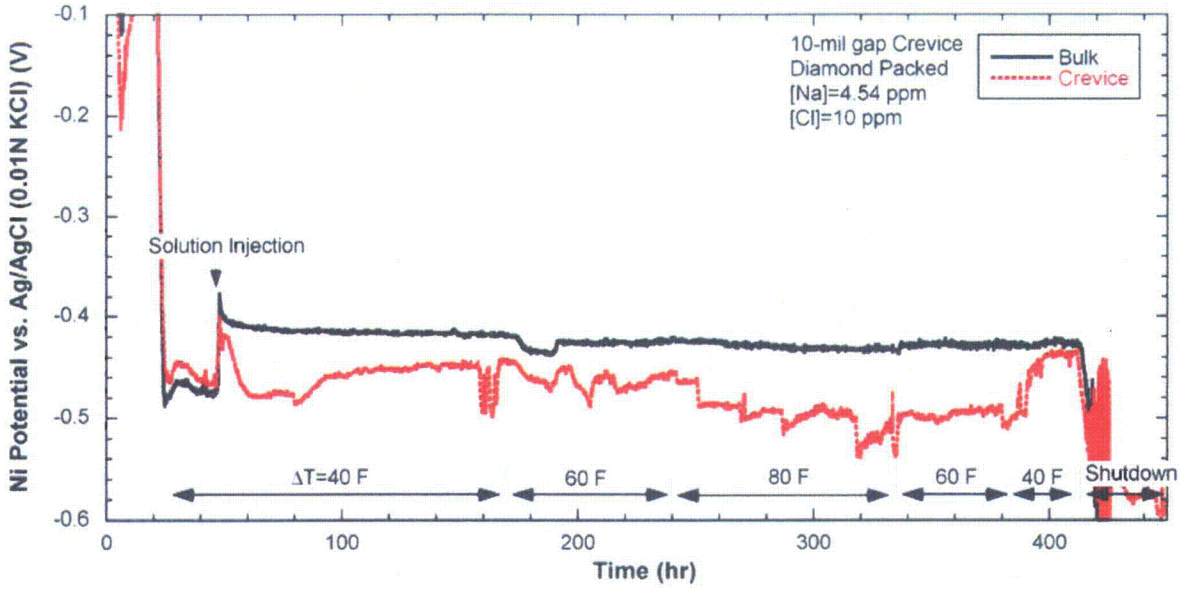

Figure 75. Variations in Ni electrode potential in bulk and 10-mil gap crevice packed with diamond (NaCl-04).

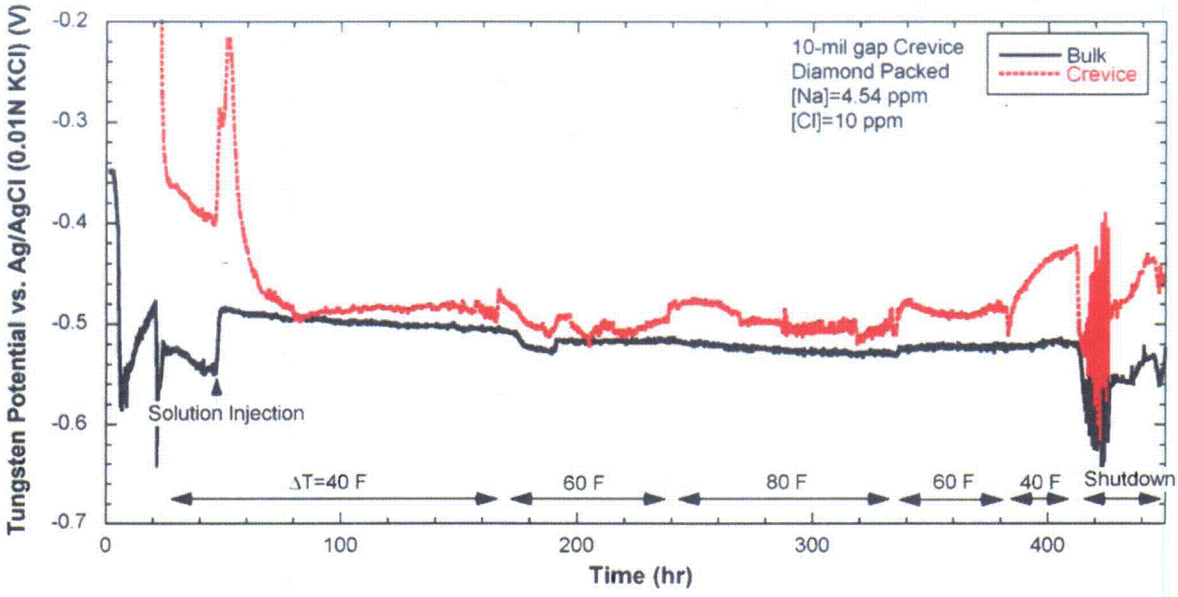

Figure 76. Variations in tungsten electrode potential in bulk and 10-mil gap crevice packed with diamond (NaCl-04).

4.4.4 Discussion of ECP and Solution Analysis

Figure 77 shows the tungsten potential difference between the crevice and the bulk with respect to the pH difference between the 10-mil gap crevice and the bulk. The pH was calculated by using MULTEQ with input from the solution sample analysis. The calculated pH indicates that the crevice pH is always lower than the bulk pH, which agrees with the measured tungsten potential difference except for one data point (indicated by a circle in Figure 77). However, even if the one data point is excluded, the potential slope with respect to pH is much lower than the Nernstian slope of -106 mV/pH at 260°C (500°F). Figure 78 shows the tungsten potential measured in the crevice and bulk as a function of the sample pH calculated by MULTEQ. The data shown in Figure 78 were corrected by considering the delay effect discussed in Section 4.3.5. The tungsten potential for the bulk solution responded in a linear fashion to the pH variation, but the crevice data did not. As observed in the NaCl-03 test, the bulk tungsten electrode behaved as a pH electrode in NaCl solution having MR=0.7.

Figure 79 shows the Na-to-Cl MR variations with time in the bulk and crevices. The MR was calculated from the bulk and crevice sample analyses. The bulk MR was stable but decreased after increasing ΔT from 60°F to 80°F. This finding indicates that Na was preferentially concentrated in crevices at ΔT=80°F. The MR for the two crevices gradually increases with increasing ΔT. The MR increase for the magnetite-packed crevice at ΔT=80°F appears to correspond with preferential Na concentration in the crevice at ΔT=80°F, but the Na concentration level in the magnetite-packed crevice, as shown in Figure 73, is too small to explain the bulk MR decrease. The crevice samples from the magnetite-packed crevice do not appear to represent the actual crevice chemistry because of the dominant steam phase in the crevice. The initial MR data for the crevices are lower than for the bulk, which indicates that some residual Cl ions from the previous test were present in the crevice. Conditions from the previous test may have affected the results of the NaCl-04 test.

From the bulk concentration data, the total accumulated moles of Na and Cl in crevices were calculated, as shown in Figure 80. Neither the Na nor Cl concentration appears to saturate at any of the ΔT's. As was expected from Figure 79, the crevice MR increased after the increase in ΔT from 60°F to 80°F. To compare the hideout rate of Na and Cl, the accumulated moles of Na and Cl in crevices were estimated with respect to each ion's exposure using the bulk concentration data, as shown in Figure 81. The initial hideout rate was almost the same for Na and Cl ions, and the rates were relatively constant until the ΔT was increased from 60°F to 80°F. From the results in Figure 81, we can expect that if the test starts with ΔT=80°F, the preferential Na concentration in the crevice would be observed from the beginning of the test.

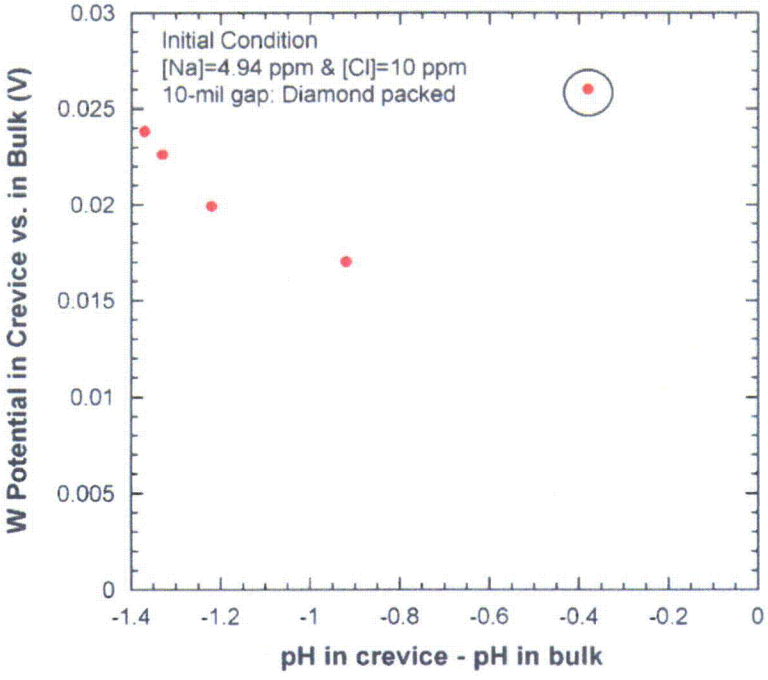

Figure 77.
Calculated pH and tungsten potential difference between the 10-mil gap crevice and bulk (NaCl-04).

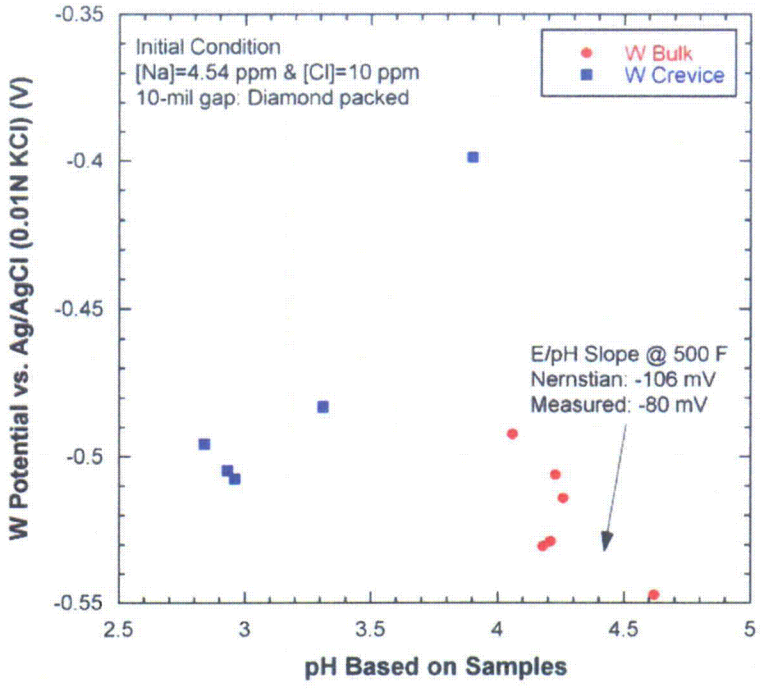

Figure 78.
Tungsten potential measured in bulk and 10-mil gap crevice as a function of calculated pH for the samples taken at the same time when tungsten potentials were measured (NaCl-04).

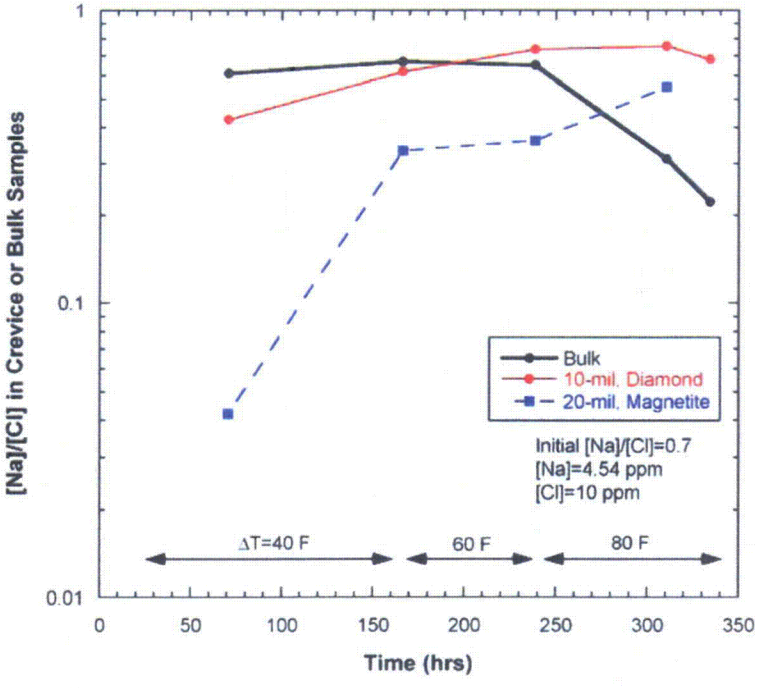

Figure 79.
Na-to-Cl molar ratio variations with time in bulk and crevices (NaCl-04).

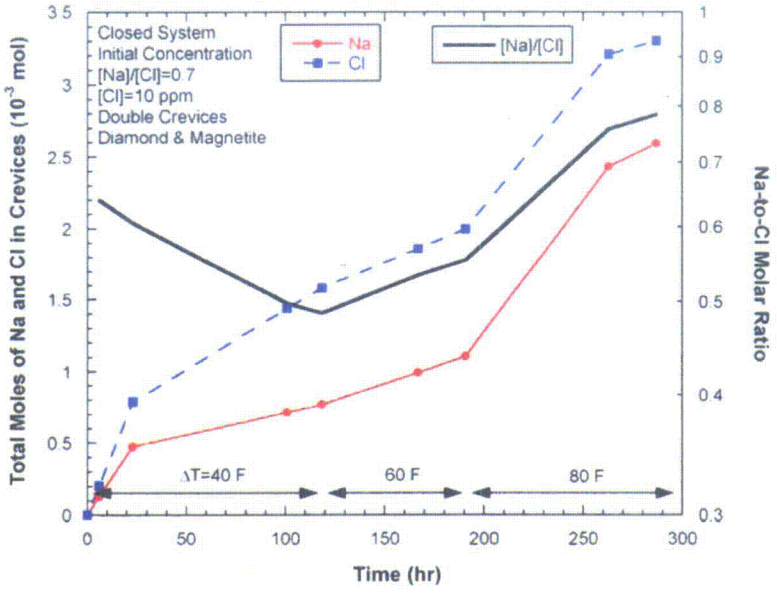

Figure 80.
Total accumulated moles of Na and Cl in crevices and their molar ratio as a function of time after the solution injection (NaCl-04).

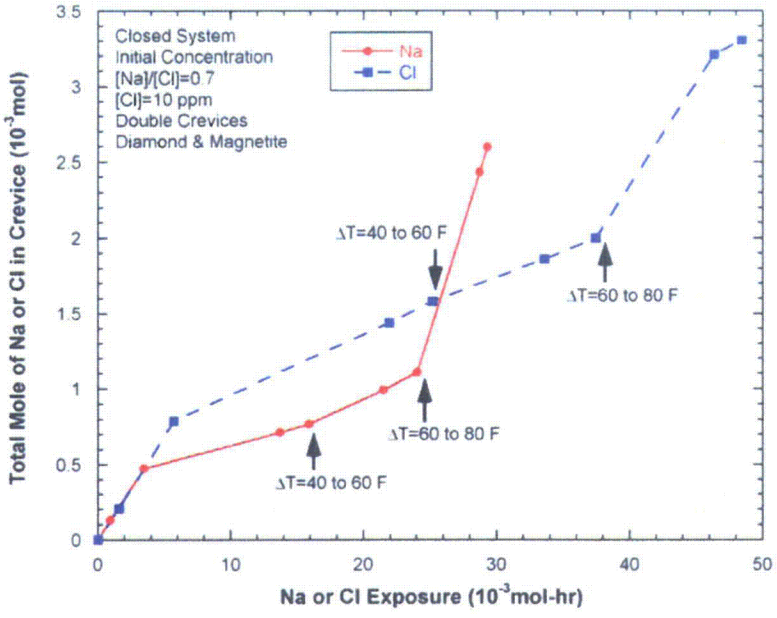

Figure 81.
Total accumulated moles of Na and Cl in crevices as a function of exposure after the solution injection (NaCl-04).

4.4.5 Post-test Examination

The post-test inspections were conducted after the NaCl-03 and -04 tests. Figure 82 shows the disintegrated Ni foam on the 10-mil gap crevice assembly. The Ni foam became thinner than its original thickness and became brittle, which was not observed in the previous two tests, NaCl-01 and -02 having an MR of 1.0. The Ni foam apparently was dissolved in the relatively acidic bulk water. Figure 83 shows that a green deposit appeared at the bottom area of the 10-mil gap crevice packed with diamond. The small particles at the upper crevice region are residual diamond particles that appeared after removal of

the crevice assembly ring. The ICP/OES analysis indicated that the main elements in the green deposit were Ni, Fe, and Cr, as shown in Table 4. Since the color of NiO and Cr_2O_3 is green, we inferred that the deposit is mainly composed of NiO and Cr_2O_3 as well as iron oxide or a nickel-chromium-iron oxide mixture. The bare tube surfaces after removal of the deposits and diamond powders are shown in Figure 84. Severe gouging was observed at the upper half, but not in the green deposit area. This gouging seems to have developed as a result of the crevice chemistry being strongly acidic and might have been enhanced by abrasion of diamond particles, as discussed in Section 3.2.1. Considering that no gouging was observed after the NaCl-01 and -02 tests having MR=1.0, the abrasion of diamond particles alone does not likely cause the gouging without severe chemical excursion. A dye penetrant test was performed to permit visual identification of any surface cracks, but no visible cracks were detected on the surface of the 10-mil gap crevice tube. Under acidic environments, alloy 600 tubing can be severely gouged, but stress corrosion cracks do not appear to easily develop as compared to caustic environments, such as in the NaOH-01 and -02 tests.

As shown in Figure 85, magnetite powder still appeared in the 20-mil gap crevice after the series of tests. A green and red deposit was observed at the upper part of the 20-mil gap crevice, as shown in Figure 86. Analysis results by ICP/OES indicated that the green and red deposit was composed of Ni and Fe oxides. The black powder observed in the 20-mil gap crevice was mainly composed of Fe, indicating magnetite, as was expected. The chemical compositions for the deposits in the 10- and 20-mil gap crevices are summarized in Table 4. After removal of the deposit in the 20-mil gap crevice, no gouging was detected on the bare tube surfaces, as shown in Figure 87.

Table 4. Chemical compositions for the deposit formed in 10- and 20-mil gap crevices after the NaCl-03 and -04 tests determined by ICP/OES.

Powder Description	Chemical Composition (wt%)*				
	Fe	Ni	Cr	Cu	Na
Green powder in 10-mil gap crevice	9.99	21.0	2.36	<0.4	<0.4
Black powder in 20-mil gap crevice	64.8	1.74	<0.05	<0.05	<0.05
Green and red powder in 20-mil gap crevice	31.3	35.7	<0.2	<0.2	<0.2

* Powder samples were pretreated and dissolved in strong acid before ICP/OES analysis. The weight of the acid is not listed in this table, which should be the balance.

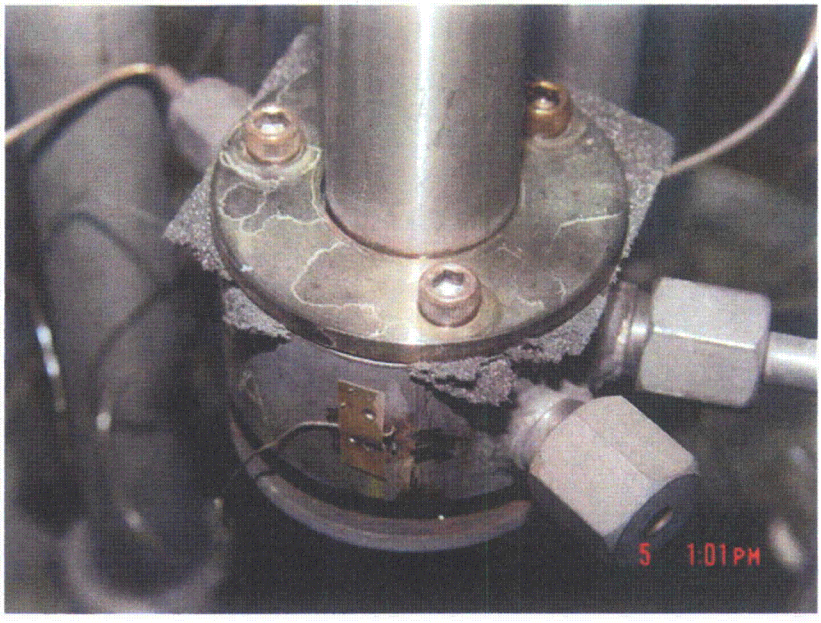

Figure 82.
Photograph of 10-mil gap crevice assembly after the NaCl-03 and -04 tests showing disintegrated Ni foam.

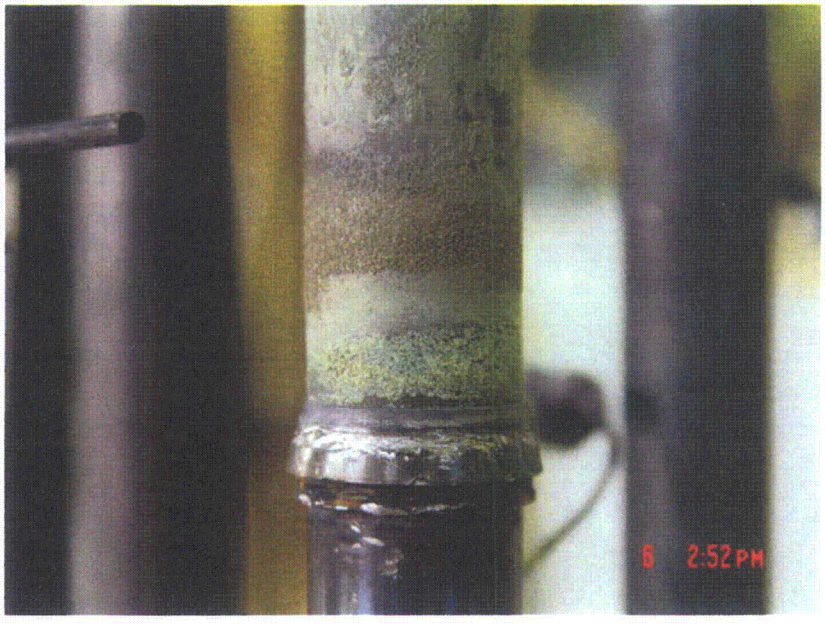

Figure 83.
Tube surfaces in the 10-mil gap crevice packed with diamond powder after removal of the crevice ring.

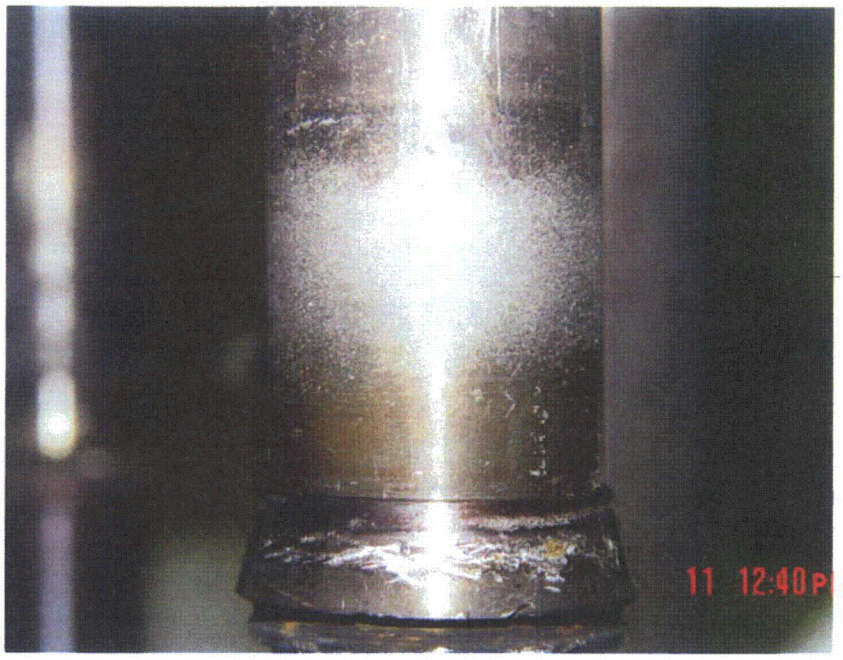

Figure 84.
Bare tube surfaces in the 10-mil gap crevice after removal of deposits and diamond powders, showing gouges (the same area as shown in Fig. 83).

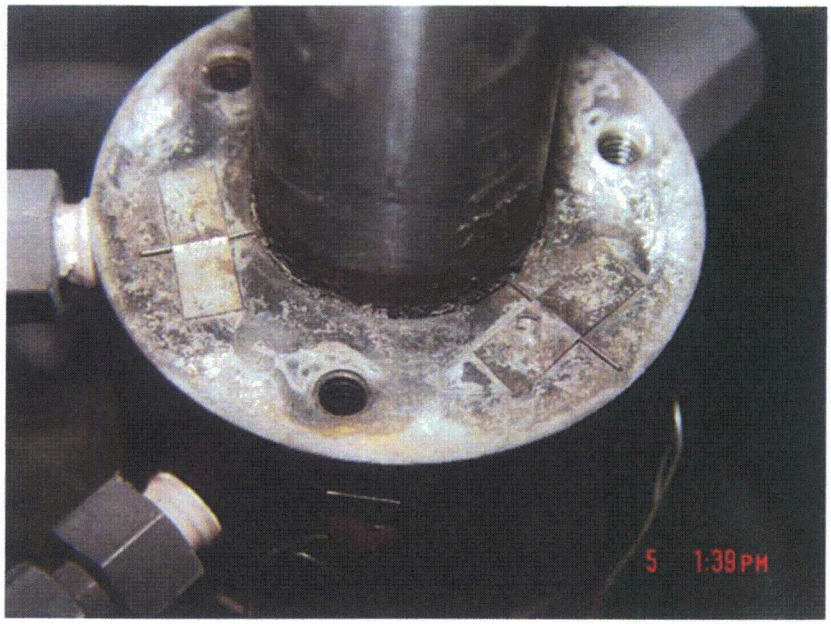

Figure 85.
Top view of 20-mil gap crevice after removal of Ni foam and retaining ring, showing the magnetite powder in the crevice after the NaCl-03 and -04 tests.

Figure 86.
Tube surfaces of 20-mil gap crevice after removal of the crevice assembly showing the deposit formed on the upper crevice region and magnetite powder.

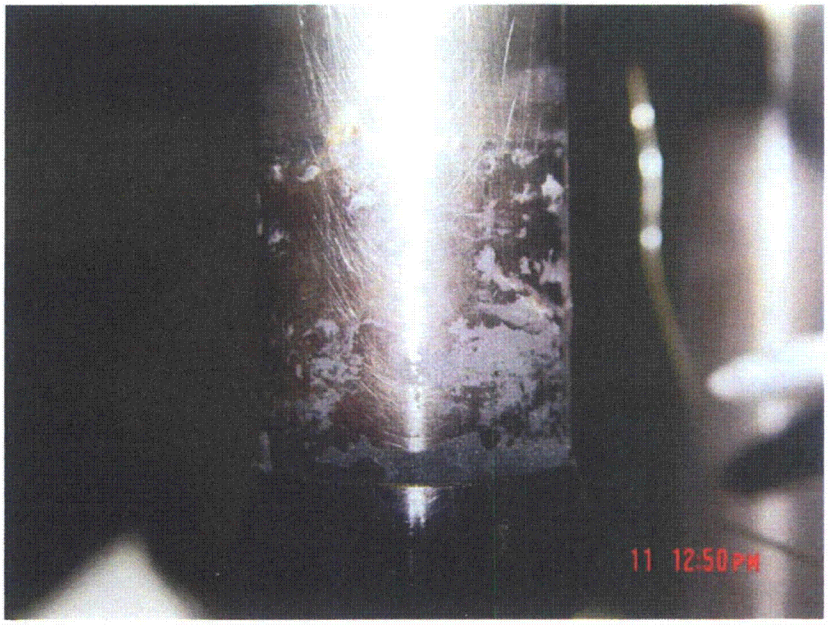

Figure 87.
Bare tube surfaces in the 20-mil gap crevice after removal of the deposit and magnetite powder, showing neither pitting nor gouges.

Two possible questions about the deposits detected in the crevices include: what is the origin of the Ni-rich deposits, and, why were the deposits located at different axial locations in the crevices having different packing materials. As shown in Figure 82, Ni dissolution occurred during the NaCl-03 and -04 tests as a result of the disintegration of the Ni foam. It is expected that this disintegration mainly occurred during the NaCl-03 test because of its more acidic bulk water. Dissolved Ni ions in the bulk water would be concentrated in the crevices, similar to the Na and Cl ions. Note that significant Cr was detected in the deposit formed in the 10-mil gap crevice. Since Cr usually does not dissolve in slightly acidic water because of the presence of a protective Cr oxide film, the origin of Cr is most likely the alloy 600 tube itself instead of the bulk water. This hypothesis is supported by the gouging shown in Figure 84.

Therefore, the deposits in the 10-mil gap crevice were formed by Ni hideout from the bulk water and gouging of the alloy 600 tubing. The Ni-rich deposits in the 20-mil gap crevice likely originate from the Ni ions in the bulk water as a result of the Ni foam dissolution.

The axial locations of the Ni-rich deposits may be related to the choice of packing material and its characteristics. The depth to which liquid phase can penetrate depends on the packing materials. The highly permeable diamond powder packing used in our tests allows liquid to penetrate deeply into the crevice, but the less permeable magnetite powder packing does not. We expect that Na and Cl hideout in the 10-mil gap crevice occurred mainly at the gouging region, and the region below the gouging region was a liquid and steam mixture. At the liquid and steam region, Ni-rich deposits having low solubility formed. Usually deposits can be formed at an intermediate region between liquid-dominant and dryout regions. For the 20-mil gap crevice, liquid could not penetrate deep enough because of the relatively less permeable magnetite packing. That is the reason that Ni-rich deposits were formed only near the crevice mouth. To verify the possibility of the Ni foam dissolution in bulk water, the Ni solubility was calculated with MULTEQ®. The calculated Ni solubility increased with decreasing pH, as shown in Figure 88. Each data set shown in Figure 88 was calculated by assuming constant Cl concentration and adjusting the Na concentration for various values of pH. The Ni solubility increased significantly with even small pH variation. It appears that approximately 10-20 ppm Ni can be dissolved in slightly acidic solutions, like the NaCl-03 test having MR=0.3. To prevent the Ni dissolution in acidic water, a corrosion-resistant metal (like chromium) can be added as an alloying element. After the NaCl-04 test, Ni-Cr-Mo alloy foams were used instead of pure Ni foams.

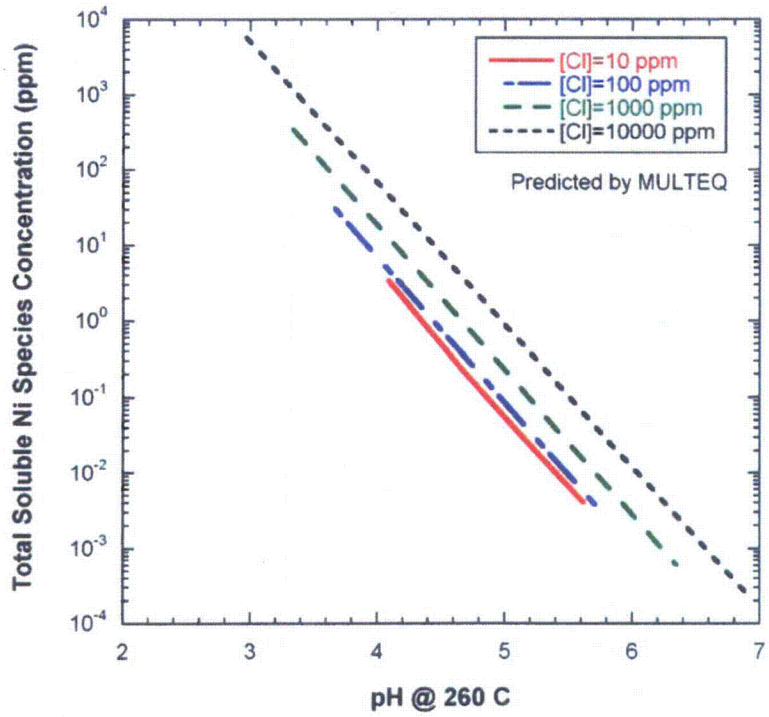

Figure 88.
Ni solubility as a function of pH and Cl concentration.

4.4.6 Comparing the Results for NaCl-02 through -04 Tests

In Figure 89, all Pt potential data collected from the three tests with different molar ratios, NaCl-02 through -04, are plotted versus the pH. The pH was determined using MULTEQ with input from the ICP/OES for Na and IC for Cl. The bulk Pt data closely follow the hydrogen electrode equilibrium line, assuming 1-ppb hydrogen concentration. The data from NaCl-03 with MR=0.3 are closer to the Ni/NiO equilibrium line than the other two data sets; this result can be explained by the dissolution of the Ni foam in the relatively acidic environment, as discussed in the previous section. Unlike the bulk Pt data, the crevice Pt data sets do not follow a linear trend. A Pt electrode usually serves as an oxidation/reduction potential electrode. To determine if other reactions are causing the mixed potential, the Fe/Fe_3O_4 equilibrium line was plotted in the same E-pH domain. The crevice data appear to be mostly located between the Fe/Fe_3O_4 and Ni/NiO lines. The scattering of crevice data might be explained by the mixed potential due to other reactions and the complexity of the heated crevice environment. However, it is still difficult to analyze the crevice potential data quantitatively.

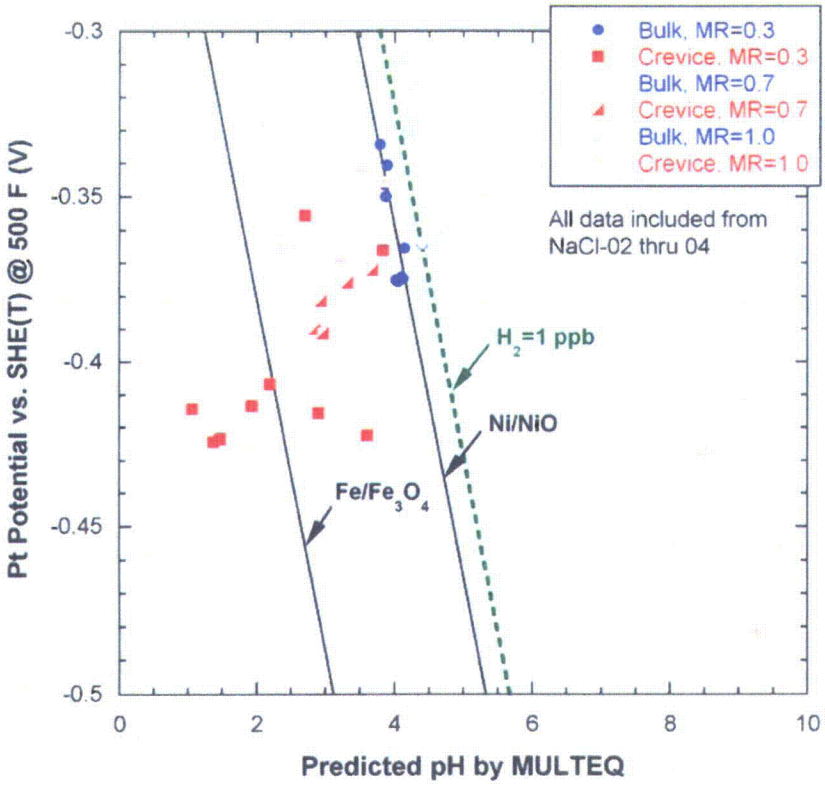

Figure 89.
Pt potential data measured in crevice and bulk water as a function of MULTEQ calculated pH based on solution sample analysis.

Figure 90 shows the tungsten potential measured in the bulk and the 10-mil gap crevice packed with the diamond powder as a function of sample pH taken at the same time as the tungsten potentials were measured. All the data from the NaCl-03 and -04 tests are included. The bulk data show good linearity, and the potential slope with respect to pH is very close to the Nernstian slope. Kriksunov and Macdonald[29] investigated the tungsten/tungsten oxide electrode as a pH sensor over the pH range of 2 to 11 at temperatures from 200 °C (392 °F) to 300 °C (572 °F). In Figure 90, the measured potential line by them at 250 °C (482 °F) is plotted. The line is about 50 mV higher than the bulk tungsten data, but this

discrepancy is not that high, considering the test temperature difference of 10 °C. It is not clear whether the crevice data are linear. If the crevice tungsten electrode follows the same tungsten oxidation reaction as the bulk tungsten electrode, the crevice data should fit on a single line.

Note that at least the bulk tungsten data and the earlier literature data are within the same intermediate tungsten oxide region, which is a compound between pentavalent (W_2O_5) and hexavalent (WO_3) forms. Additional data would be needed to confirm whether it is appropriate to use the tungsten electrode as a pH electrode under such a complicated crevice environment. To reduce the chemical complexity in a crevice, a crevice hideout test with highly soluble NaOH water chemistry appears to be an appropriate means to confirm the functionality of the tungsten electrode as a pH electrode under crevice environments.

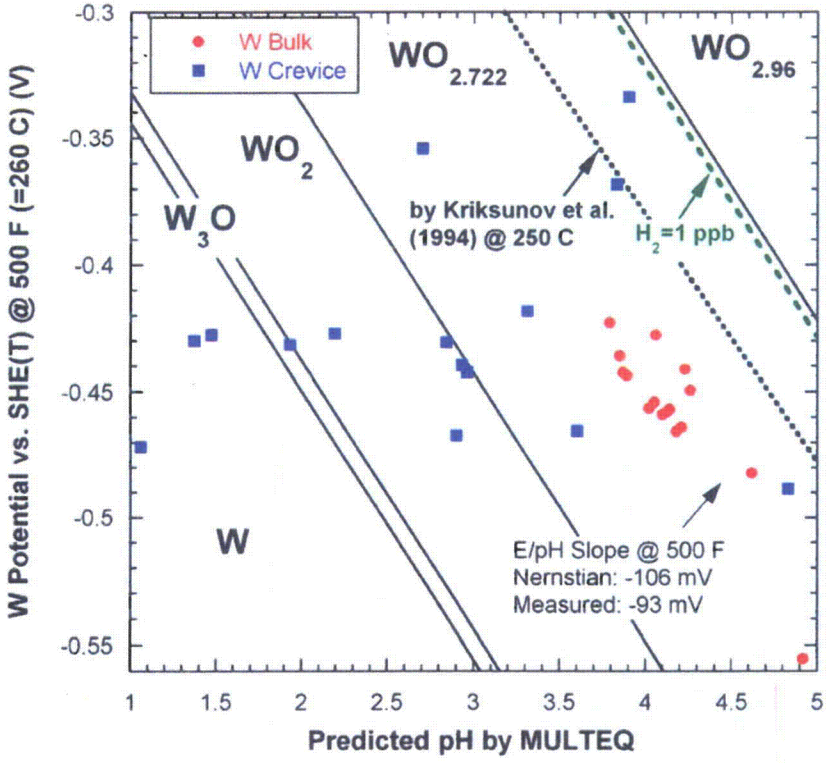

Figure 90. Tungsten potential measured in bulk and crevice as a function of sample pH, including all data from NaCl-03 and -04 tests plotted in a potential-pH diagram of W-H_2O system predicted by the thermodynamic code HSC Chemistry.

4.4.7 Summary

The NaCl-04 test followed the NaCl-03 test without the MB being opened. The NaCl-04 test appears to have been affected by residual chemicals from the NaCl-03 test. In the NaCl-03 and -04 tests, the tungsten electrode behaved as a pH electrode in the bulk water, but the crevice tungsten electrode data did not linearly fit the sample pH data. The crevice tungsten electrode tip appeared to be too far from the tube surface to represent the actual crevice pH variation. The crevice samples in the NaCl-04 test

indicated less acidic pH than those in the NaCl-03 test. The post-test examinations after NaCl-03 and -04 showed that gouging occurred on the alloy 600 tube surfaces in the 10-mil gap crevice packed with diamond, but no cracks were detected. This result indicates strong acid conditions developed during the NaCl-03 and -04 tests, mostly during the NaCl-03 test. The magnetite-packed crevice did not show any corrosion on the tube surfaces. To maximize the advantage of a closed system and evaluate the crevice hideout characteristics from bulk concentration data, a single crevice was tested instead of a double crevice.

5. Single Crevice Test

5.1 Background

As discussed in Section 4, in the double crevice tests having different packing materials, we had difficulty in analyzing the crevice concentration behavior with results from bulk water chemistry analysis. In contrast, use of only one crevice packed with one kind of packing material should make it much easier to analyze the crevice chemistry from bulk chemistry data because the MB is a closed system and there is only one crevice where hideout can occur.

5.2 NaOH-03: NaOH Test

The main objective of the NaOH-03 test is to confirm that the W/WO_x electrode can work as a pH electrode even in complex crevice environments. Since the behavior of the NaOH chemistry is much simpler than the NaCl chemistry, testing with NaOH bulk water is valuable. This testing will furnish a much simpler starting point for developing and confirming the adequacy of our chemical instrumentation. The 10-mil gap crevice was packed with diamond powder, and the 20-mil gap crevice was left unpacked. The estimated porosity of the 10-mil gap crevice was 35 %. This simplified configuration allows us to better model crevice behavior and perform chemical balances accounting for what happens between a single crevice and the bulk water. The bulk water was an 11.5-ppm Na solution as NaOH, which is the same Na level as NaOH-01 and -02 tests.

Leakage from the primary to secondary chamber occurred, and the system was automatically shut down after about 400 hours. Multiple through-wall cracks were detected in the unpacked crevice tubing, which had been used during prior tests. A through-wall crack was found in the packed crevice tubing, which was being used for the first time in the MB. The starting point of the leak was carefully determined, and only test results acquired before the start of the leak were used in the crevice chemistry analysis.

5.2.1 Temperature Data

As shown in Figure 91, all the crevice temperatures in the diamond-packed 10-mil gap crevice started to increase immediately after the injection of the 11.5-ppm Na solution, followed by stabilization 20 hours later. This temperature increase is attributed to Na concentrating in the crevice and resulting in elevation of the boiling point. The temperature increase after solution injection was about 5°F. After increasing the primary temperature from 540°F to 560°F, the crevice temperature increased immediately but did not show any additional temperature increase. The thermocouple labeled T3 indicated temperature instability at ΔT=60°F and a noisy signal at ΔT=100°F, a sign of leakage. The primary temperature was increased to 600°F to evaluate the reproducibility of the NaOH-01 and -02 test results. However, the reproducibility test was shut down due to the leakage. In Figure 92, the temperature in the 20-mil gap crevice did not increase even after NaOH solution injection. The non-packed condition and wider gap induced violent mixing between the crevice and bulk environments, which led to only minor hideout and boiling point elevation. Crevice solution samples for the unpacked crevice also showed only minor Na hideout. Thermocouple T5 indicated temperature fluctuation at ΔT=60°F. Since through-wall cracks were detected at the open crevice, the noisy temperature signal appears to indicate the start of leakage. Since the primary water temperature is higher than the secondary water temperature, we inferred that as the crack length became longer and the steam leak rate became higher, the upper bound of the noisy temperature became higher.

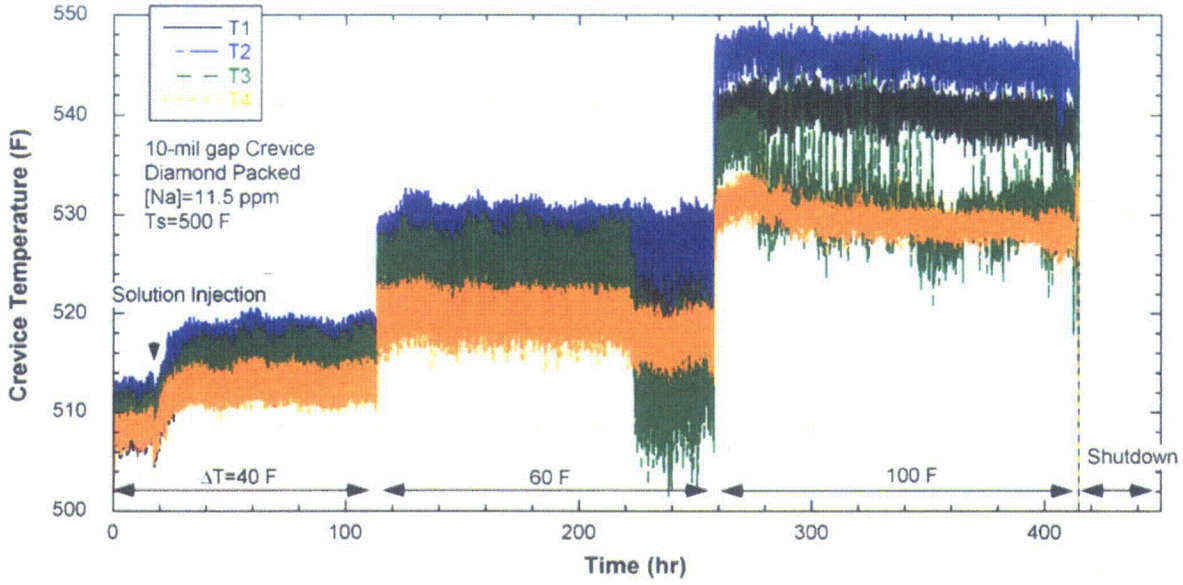

Figure 91. Crevice temperature variation in the 10-mil gap crevice packed with diamond (NaOH-03).

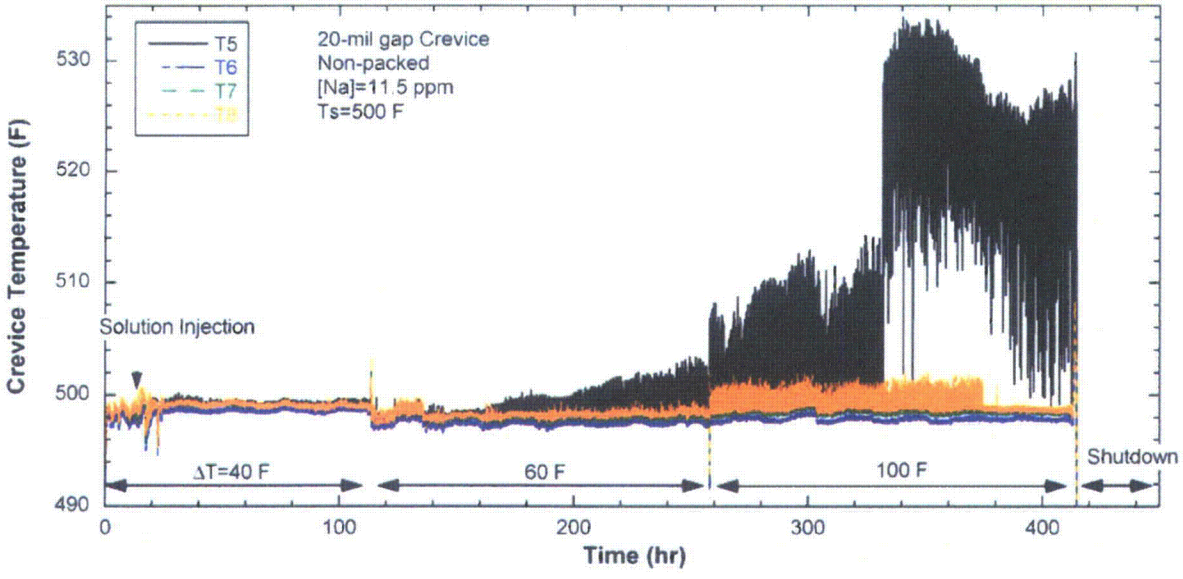

Figure 92. Crevice temperature variation in the 20-mil gap crevice without packing (NaOH-03).

The crevice temperatures were normalized by using the primary and secondary temperatures, as shown in Figure 93. The temperature increase is clear after the solution injection. The normalized temperatures slightly increased after raising the primary temperature from 540°F to 560°F. Temperature fluctuations became smaller after increasing the primary temperature from 560°F to 600°F except for T3. This result indicates that the two-phase mixture zone became smaller at the thermocouples in the crevice, and the steam phase became dominant.

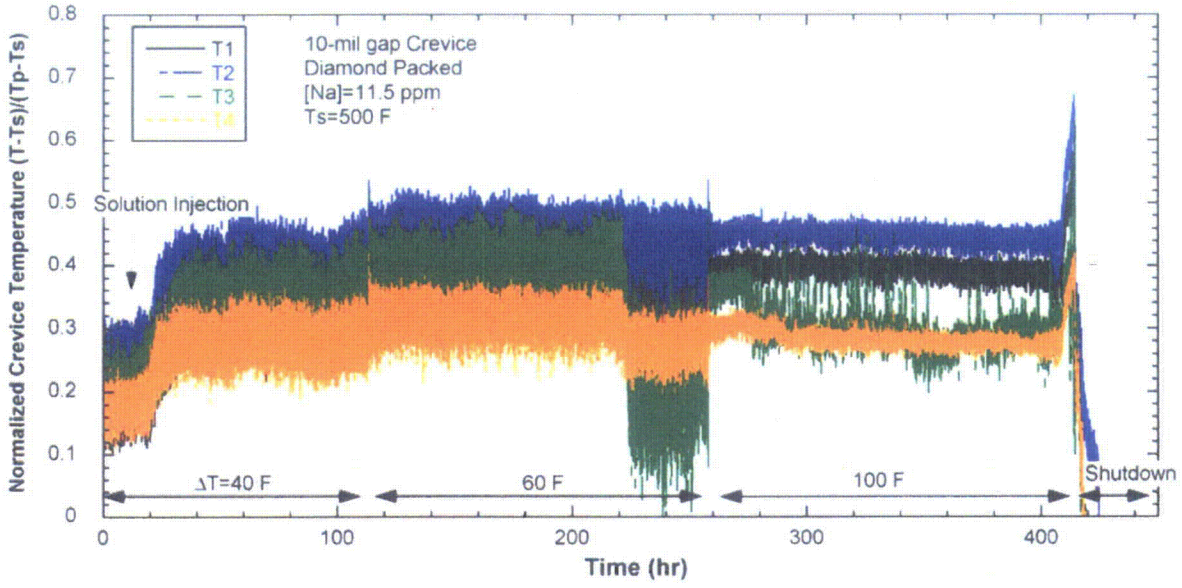

Figure 93. Normalized crevice temperature in the 10-mil gap crevice packed with diamond (NaOH-03).

5.2.2 Bulk & Crevice Chemistry

The bulk conductivity responded very quickly to the solution injection but exceeded the upper limit of the conductivity meter with 20-ppm NaOH solution, as shown in Figure 94. After changing the range module in the conductivity meter, the recording of the bulk conductivity was resumed. Based on the analysis results for bulk samples, the Cl ion concentration was around 0.6 ppm. This test can be considered as having a high Na-to-Cl molar ratio. The source of Cl ions is not clear, but some Cl ions adsorbed on the oxide surface of the secondary chamber during the previous NaCl tests may have been released. The Na concentration decreased continuously, but the Cl concentration remained the same value. After changing ΔT from 60°F to 100°F, the conductivity reduction rate increased more than before. But a certain transition appears before and after a lapse of 280 hours. This transition may be another indication of the start of leakage from the primary to secondary chamber. As compared with the temperature indication for leakage, the bulk conductivity was less sensitive to leakage because the bulk conductivity reduction could be interpreted as Na hideout in the crevice as well as primary-to-secondary leakage.

In Figure 95, crevice conductivity can be seen to increase a few hours after the solution injection. This finding indicates that a certain time is needed for the concentrated solution to penetrate into the bottom region of the crevice and replace the steam phase. Crevice conductivity also exceeded the upper limit of the meter. In the NaOH-03 test, the contribution of the OH^- ion to total conductivity became larger than that in the previous NaCl tests, because the total OH^- ion concentration is higher and the conductance of the OH^- ion is about two times higher than the Na^+ or Cl^- ion at 500°F.[38] After replacing the range module, we resumed the crevice conductivity recording. The crevice conductivity at ΔT=60°F showed a gradual decrease followed by an increase. At ΔT=100°F, the conductivity dropped quickly after increasing the primary temperature because the steam phase became dominant in a very short time. Then, the conductivity increased rapidly, which indicates Na hideout. Subsequently, the conductivity started

decreasing again followed by oscillations. The crevice conductivity oscillations appear to be the effect of the steam leakage through a crack.

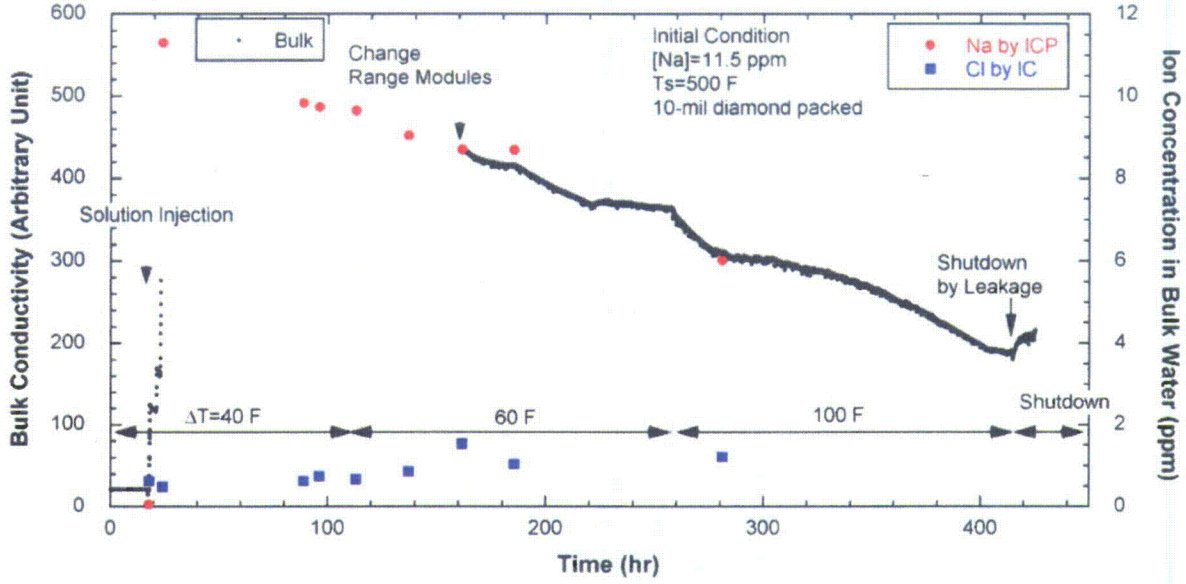

Figure 94. Bulk conductivity variation with time and impurity concentrations in bulk solution (NaOH-03).

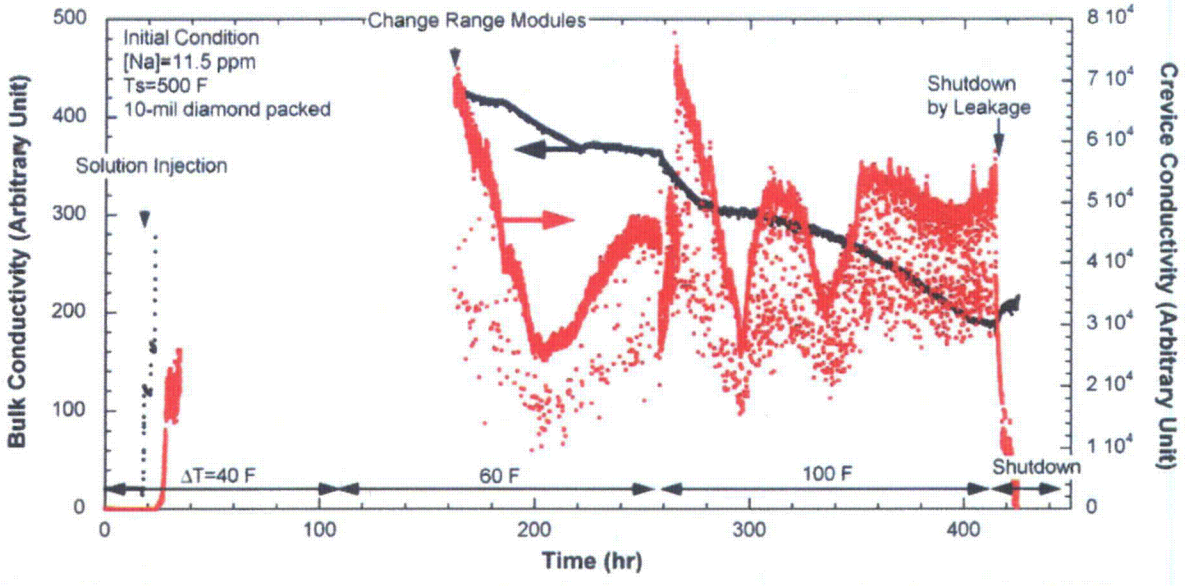

Figure 95. Crevice conductivity variation in the 10-mil gap crevice packed with diamond (NaOH-03).

Solution samples were taken from the 10-mil gap crevice and analyzed by ICP/OES or IC. Figure 96 shows the chemical analysis results for the crevice samples. At ΔT=40°F the maximum crevice concentration for Na was 12,500 ppm, as shown in Figure 96. The samples taken just before increasing the ΔT showed low concentration, but they recovered to higher concentration again one day later. At ΔT=60°F the maximum crevice concentration for Na was 31,400 ppm. Note that the variation of the Cl concentration in the crevice follows that of the Na ion. The concentration factor for Cl is around 10^3 as

compared with the bulk Cl concentration. This observation suggests that the total ion concentration in a crevice is proportional to the bulk impurity concentration.

A time delay appears to occur between solution samples and actual crevice chemistry. The first sample showing high concentration of Na was taken after a lapse of 100 hours, but the tungsten potential had already decreased indicating a high concentration of Na after about 50 hours elapsed. As discussed before, the volume of the sampling line and valve is about 90 μL, and the sampling volume is usually 50-100 μL, which causes the time delay. We can assume no time delays for bulk samples because we flushed the bulk sampling line before taking samples and the volume of the bulk sample is about 1500 μL. Figure 96 shows ion concentration versus time in the crevice not corrected for the time delay. To make the crevice samples more representative of the actual crevice chemistry, the analyses were corrected for the time delay. We assumed that a solution sample extracted at a certain time represents the crevice chemistry at the previous sampling time. The corrected chemical analyses are shown in Figure 97. Crevice concentration started to decrease after 160 hours for both crevices. For the unpacked crevice, the Na concentration did not exceed 100 ppm, which is consistent with the earlier test results described in Section 3.1. The crevice concentration decrease observed at ΔT=60°F is another indication of leakage.

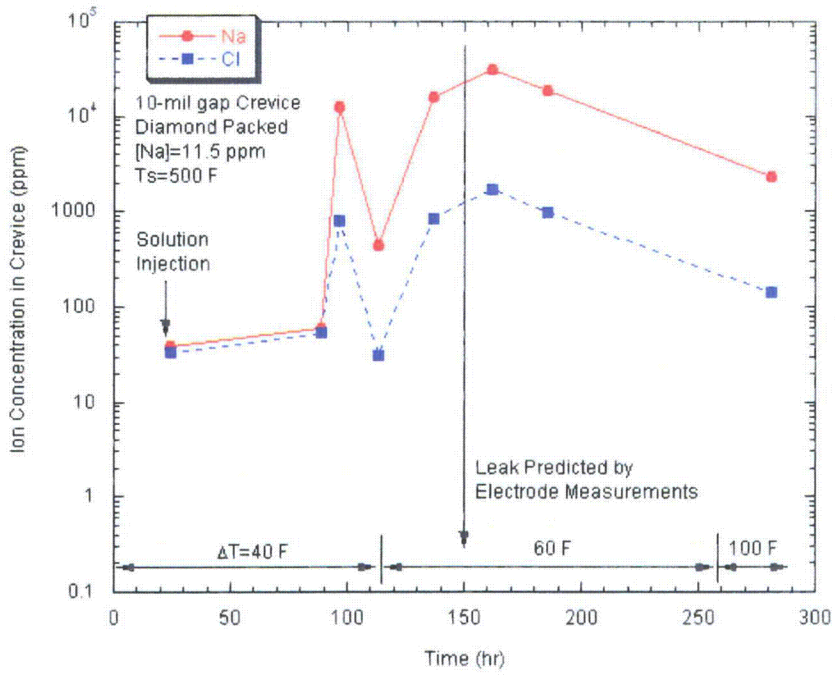

Figure 96. Chemical analyses of the samples taken from the 10-mil gap crevice packed with diamond dust (NaOH-03).

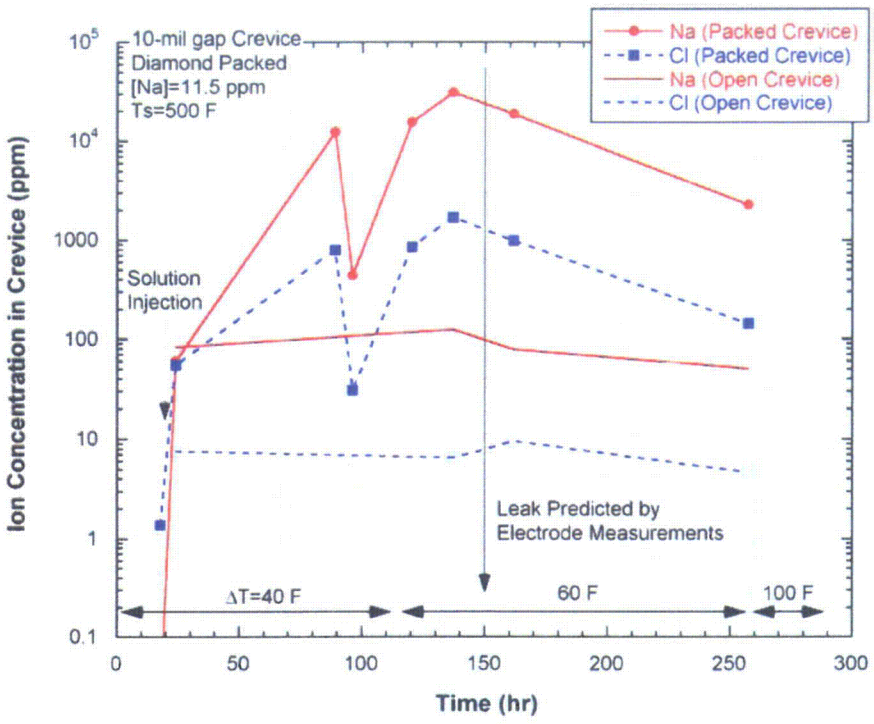

Figure 97. Chemical analyses of crevice samples corrected for sampling time (10-mil gap crevice: diamond packed, 20-mil gap crevice: open crevice).

5.2.3 ECP Measurement

Two tungsten/tungsten oxide electrodes were installed in the 10-mil gap crevice separated by 30 degrees at the same crevice elevation. Before the solution injection, one tungsten electrode exhibited noisy behavior, as shown in Figure 98. The other tungsten electrode was stable before and after the solution injection. After the solution injection, the two tungsten potentials became almost the same, suggesting that there is no significant chemical concentration gradient with circumferential location at ΔT=40°F. The bulk tungsten potential quickly responded to the NaOH injection, and the decrease of potential indicated an increase of bulk pH. The bulk potential change after the NaOH injection was 263 mV. The pH change calculated by MULTEQ was 3.0 at 500°F. If the tungsten electrode follows the Nernstian potential/pH slope, -106 mV at 500°F, this pH change will cause potential decreases of 318 mV, which is close to the measured bulk tungsten potential change. The crevice tungsten potential changes before and after injection was -588 mV at ΔT=40°F, and the pH change based on the solution samples was 5.7. If the crevice tungsten electrode follows the Nernstian potential/pH slope, this pH change will cause a potential decrease of 600 mV, which is very close to the measured value, -588 mV. Based on the crevice temperature data, the boiling point elevation at ΔT=40°F was 5°F higher in this case than that observed in high purity water. The calculated crevice pH and concentration factor corresponding to this boiling point elevation are 10.33 and 2500, respectively. The measured pH and the maximum concentration factor at ΔT=40°F are 10.11 and 1300, respectively. This discrepancy is probably due to an overestimation in the calculation of crevice concentration or dilution of the crevice solution during the sampling. At ΔT=60°F, the potential spikes were not observed immediately after changing ΔT from 40°F to 60°F, but some spikes were observed 40 hours later. These potential spikes can be considered an indication of leakage. In contrast to the crevice conductivity data shown in Figure 95, oscillations in crevice potential data are not apparent, but a small fluctuation in the tungsten potential denoted as "Crevice A2" appears at ΔT=60°F and 100°F.

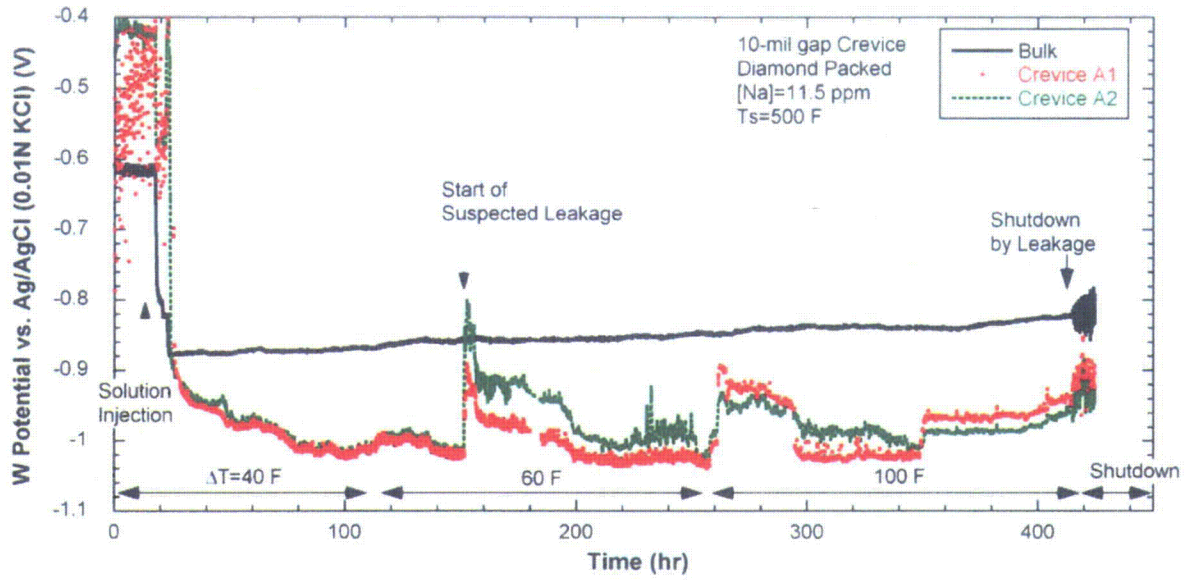

Figure 98. Tungsten potential variation in bulk and 10-mil gap crevice packed with diamond powder (NaOH-03).

Figure 99 shows the variations in Pt electrode potential for the bulk and 10-mil gap crevice packed with diamond powders. The bulk and crevice potentials are almost identical to those of the tungsten electrodes, as shown in Figure 98. The crevice Pt electrode potential shows noisy behavior before the solution injection, suggesting that the steam phase was dominant around the Pt wire electrode due to vigorous boiling. The subsequent stabilization of the potential was caused by Na concentrating in the crevice and the resultant increase in the concentrated liquid phase. Figure 100 shows the alloy 600 electrode potential variations in the bulk and crevice. Alloy 600 electrodes also show identical behavior to the tungsten electrode. Based on these observations, under deaerated NaOH water chemistry, alloy 600 and Pt electrodes can be used as a pH electrode, just as the W/WO_x electrode.

To determine if any relationship exists between conductivity and measured potential in the crevice, data for tungsten and alloy 600 are plotted along with the conductivity in Figure 101. After the solution injection, the potential decreased as the conductivity increased. After a potential spike, the alloy 600 potential in the crevice appears to follow the oscillations of crevice conductivity. If the conductivity depends on ion concentration in the liquid and the alloy 600 electrode behaves as a hydrogen electrode in the crevice, the alloy 600 potential should go in the negative direction when the conductivity increases. However, conductivity also depends on the ratio between steam and liquid phase as well as the liquid concentration, which complicates any simple comparison.

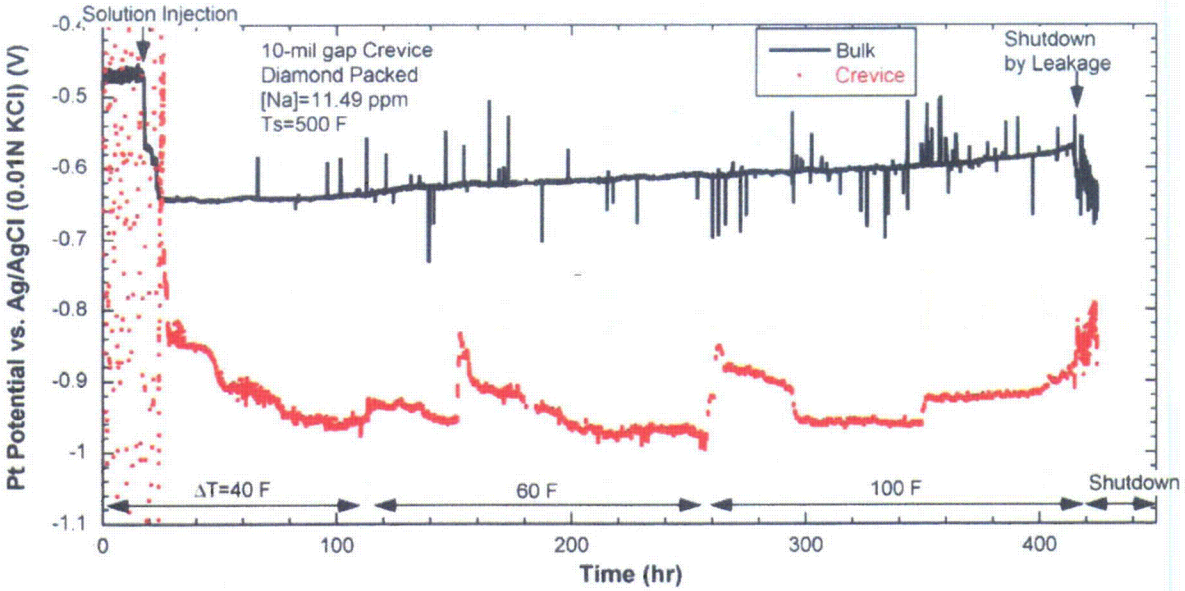

Figure 99. Pt potential variations in bulk and 10-mil gap crevice packed with diamond powder (NaOH-03).

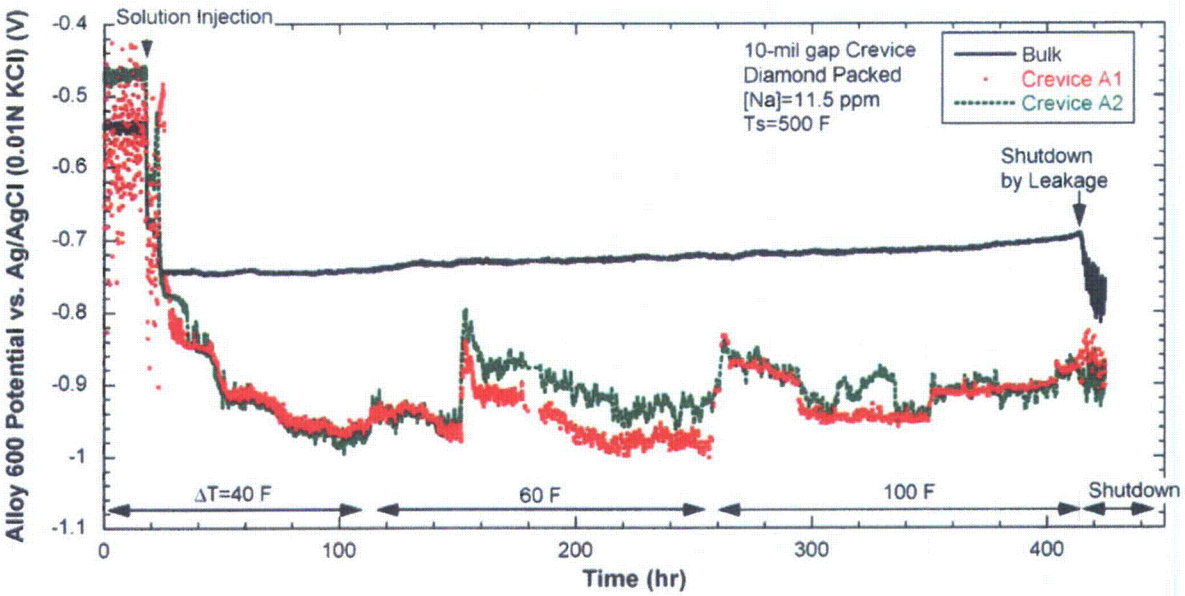

Figure 100. Alloy 600 potential variations in bulk and 10-mil gap crevice packed with diamond powder (NaOH-03).

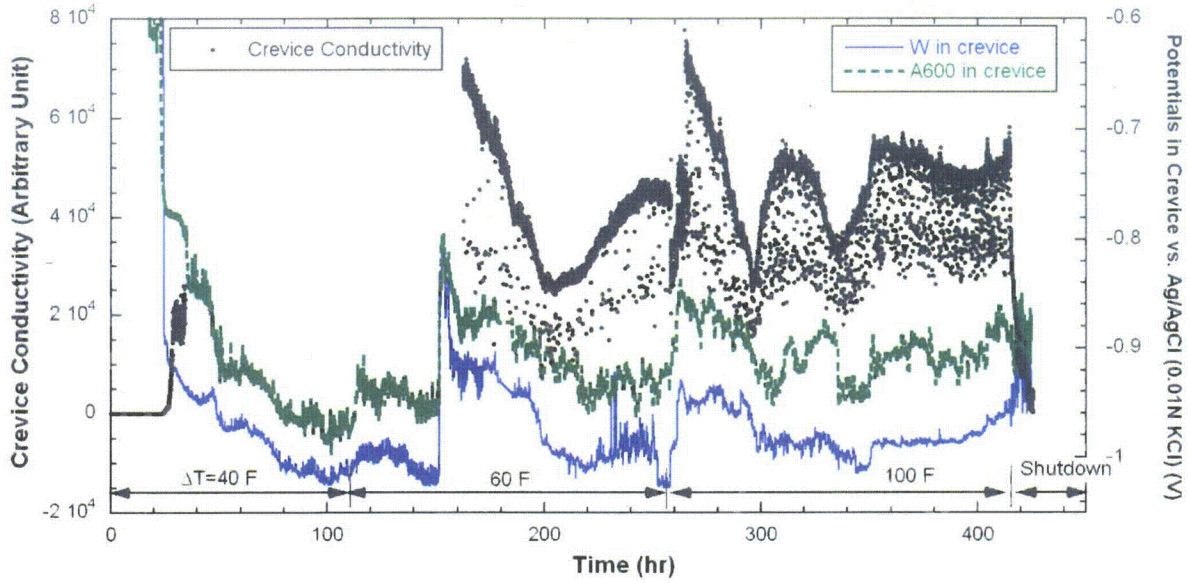

Figure 101. Tungsten and alloy 600 potentials in 10-mil gap crevice packed with diamond as compared with crevice conductivity variation (NaOH-03).

5.2.4 Post-Test Examination

Figure 102 shows the bare surfaces of alloy 600 tubing in the 10-mil crevice region, which indicate severe gouging. The gouging looks similar to that observed after the NaOH-01 and -02 tests shown in Figure 24. As discussed in Section 3.2.1, the gouging may be enhanced by abrasion caused by hard diamond particles. However, the total exposure time before the leakage is much shorter than that of NaOH-01 and -02 tests. In this test the total exposure time was about 160 hours, but in the NaOH-01 and -02 tests the leakage was detected after about 590 hours. The only difference between the two cases is ΔT. A higher ΔT is supposed to result in higher impurity concentration in a crevice. In the NaOH-01 and -02 tests, since the temperature was the only crevice monitoring parameter, the leakage might be detected later than its actual start time. Based on dye penetration test results, the crack depth in the previous NaOH tests appears to be deeper than that in the NaOH-03 test. Figure 103 shows the bubble test result for the packed crevice tubing. The tubing was pressurized up to 350 psig and put in a water bath. A 5-mm-long axial crack was detected where a Teflon cone ring and a stainless steel back ferrule had sat. These results suggest that low-temperature mill-annealed alloy 600 is very weak to cracking under NaOH solution with only operational hoop stress. Figure 104 shows the dye penetration results for the packed crevice tubing. Many axial cracks were detected around the tube surfaces. At the bottom of the crevice, the cracks linked together forming what looked like a circumferential crack.

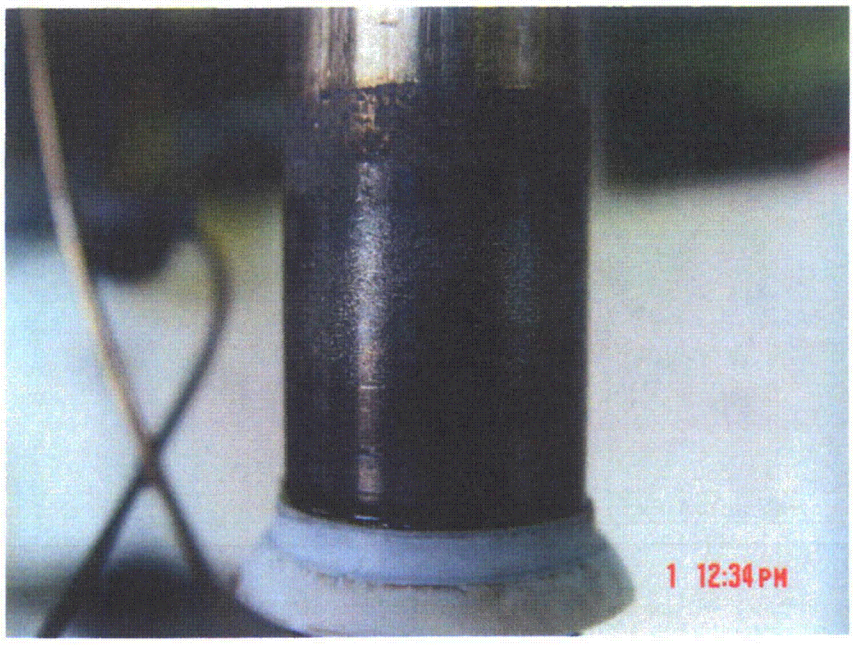

Figure 102.
Bare surface of alloy 600 tubing showing severe gouging due to caustic crevice chemistry.

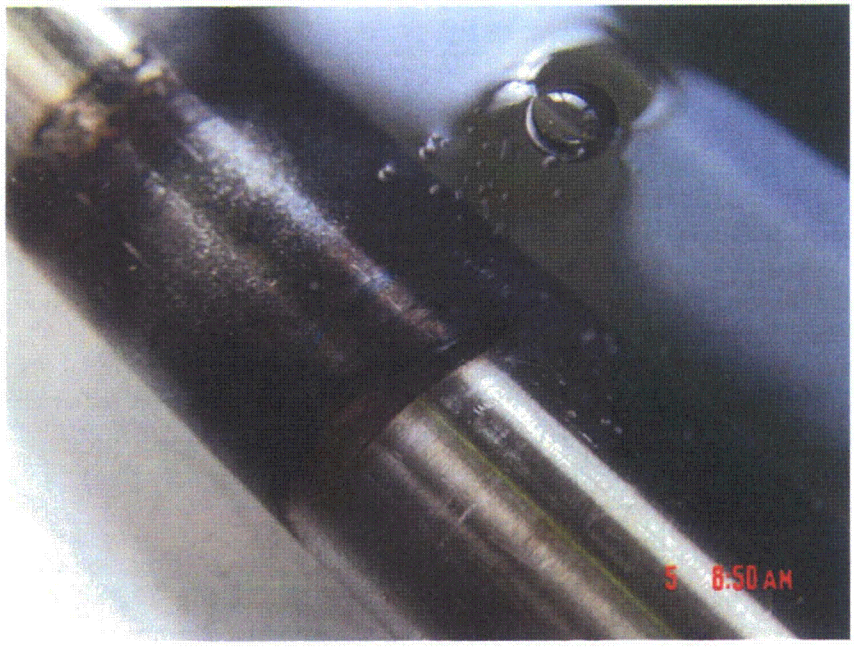

Figure 103.
Gas bubbles coming out of a through-wall crack detected underneath the Teflon swaging ferrule and developed inside the 10-mil gap crevice packed with diamond dust.

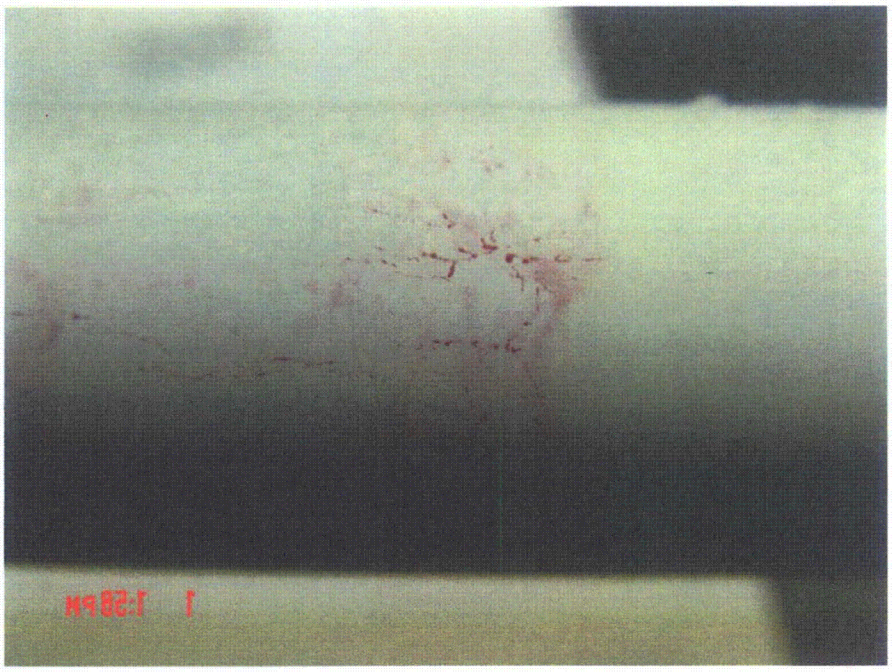

Figure 104.
Axial cracks developed inside the 10-mil gap crevice packed with diamond dust and visually enhanced by dye penetration (left side: crevice top, right side: crevice bottom).

Figure 105 is a photo of a bubble test showing multiple axial cracks developed at the 20-mil gap crevice without packing. In Figure 106 the cracks were visually enhanced by dye penetration. All cracks were detected at the middle or slightly upper region of the crevice, not at the bottom where the impurity concentration is expected to be higher than other areas, and residual stress is supposed to be higher because of a swaging ferrule. The tubing used for the open crevice had been exposed to NaOH or NaCl solution since the beginning of MB tests.

We can discuss two aspects of the through-wall cracks in the 20-mil gap crevice: crack initiation and propagation to the through-wall condition. In the previous series of NaCl tests, magnetite was packed in the 20-mil gap crevice. Since no gouging was observed on the tube surfaces, it is not likely that cracks were initiated during the previous NaCl tests. Cracks appear to have developed during the NaOH-02 tests because the packed diamond powders were blown out of the crevice during the NaOH-01 test. The crack propagation also appears to have occurred mainly during the NaOH-02 and this test, NaOH-03. A gas pressurization test before starting the NaOH-03 test confirmed that there was no through-wall crack. The question is how cracks can propagate under the unpacked condition. The crack itself can be considered as a crevice, which can cause impurity hideout if it is wide and deep enough. As shown in Figure 97, the crevice samples from the unpacked 20-mil gap crevice did not show high hideout. However, if a deep and long crack had developed, impurity hideout might have occurred inside the deep crack, which made the crack grow during this test.

The test results indicate that hideout/cracking can easily occur in Na-concentrated crevices, even with less flow-restrictive packing like diamond powder. A crack growing in a crevice that was cleaned is potentially very important to SG operators. It suggests that cracks or scratches themselves can become hideout crevices. It may be worthwhile to grow 20-40% though-wall cracks and then test them in the MB to determine if they will increase to 100% through-wall without any crevice or packing present.

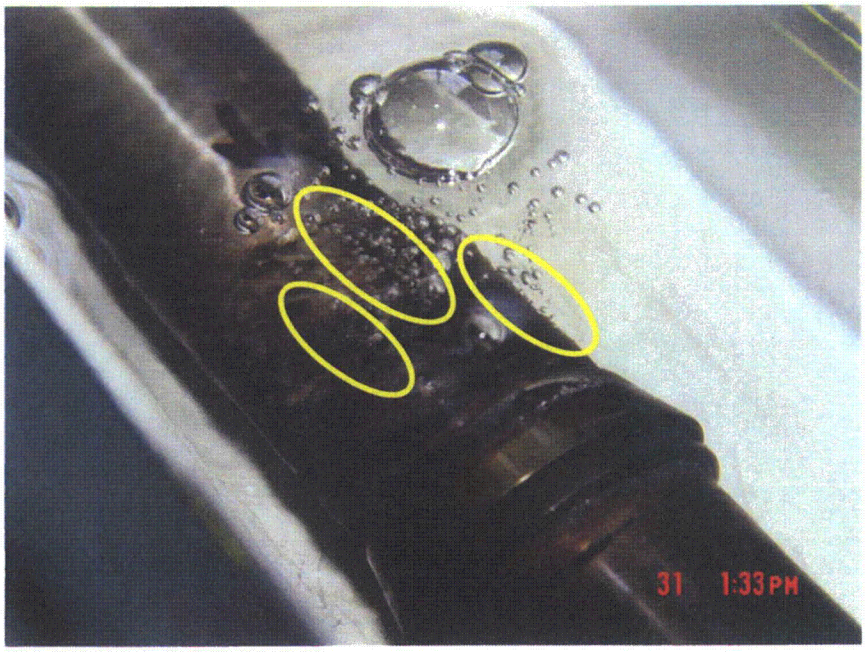

Figure 105.
Gas bubbles coming out of through-wall cracks developed inside the unpacked crevice region having a 20-mil radial gap.

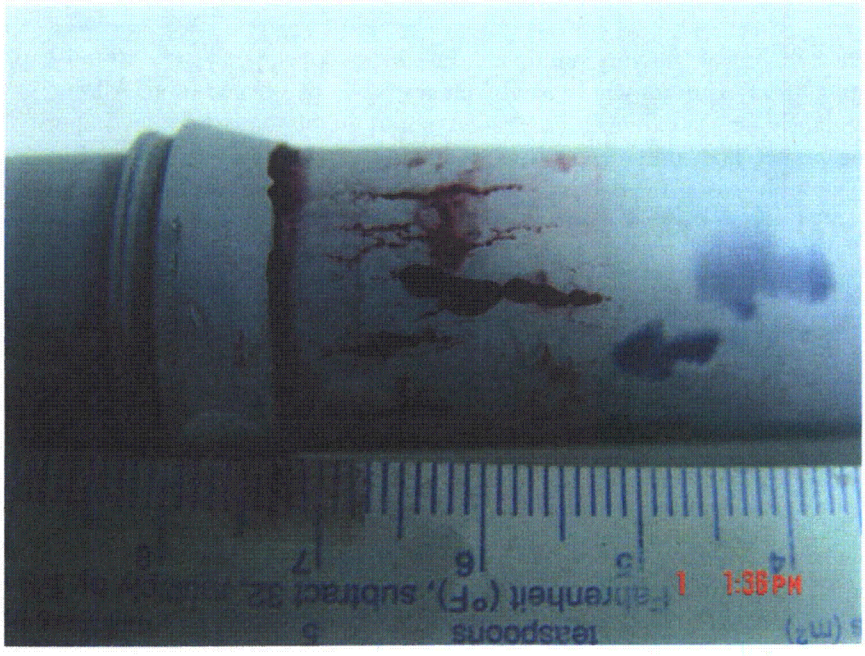

Figure 106.
Axial cracks developed inside the unpacked crevice region and visually enhanced by dye penetration.

5.2.5 Discussion

Starting Point of Leakage

It is important to know when the leakage started from the primary to secondary chamber because leakage could affect the data being analyzed. The primary and secondary water temperatures were plotted as a function of time, as shown in Figure 107. Since the primary and secondary temperatures were well controlled by heater power regulators and a cooling fan, no leakage was evident from the primary and secondary water temperatures. The primary and secondary pressures were also plotted as a function of time, as shown in Figure 108. Again, it was difficult to find any indication of leakage.

The cooling fan speed is plotted as a function of time in Figure 109. Since three rather than two fans were used at $\Delta T=100°F$, each fan speed was automatically readjusted after the change in ΔT from 60°F to 100°F. Cooling fan speed started to increase gradually at 330 hours, which indicates an increase of the thermal load in the secondary chamber because of leakage from the primary side.

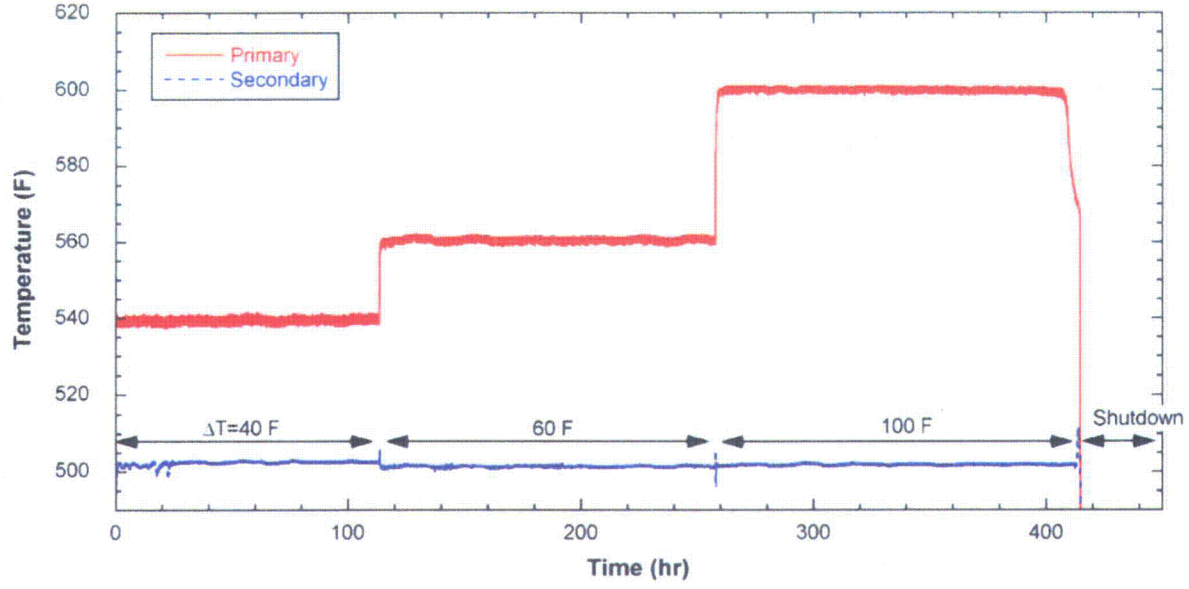

Figure 107. Primary and secondary water temperature variation with time (NaOH-03).

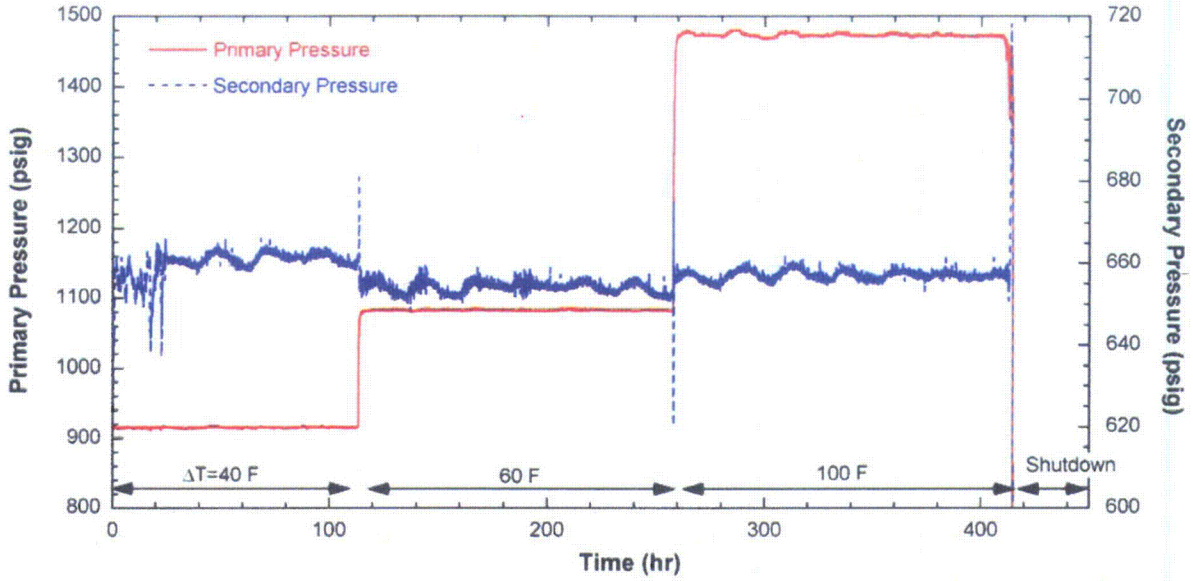

Figure 108. Primary and secondary pressure variation with time (NaOH-03).

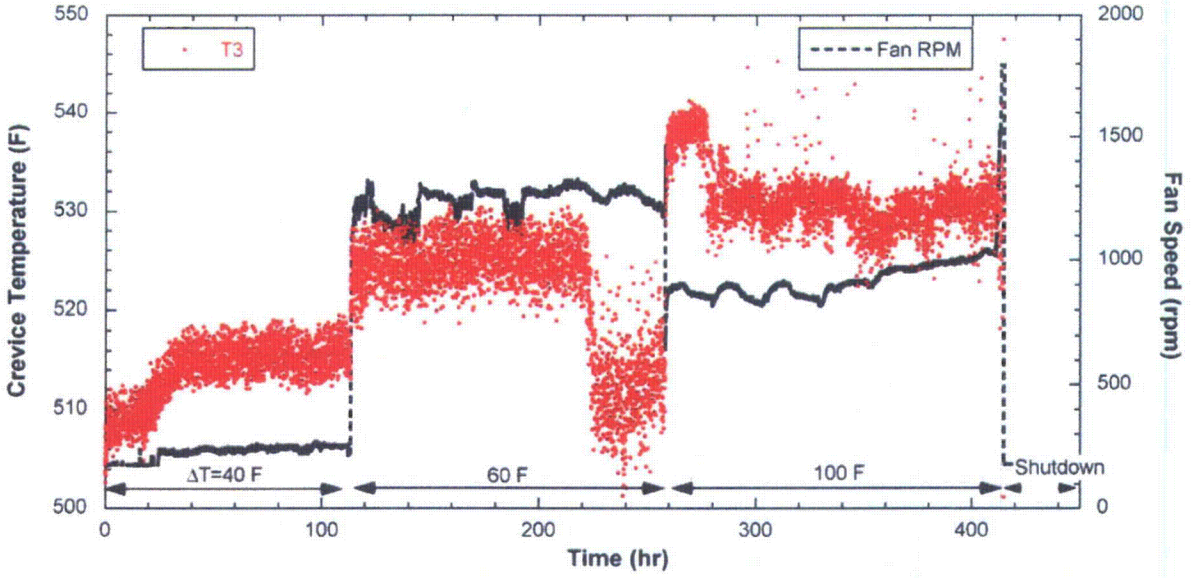

Figure 109. Cooling fan speed and crevice temperature (T3) variations with time (NaOH-03).

Table 5 summarizes the parameters monitored and the suggested starting time of the leak based on an evaluation of the data. The parameters measured in the bulk water, such as cooling fan speed or bulk conductivity, are less sensitive than the crevice monitoring parameters, as expected.

Table 5. Summary of monitoring parameters and each corresponding time indicating leakage from primary to secondary side.

Monitoring Parameter		Time Indicating Leakage	Comments
10-mil Crevice (Packed)	Crevice Temperature	220 hr	Figure 91
	Crevice Conductivity	Earlier than 160 hr	Figure 95
	Crevice Potentials	150 hr	Figure 98
	Crevice Solution Samples	Earlier than 162 hr	Figure 97
20-mil Crevice (Unpacked)	Crevice Temperature (Unpacked Crevice)	160 hr	Figure 92
	Crevice Solution Samples	Earlier than 162 hr	Figure 97
Bulk	Cooling Fan Speed	330 hr	Figure 109
	Bulk Conductivity	280 hr	Figure 94

ECP and pH Data Analysis

In Figure 110, variations in crevice and bulk tungsten potentials are plotted as a function of crevice pH based on sample analysis results. As mentioned with regard to Figure 97, a correction for sampling time was applied. For the bulk water data the correction was not applied because the bulk samples have enough volume to overcome the dead volume of the sampling line. Only the crevice samples taken before the start of leakage were considered in this analysis. As compared with Figure 110(a), the crevice tungsten data after the sampling time correction in Figure 110(b) appear to better fit a single line. The bulk tungsten data show a linear behavior, and their slope is -85 mV/pH, which is less than the Nernstian slope of -106 mV/pH at 500°F, but the slope becomes closer to the Nernstian one when combined with NaCl test data (see Figure 114). The corrected data for crevice tungsten potential and bulk potential were plotted in a potential-pH diagram for the W-H_2O system, shown in Figure 111. The data from the NaCl-03 and -04 tests are plotted in the same figure. The bulk tungsten data in the NaOH test are well fitted to a line with the bulk solution data in NaCl tests, and the slope of the line appears to be close to the theoretical slope, -106 mV. The crevice tungsten data appear to be linear for the overall pH range, but data scatter occurs in the local caustic pH range. As compared with the bulk data, the crevice data in the NaOH test tend to have higher potentials at the same pH level. The oxidation states of the crevice W/WO_x electrode might be different from the bulk water, or the boiling liquid around the crevice tungsten wire tip might affect the potential value. The main purpose of the NaOH-03 test was to confirm the functionality of overall instrumentation. From this point of view, within the pH range of 5-10 at 500 °F, the instruments at the crevice and bulk appear to generate reasonable data.

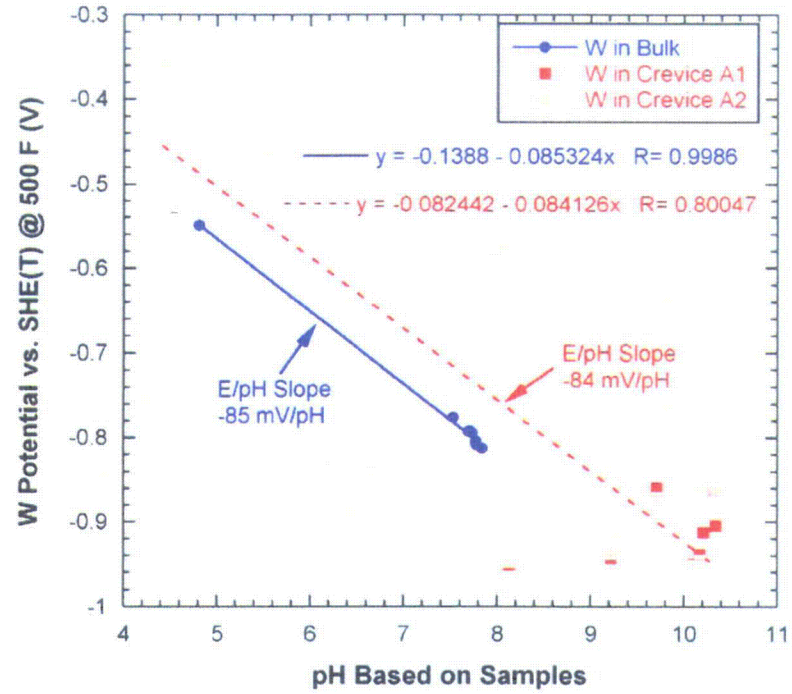

(a) Before sampling time correction

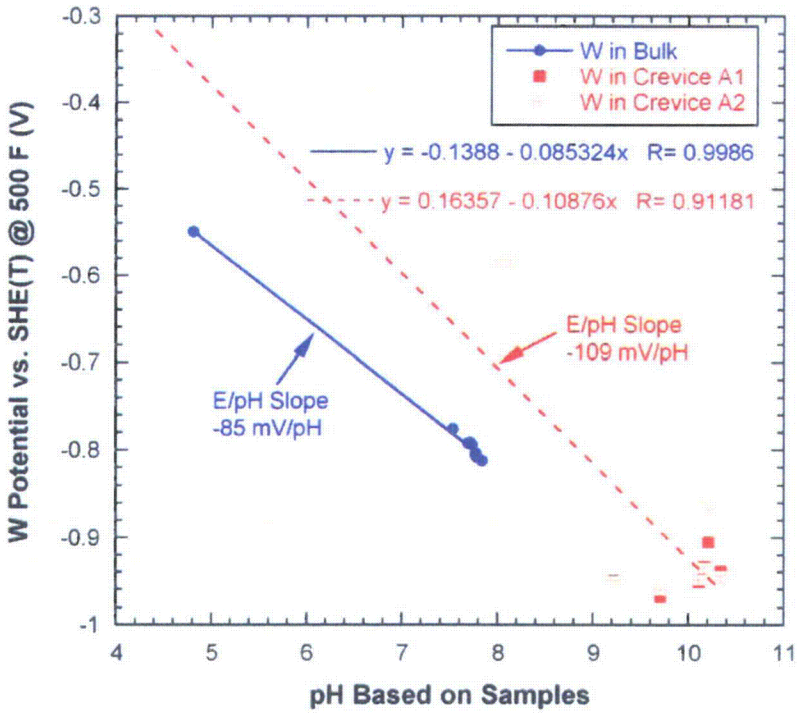

(b) After sampling time correction

Figure 110. Crevice and bulk tungsten potential variation as a function of crevice pH based on samples (NaOH-03).

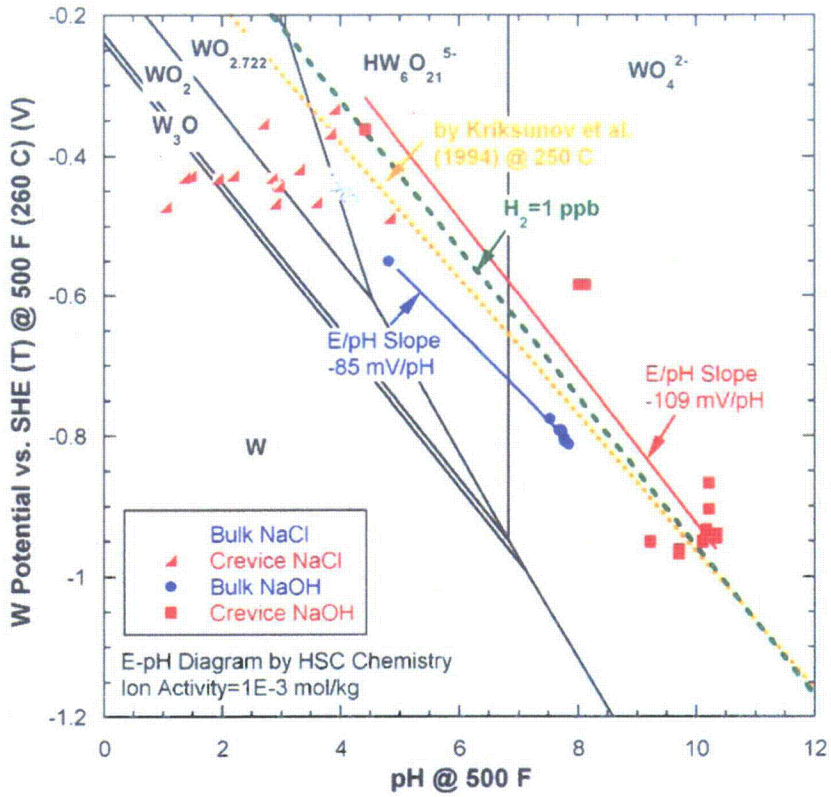

Figure 111. Tungsten potentials in bulk and crevice as a function of pH by sampling results in a potential-pH diagram of W-H_2O system predicted by the thermodynamic code HSC Chemistry.

Crevice Concentration Estimation

Figure 112 shows the variation in integrated-volume averaged crevice Na concentration as a function of time. The crevice Na concentrations were estimated from the data on bulk chemistry, crevice potential, and crevice temperature and compared with concentrations determined from the crevice samples. When estimating the concentration using the bulk samples, we assumed that all of the Na that left the bulk water was concentrated in the 10-mil gap crevice region, which is a credible assumption. The volume-averaged crevice concentration was calculated based on the total Na hideout mass and crevice porosity. The crevice samples showed lower concentrations than the three other estimated values.

The method for estimating the crevice concentration from the crevice temperature is as follows. The boiling point elevation was assumed to be as the temperature difference between the crevice temperature and the secondary saturation temperature of 500°F. As shown in Figure 113, MULTEQ® can predict the relationship between crevice concentration and corresponding BPE. The relationship is represented as follows:

$$[Na\,(ppm)] = \frac{BPE\,(F) + 0.053497}{0.00019134} \qquad (4)$$

In this MULTEQ calculation, a static condition and steam-retained option were selected. By means of Eq. (4), we estimated the Na concentration from the crevice temperature data. The crevice tungsten potential data can also give the Na concentration in the crevice. Before NaOH solution injection, the

crevice tungsten potential and pH were -0.362 V (vs. a standard hydrogen electrode) and 4.42, respectively. If the slope of the line relating potential to pH is determined, the crevice pH can be estimated from the crevice tungsten potential data. As shown in Figure 114, the potential/pH slope for the tungsten/tungsten oxide electrode was determined from the tungsten potential data for the bulk solution. Since we know the tungsten potential/pH slope and we have the pH and corresponding potential for one instant in time in the crevice, a linear equation can be derived for the relationship between crevice tungsten potential and crevice pH. The data in Figure 113 (from MULTEQ®) can then be used to relate the crevice pH (determined from the crevice potential) to the Na concentration. Based on the data in Figure 113, the logarithmically fitted equation was derived:

$$[Na(ppm)] = 10^{\frac{pH-7.3378}{0.67514}} \tag{5}$$

From Eq. (5), the crevice Na concentration was estimated from the crevice tungsten potential data. The estimated Na concentration was similar to the estimated value from the crevice temperature data at ΔT=40°F and slightly lower at ΔT=60°F, as shown in Figure 112. If the test had been continued without the leakage at ΔT=60°F, the discrepancy between the two data sets might have decreased.

Based on the comparison results shown in Figure 112, the Na concentration determined from the crevice samples tends to follow the same general trend as the Na concentration determined by other methods but they are lower than those estimated using other methods. The crevice samples may be diluted because less concentrated solution from the bulk region is mixed with the solution from the crevice bottom region, even though the sampling line itself is located at the crevice bottom region.

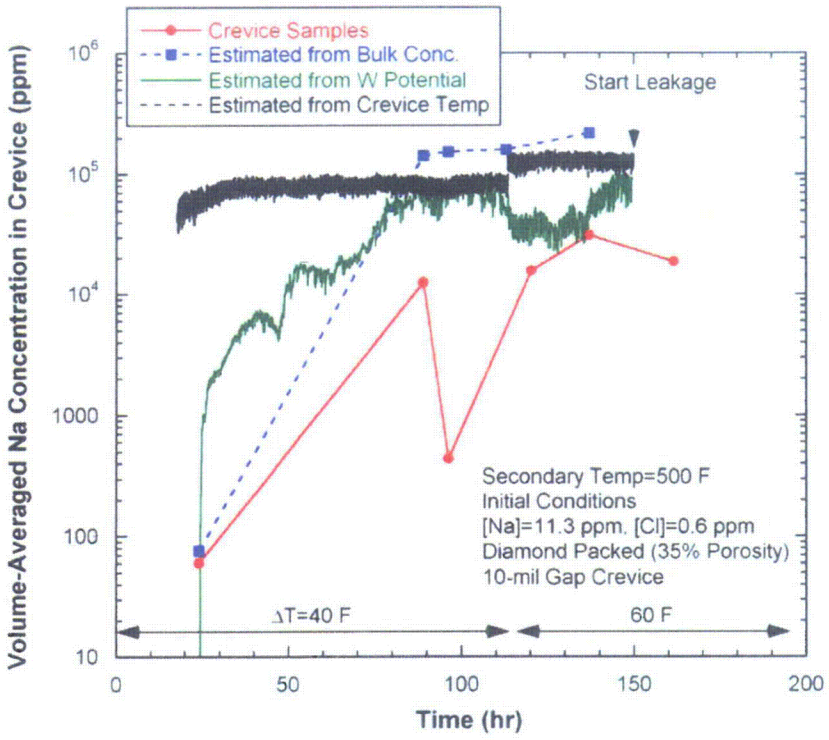

Figure 112.
Volume-averaged crevice Na concentration estimated from bulk chemistry data, tungsten potential in crevice, and temperature data in crevice as compared with the analyses for crevice samples (NaOH-03).

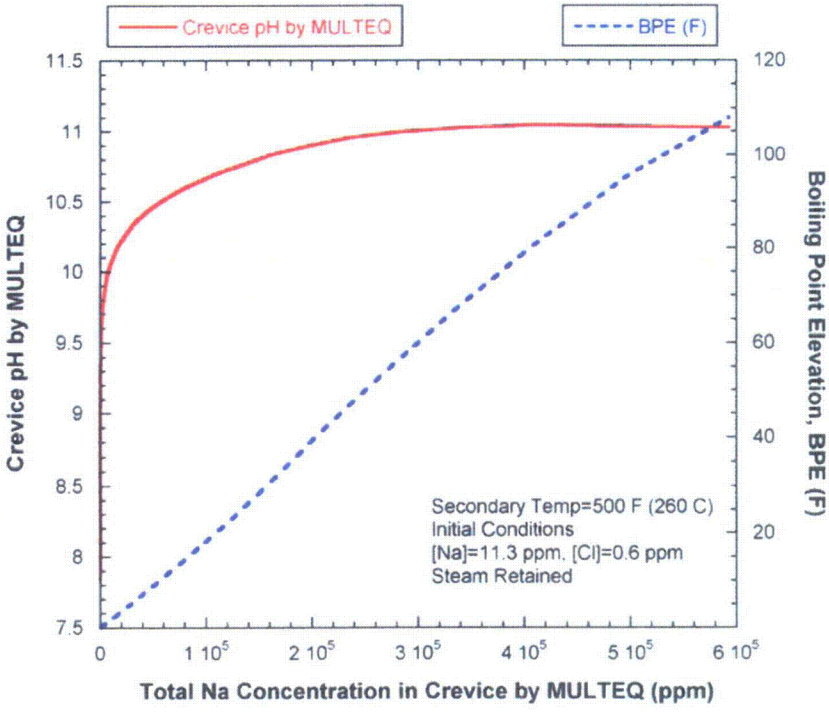

Figure 113.
Calculated pH and boiling point elevation variation as a function of total Na concentration in crevice predicted by MULTEQ.

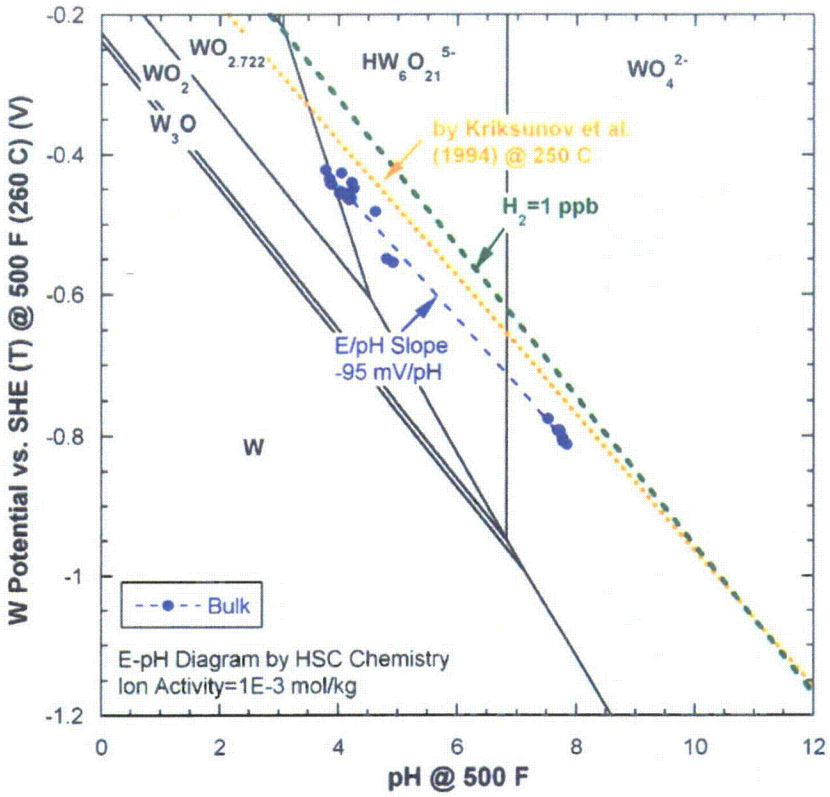

Figure 114. Measured tungsten potentials as a function of pH based on bulk solution samples plotted in a potential-pH diagram of W-H_2O system predicted by the thermodynamic code HSC Chemistry.

5.2.6 Summary

The NaOH-3 test involved a NaOH solution and only one crevice packed with diamond powder. The tungsten potential data for the bulk solution were consistent with the previous data measured in tests with NaCl chemistry. The crevice tungsten potential data showed good linearity within the pH ranges of 5-10, even though data scatter occurred in narrow pH ranges. Based on these results, the crevice chemistry instrumentation itself appears to work properly under the NaOH chemistry. The integrated-volume averaged Na concentrations in the crevice were estimated from the bulk samples analysis results, the crevice temperature, and crevice tungsten potential, and compared with Na concentrations estimated from the crevice solution samples. The estimated crevice concentrations from the bulk samples, the temperature, and tungsten potentials are higher than that by the crevice samples which might be diluted during sampling processes by being mixed with bulk solution, but the three data sets follow similar trends. Through-wall cracks developed in the unpacked crevice during this test. Crack growing in a crevice that was cleaned is potentially very important to SG operators. It may indicate that cracks or scratches themselves can become hideout crevices.